PROCESS OPTIMIZATION FOR PARTIAL OXIDATION OF BACTERIAL SLUDGE IN A SONOCHEMICAL REACTOR

by

Analene Beyers

Thesis presented in partial fulfilment

of the requirements for the Degree

of

MASTER IN ENGINEERING

(CHEMICAL ENGINEERING)

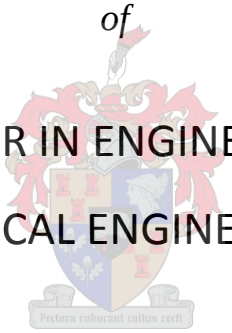

in the Faculty of Engineering

at Stellenbosch University

Supervisor

Dr. Linda Callanan

Co-Supervisor

Prof. Chris Aldrich

April 2014

Declaration

By submitting this thesis electronically, I declare that the entirety of the work contained therein is my own, original work, that I am the sole author thereof (save to the extent explicitly otherwise stated), that reproduction and publication thereof by Stellenbosch University will not infringe any third party rights and that I have not previously in its entirety or in part submitted it for obtaining any qualification.

Analene Beyers 29 November 2013

....

Signature Date

ABSTRACT

It was found that bacterial sludge from anaerobic water treatment systems is produced internationally at a rate of 60 grams per person per day and the accumulation of the potentially hazardous by-product has become of increasing concern. The produced bacterial sludge is frequently pumped into dams, dried out and used as agricultural fertilizer. This bacterial sludge is expected to have a relatively high heating value and as such, has the potential to produce energy from the biomass. It is, therefore, advisable to utilize this energy potential as an alternative to conventional sludge disposal.

This project aimed to improve the yield of syngas by optimizing the reactor design to partially oxidize bacterial sludge using a sonochemical reactor that is operated at bulk atmospheric conditions. The effect of different conditions was investigated and the optimum settings for syngas production were found by investigating temperature, pressure and the effect of the amplitude of operation that regulates the energy input by the ultrasonic equipment. The optimum conditions were used to investigate the kinetics involved in this process as well as to determine the energy consumption by the process. It was also required to study the feasibility of partially oxidizing bacterial sludge using a sonochemical reactor instead of conventional steam gasification and also as an alternative means of sludge disposal.

By eliminating this pollutant source, the future environmental threat posed by an increasing population size will be minimized and energy will be utilized from a thus-far wasted energy source. The syngas that is produced is used as a green alternative to fossil fuels in the Gas-to-Liquids (GTL) process to produce liquids fuels. A thus-far wasted energy source will be consumed and fossil fuels can be saved in the process.

It was found that the maximum hydrogen mole percentage produced is 0.141 mole % of the vapour phase with the maximum carbon monoxide mole percentage in the vapour phase at 1.896 mole %. This shows an improvement on work conducted by Beyers (2011) of 59 % for hydrogen, 92% for carbon monoxide and a reduction of 49 % for carbon dioxide. A kinetic study of the process indicated that the rate equations that describe the hydrogen and carbon monoxide production are zero order and, therefore, independent of initial concentration of the sludge. The rate constants were 0.0146 (mol % hydrogen/s) and 0.0183 (mol % hydrogen/s) for hydrogen and carbon monoxide, respectively. It was found that the most severe change to the higher heating value of the

feed was a mere 0.27 mJ/kg from an original value of 9.81 mJ/kg. This therefore confirms that the reaction has not proceeded to completion. The statistical model predicted a maximum value for hydrogen production at 0.151 mole % in the product gas, 0.01 mole % from the measured maximum.

It was also found that hydrogen is produced during the sonolysis of distilled water and that this confirms that the hydrogen production during partial oxidation of the sludge sample comes mainly from the water present in the sludge. The hydrogen produced when only using water, was found to be 0.127 mole % and when using the active sludge, the value was 0.116 mole % hydrogen in the vapour phase. The thermal decomposition of calcium carbonate in the lime that is used to treat the pH of the unit where the sludge originates from, followed by the formation of carbon monoxide during the Boudouard reaction, led to an increased amount of carbon monoxide present in the product gas.

Ultrasonic intensity is defined as the amount of energy that is transferred to the sample per cubic meter of the internal surface area of the reactor vessel. It was found that the intensity that was delivered to the reactant was lower than expected as the reactor was operating at an efficiency of only 36%. The design intensity was 1.44 W/m^2 and the actual delivered intensity was 0.52 W/m^2.

Based on a maximum yield of 0.00012 Nm^3/kg, the cost of syngas production under the conditions described by this study, would amount to R 19.98/Nm^3. This cost only implicates the operational expenses and does not take further downstream processing and initial capital investment repayments into account. Conventional steam gasification at a yield of 0.67 Nm^3/kg has an operational syngas production cost of R 1.48/Nm^3. This process was therefore found to not be economically feasible as the cost of utilizing ultrasound as opposed to normal steam gasification is more than ten times more expensive.

It was concluded that the process was successfully optimized by the redesigning of the reactor and that carbon dioxide production was limited by excluding oxygen from the feed gas. It was also concluded that the sonolysis of water and the thermal decomposition of calcium carbonate, followed by the conversion of carbon dioxide to carbon monoxide, supplements the syngas production under the current operational conditions.

Based on the production of no methane during the course of this study, the sonochemical process can be tied into the GTL process after the steam reforming unit. Due to the relatively high carbon

dioxide content, the process will need to join the main feed gas stream that is fed into the carbon dioxide removal unit before it enters the GTL process to correct the desired feed gas ratio.

Based on the very low syngas yields, the low hydrogen to carbon monoxide ratio in comparison to the required ratio of 2 as well as the high energy intensity required for this process, it can be concluded that the partial oxidation of biomass sludge in a sonochemical reactor is not feasible as an alternative technology to conventional steam gasification. The operating costs of the sonochemical unit would be nearly ten times that of steam gasification and is therefore concluded to not be a competitive technology to conventional steam gasification.

It is recommended that the reactor design is reinvestigated to improve the delivered ultrasound intensity as well as the surface area where the ultrasonic waves are intensified. This would eliminate dead-zones. It was also recommended that the argon gas is continuously bubbled through the reactant mixture during experiments to eliminate the degassing effect caused when the ultrasound is initially emitted. The gas outlet of the process can then be connected to an online gas chromatograph (GC) with a thermal conductivity detector (TCD) and flame ionization detector (FID) methanizer in series as the TCD does not destroy the sample and this setup would improve the analytical process.

The production of carbon monoxide from lime as well as the production of hydrogen from water during sonolysis needs to be investigated. The effect of radicals can also be studied by the addition of a radical scavenger to the process.

It is recommended that the experimental design is reinvestigated and a design that will deliver similar information utilizing fewer data points should be chosen. Based on this model as well as further kinetic testing, it is recommended that a complete ASPEN model is developed to simulate the energy requirements to tie the ultrasonic process into the commercial plant. Based on this model, a complete feasibility study can then be conducted to determine the capital costs involved, the operating costs, the repayment period as well as taking the current costs of sludge disposal into account.

OPSOMMING

Daar is gevind dat bakteriele slik internasionaal geproduseer word deur anaerobiese waterbehandelingseenhede teen ‘n tempo van 60 gram per person per dag en dat die opberging van hierdie gevaarlike byproduk ‘n groeiende probleem word. Die geproduseerde bakteriele slik word in damme gestoor, uitgedroog of gebruik as kunsmis in die landbou bedryf. Daar word vermoed dat hierdie baketriele slik oor ‘n hoe verwarmings waarde beskik en het daarom die potensiaal om energie te produseer uit die biomassa. Daarom is dit voorgestel om alternatiewe prosesse te ondersoek om van hierdie slik ontslae te raak en moontlik die energie wat beskikbaar is te gebruik.

Die projek is daarop gefokus om die produksie van syngas te verbeter deur die reaktorontwerp te optimeer deur gebruik te maak van parsiele oksidasie van slik onder atmosferiese kondisies deur klankgolwe te gebruik. Die effek van verskillende operasionele kondisies is ondersoek en die optimale vlakke van syngas produksie is gevind deur temperatuur, druk en amplitude wat die hoeveelheid energie wat oorgedra word aan die reaktor reguleer, te ondersoek. Die optimale kondisies is ook gebruik om die kinetiese aspekte van die proses te ondersoek en ook om te kyk wat die sisteem se energie benodighede behels. Die haalbaarheid om baketriele slik parsieel te oksideer in ‘n sonochemiese reaktor is vergelyk met dit van konvensionele stoom vergassing van die biomassa en is ook ondersoek as ‘n alternatief om van die slik ontslae te raak.

Deur die slik te verwyder as ‘n potensiele bron van besoedeling, kan die toekomstige omgewing’s risiko wat deur die toename in die bevolkkingsgroote tot gevolg is, verwyder word deur ‘n energie bron te gebruik wat tot dusver geignoreer is. Die syngas wat geproduseer word kan dan gebruik word in die “Gas-to-Liquids” (GTL) process om vloeistof brandstowwe te produseer. Dus sal ‘n omgewingsrisiko verminder word, ‘n energiebron word benuttig wat nooit van tevore benuttig is nie en fosiel brandstowwe kan gespaar word.

Die maksimum waterstof wat geproduseer is, was 0.141 mol % in die gas fase met ‘n maksimum waarde vir koosltof monoksied van 1.896 mol % in die gas fase. Dit toon ‘n verbetering van 59 % vir waterstof, 92 % vir koolstof monoksied en ‘n vermindering van 49% in die koolstof dioksied wat deur Beyers (2011) geproduseer is. Die kinetiese studie het ondervind dat die “rate equation” van waterstof en koolstofmonoksied beskryf word deur nul-orde kinetika. Hierdie konstantes was 0.0146 (mol % waterstof/s) en 0.0183 (mol % waterstof/s) vir waterstof en koolstofmonoksied.

Daar is ook gevind dat die grootste moontlik verandering in die hoe verwarmings waarde van die biomassa is ‘n skamele 0.27 mJ/kg van die oorspronklike waarde van 9.81 mJ/kg. Hierdie waarneming staaf dus die uitkoms dat die reaksie dus nie tot die einde verloop het nie. Die statistiese model het ‘n maksimum van 0.151 mol % voorspel wat 0.01 mol % meer was as die waarde wat gemeet is.

Dit is ook gevind dat waterstof geproduseer word deur die sonoliese van water en dat hierdie bykomende waterstof deel uitmaak van die produkgas aangesien die slik grootliks uit water bestaan.Die hoveelheid waterstof in die gas fase wat geproduseer is tydens sonoliese van ‘n suiwer water monster, was 0.127 mol %. Die hoeveelheid waterstof in die gas fase wanneer die slik behandel is ten optimal kondisies, was 0.116 mol % gemiddeld. Die hitte degradering van kalsium karbonaat wat teenwoordig is in die kalk wat gebruik word om die pH van die produksie eenheid te reguleer, gevolg deur die Boudouard reaksie, het tot gevolg dat addisionele koolstof monoksied ook gevorm word.

Ultrasoniese intensiteit kan gedefineer word as die hoeveelheid energy wat oorgedra word aan ‘n reaktant gebasseer op die oppervlak area aan die binnekant van die reaktor. Die intensiteit waarteen die voermateriaal blootgestel word aan die klankgolwe was laer as verwag met ‘n 36 % effektiwiteit. Die ontwerp spesifiseer ‘n intensiteit van 1.44 W/m^2 en die intensiteit wat fisies gelewer is, was 0.521 W/m^2.

Die maksimum produksie van syngas was 0.00012 Nm^3/kg, wat lei tot ‘n operasionele koste van R 19.98/Nm^3 onder die kondisies van hierdie studie. Hierdie koste neem nie die oorsponkilke kapitaal vir die konstruksie, of die koste van verdere behandelik van die gas, in ag nie. Konvensionele stoom vergassing teen ‘n opbrengs van 0.67 Nm^3/kg het ‘n operasionele koste van R 1.48/Nm^3 tot gevolg. Die proses is dus ekonomies nie ‘n aantreklike opsie nie aangesien die kostes van syngas produksie met ultraklank meer as tien keer meer is as konvensionele stoom vergassing.

Daar is tot die gevolgtrekking gekom dat die reaktor optimering suksesvol was en deur geen stuurstof te voer nie, die koolstofdioksied persentasie verminder is. Daar is ook tot die gevolgtrekking gekom dat die sonoliese van water, en die hitte degradering van kalsium karbonaat, gevolg deur die Boudouard reaksie, die syngas produksie supplementeer.

Aangesien geen metaan gedurende hierdie studie geproduseer is nie, kan die sonochemiese proses inskakel by die GTL aanleg na die stoom hervormingseenhed. As gevolg van die hoe koolstofdioksied konsentrasie, sal die prosesstroom gemeng moet word met die produk stroom uit die stoom hervormings proses, wat gevoer word na die koolstofdioksied verwyderings eenheid. Hierdie eenheid is daarvoor verantwoordelik om die korrekte verhouding van gasse vir die GTL voer stroom te reguleer.

Gebasseer op die baie lae syngas opbrengs, die lae waterstof tot koolstofmonoksied verhouding en die hoe energie behoeftes, is daar tot die gevolgtrekking gekom dat die parsiele oksidasdie van die biomassa in ‘n sonochemiese reaktor nie ‘n haalbare alternatief is vir konvensionele stoom vergassing nie. Die operasionele koste van die sonochemiese eenheid is ongeveer tien keer meer as die van stoom vergassing en daarom is die proses nie kompeterend nie.

Daar word voorgestel dat die reaktor ontwerp hersien word om die gelewerde intensiteit te verbeter, sowel as om die kontak area waar die klankgolwe gekonsentreer is, te vergroot. Dit sal dooie sones uitskakel. Daar word ook voorgestel dat argon gas gedurende die eksperiment aanhoudende geborrel word deur die reaktant vloeistof in die reaktor om die ontgassingseffek uit te skakel sodra die klankgolwe aangeskakel word. Die gas uitlaat kan dan inlyn gekoppel word aan ‘n gas chromatograaf met ‘n termiese geleidings detektor (TCD) en ‘n vlam ionisasie detektor (FID) met metaan omskakeling, aangesien die TCD nie die monster vernietig nie. Hierdie opstelling behoort analitiese methodes te verbeter.

Die produksie van koolstofmonoksied uit kalk sowel as die produksie van waterstof uit water gedurende sonoliese, moet verder ondersoek word. Die effek van radikale kan ook verder bestudeer word deur die gebruik van ‘n radikaal rower gedurende die proses.

Daar word ook voorgestel dat die statistiese ontwerp herondersoek word sodat minder eksperimente gebruik kan word om soortgelyke resultate te bekom met minder data punte. Gebasseer op hierdie nuwe model en ‘n kinetiese studie, word dit aangeraai dat ‘n volledige ASPEN model gebou word om te simuleer hoe hierdie sonochemiese eenheid sal inskakel met die kommersiele eenheid.

Dit sal dan moontlik wees om die energie benodighede van die proses te verstaan en gebasseer daarop, kan ‘n volledige haalbaarheid studie gedoen word wat kyk na oorspronklike installasie

kostes, onderhouskostes, operasionele kostes sowel as die terugbetaling van die konstruksie kostes. Dan kan ‘n vergelyking getref word met die huidige kostes om van hierdie slik ontslae te raak en om die slik as ‘n brandstof te benut.

ACKNOWLEDGEMENTS

I would especially like to acknowledge the following persons for their contribution to me completing this thesis:

Dr. Linda Callanan

Prof. Chris Aldrich

Mrs. Hanlie Botha

Dr. L.J. du Preez

Mr. Jannie Barnard

Mr. Alvin Petersen

Mr. Elton Thyse

Mr. Max van Baarsel

Dr. Marion Carrier

Mrs. Jeanne du Preez

Mr. Mark Hobbs

Dr. JO Van Vuuren

Mr. Raoul Coetzee

And then a special thank you to my friends and family for their patience and understanding over the last two years.

TABLE OF CONTENTS

ABSTRACT iii

OPSOMMING vi

ACKNOWLEDGEMENTS x

TABLE OF CONTENTS xi

LIST OF FIGURES xiv

LIST OF TABLES xvi

NOMENCLATURE xvii

SECTION I - THE LITERATURE REVIEW 1

1. INTRODUCTION 1

2. LITERATURE REVIEW 3

2.1 The role of the GTL industry in liquid fuels production 3
2.2 The production of syngas from biomass 4
2.3 The production of syngas from bacterial sludge 4
2.4 The difference between biomass gasification and partial oxidation 7
2.5 Partial Oxidation Reactions 9
2.6 Sonolysis of water using Ultrasound 10
2.7 Thermal Decomposition of Lime 11
2.8 Sonochemical Reactor 11
2.8.1 The sonochemical reactivity two-site model 12
2.8.2 Sonochemical reactor considerations 13
2.9 Reaction mechanism involving OH radicals 15
2.10 Partial Oxidation of bacterial sludge using a sonochemical reactor 16
2.11 Effect of Pressure on Sonochemistry 17

3. THEORETICAL FRAMEWORK 18

3.1 Response Surface Methodology - Rotatable CCD 18
3.1.1 Regression 20
3.1.2 Stationary Point 21
3.1.3 Generalized Reduced Gradient Method to obtain local maxima 21
3.1.4 Desirability Approach 22
3.2 Kinetic and Mechanistic Effects of Ultrasound 22
3.3 Compressibility for gas mixtures 24
3.4 Solubility of gases in water 25
3.5 Estimation of Biomass Synthesis Gas Composition using Equilibrium Modelling 26

4. PROBLEM STATEMENT 28

5. HYPOTHESIS 29

6. PROJECT SCOPE 30

7. PROJECT OBJECTIVES 31

SECTION II – PRELIMINARY STUDIES 32

8. Biomass Sample Preparation 32

9. Sludge Characteristics 34

10. Reactor set-up and supporting equipment 42

11. Gas Chromatography 48

11.1 Overview 48
11.2 Thermal Conductivity Detector 49
11.3 Flame Ionization Detector with a methanizer 49
11.4 Column Conditioning 50
11.5 Column Operating Method Selection 50
11.6 Calibration 51

12. Variable Selection and Range Testing 54

13. Experimental Planning 56

13.1 Central Composite Experimental Design 56
13.2 Introductory Experiments to establish variable ranges 56
13.3 Sampling Techniques 58
13.4 Experimental Procedure 58
13.5 Solid and Gas Sample Analysis 60
13.5.1 GC Start-up Procedure: 60
13.5.2 GC Operating Procedure: 60
13.5.3 GC Shut-down Procedure: 61
13.5.4 Solid sample analysis: 62

SECTION III – REACTOR COMMISSIONING AND TESTING 63

14. Physical behaviour in the sonochemical reactor 63

15. Product Gases 66

16. Mass- and Energy Balance 74

17. Kinetics 81

18. Control Experiments 85

19. Evaluation of Optimum Design 88

20. CCD Results and Optimization 90

20.1 Basic Statistical Analysis and Model determination 90
20.2 ANOVA Assumptions for the hydrogen model 91
20.3 Adequacy of the hydrogen model 93
20.4 ANOVA Assumptions for the carbon monoxide model 94
20.5 Adequacy of the carbon monoxide model 96

20.6 Regression Model Description 96
21. Cavitation effect on equipment 100
22. Commercial Plant input 100
23. Improvement on previous work 102
24. Feasibility 102
SECTION IV – CONCLUSIONS AND RECOMMENDATIONS 104
25. CONCLUSIONS 104
26. RECOMMENDATIONS 107
REFERENCES 109
Appendix 114
A. Personal Protective Equipment and Safety Considerations 114
B. GC Method Used 115
C. GC Calibration Curves 117
D. RAW Data Tables 125
E. ANOVA Outputs 127
F. Particle Size Analysis 133
G. Materials used 142

LIST OF FIGURES

Figure 1: Schematic of Activated Sludge process (LennTech Water Treatment Solutions, 2003)..... 5
Figure 2: Schematic of normal Biomass Gasification (Fuel.com, 2008)..... 8
Figure 3: Cavitational growth and collapse of bubble (Timothy J. Mason, Dietmar Peters, 2003)..... 13
Figure 4: Schematic of Central Composite Design parameter settings..... 19
Figure 5: Sludge Mixing Vessel..... 33
Figure 6: Sample Weight Distribution of sludge feed..... 33
Figure 7: Sludge Ultimate Analysis..... 36
Figure 8: Sludge Proximate Analysis..... 37
Figure 9: TGA Graph of Sample B85-2013..... 38
Figure 10: Sludge Cumulative Finer Volume % from Particle Size Analysis..... 39
Figure 11: Sludge Particle Size Distribution..... 40
Figure 12: Partial Oxidation of bacterial sludge Process Flow Diagram..... 42
Figure 13: Experimental Setup for partial oxidation of bacterial sludge using ultrasound..... 43
Figure 14: Reactor Probe..... 43
Figure 15: Reactor Gas outlet..... 44
Figure 16: Reactor Flange at gas outlet..... 44
Figure 17: Mesh Wire Water Trap..... 44
Figure 18: Reactor temperature gradients..... 45
Figure 19: Detailed Sonochemical reactor drawing with cooling water jacket..... 47
Figure 20: Hydrogen and Carbon Monoxide Production during Screening Experiments at 70%..... 55
Figure 21: Hydrogen and Carbon Monoxide Production during Screening Experiments at 50%..... 55
Figure 22: Pressure and Temperature Changes during Sonochemical Experimental Runs..... 63
Figure 23: Pressure changes over time during Sonochemical Experimental Runs..... 64
Figure 24: Hydrogen Mole % formed during Sonochemical Experimental Runs..... 66
Figure 25: Carbon Monoxide Mole % Formed during Sonochemical Experimental Runs..... 67
Figure 26: Product Gas Contributions during Sonochemical Experimental Runs..... 68
Figure 27: Hydrogen to Carbon Monoxide Ratio for Sonochemical Experimental Runs..... 69
Figure 28: Normalized Average Reactor Composition after Sonochemical experiments excluding Argon as inert gas..... 70
Figure 29: Ultrasound delivered Intensity and Pressure correlation during Sonochemical Experimental Runs..... 71
Figure 30: Ultrasound Delivered Intensity and Amplitude Pressure correlation during Sonochemical Experimental Runs..... 72

Figure 31: Ultrasound power input during 40 minutes kinetic run at optimum conditions 78
Figure 32: Energy Flow of Sonochemical Reactor System with Cooling 79
Figure 33: 40 min Kinetic Run Power Input at optimum conditions 79
Figure 34: Hydrogen zero order Kinetics at optimum conditions 82
Figure 35: Carbon Monoxide zero order Kinetics at optimum conditions 83
Figure 36: Carbon Monoxide 1st Order Kinetics at optimum conditions 84
Figure 37: Carbon Monoxide 2nd Order Kinetics at optimum conditions 85
Figure 38: Results from Control Experiments using distilled water, previously sampled sludge as well as new sludge at optimum conditions 86
Figure 39: Higher Heating Value of untreated sludge and treated sludge at optimum conditions 88
Figure 40: Constant Variance H_2 Model using data points obtained during Ultrasonic Experiments .. 92
Figure 41: Independent Errors for H_2 Model using data points obtained during Ultrasonic Experiments 92
Figure 42: Normal Probability Plot for H_2 Model obtained during Ultrasonic Experiments 93
Figure 43: Constant Variance CO Model using data points obtained during Ultrasonic Experiments . 94
Figure 44: Independent Errors for CO Model using data obtained during Ultrasonic Experiments 95
Figure 45: Normal Probability Plot for CO Model using data points obtained during Ultrasonic Experiments 95
Figure 46: Comparison of predicted and actual values for H_2 Model 96
Figure 47: Contour plot of maximum values for H_2 production obtained by response surface methodology 98
Figure 48: 3D Plots of maximum values for H_2 production obtained by response surface methodology 99
Figure 49: Ultrasonic Probe tip damage after experiments were conducted 100
Figure 50: Ultrasonic Syngas Production Process Integration into GTL stream 101

LIST OF TABLES

Table 1: Estimates of GTL Contribution to overall liquid fuel generation (Adbel-Kreem, Bassyouni, Abdel-Hamid, & Abdel-Aal, 2009) 3
Table 2: Annual Sewage Sludge Production by Country (Lux Research Inc, 2009) 7
Table 3: Heats of Reaction @ 298 K (Probstein and Hicks, 1982) 10
Table 4: Coded CCD Design Matrix 20
Table 5: Sludge Properties 34
Table 6: Experimental and Calculated HHV 35
Table 7: Gas standard Composition 52
Table 8: Factor Ranges for Screening Experiments 54
Table 9: Factor Settings 56
Table 10: Experimental Design 57
Table 11: Gas Composition Errors and Standard Deviations 70
Table 12: Summary of results 73
Table 13: Mass Balance – 40 minute kinetic run as basis 77
Table 14: Energy Removed by Cooling Water 80
Table 15: Internal Energy Calculation 80
Table 16: Adequacy of H_2 Model 93
Table 17: Adequacy of CO Model 96
Table 18: Comparison of actual data with RSM and Solver results 98
Table 19: Comparison of optimum responses 99
Table 20: Effect of Design Changes to Equipment 102

NOMENCLATURE

$D = desirability\ function$

$H_A(T) = Henry's\ constant\ for\ component\ A$

$K = Polytropic\ Index\ for\ gas\ mixture$

$k = reaction\ rate\ constant$

$n = amount\ of\ factors$

$P = System\ Pressure$

$p_A = Partial\ Pressure\ of\ component\ A$

$P_c = critical\ pressure$

$P_h = Hydrostatic\ Pressure$

$P_m = Pressure\ in\ liquid\ at\ moment\ of\ transient\ collapse$

$P_{max} = maximum\ Pressure\ at\ moment\ of\ total\ collapse$

$P_R = reduced\ pressure$

$P_v = vapour\ pressure\ inside\ bubble$

$$Q = \frac{Resonance\ amplitude}{Static\ Amplitude\ of\ Vibration}$$

$r_A = reaction\ rate$

$T_0 = Initial\ Temperature$

$T_c = critical\ temperature$

$T_{max} = maximum\ Temperature\ at\ moment\ of\ total\ collapse$

$T_R = reduced\ temperature$

$x_A = Liquid\ fraction\ of\ component\ A$

$X_i = Independent\ Conditions$

$X_j = Independent\ Conditions$

$y_A = Vapour\ Fraction\ of\ component\ A$

$Y_i = Response\ Variable$

$z = compressibility\ factor\ to\ account\ for\ non - ideality$

$\beta_0 = Intercept\ value\ of\ regression\ coefficient$

$\beta_i = Linear\ regression\ Coefficient$

$\beta_{ij} = Interaction\ regression\ Coefficient$

$\varepsilon_i = Experimental\ Errors$

$\gamma = gas\ specific\ heat\ ratio$

$\propto = rotatability\ requirement$

SECTION I - THE LITERATURE REVIEW

1. INTRODUCTION

Bacterial sludge is produced daily at a rate of 60 grams per person on average (Lux Research Inc, 2009) and the accumulation of this hazardous by-product has become of increasing concern internationally. The produced bacterial sludge is frequently pumped into dams, dried out and used as agricultural fertilizer. As these sludge dams are not always well maintained, the contamination of any near-by area is of grave concern. Heavy metals, which are also found in this sludge, end up in the water table when used as agricultural fertilizer. As a result, government regulations now apply and this sludge may no longer be spread out on soil. It is therefore very important that an environmentally friendly, alternative means of disposal is found that could potentially be profitable. This bacterial sludge is expected to have a relatively high heating value and, as such, there is the potential to produce energy from the biomass.

It was found by Beyers (2011) in a proof of concept study that it is possible to partial oxidise bacterial sludge in a sonochemical reactor, but very limited amounts of hydrogen, methane and carbon monoxide were produced. A significant amount of carbon dioxide was an undesired by-product of this experimental work.

As such, an improved sonochemical reactor is being studied to investigate if reactor design improvements could result in more significant syngas yields and a reduction in the production of carbon dioxide. It, therefore, needs to be established if the production of syngas from bacterial sludge using ultrasound can be optimized. The yield of syngas produced using ultrasonic cavitation needs to be established to determine if the ultrasonic cavitational process can be compared to a conventional steam gasification process.

A mathematical model that describes the hydrogen yield in the product gas is to be developed and tested at maximum yield conditions. This model can then be used to predict the process output of syngas when varying process conditions. It is also required to study a range of varying sludge compositions to see how the process would react to upstream plant changes.

If the study produces feasible yields, a thus-far wasted energy source, which is produced on a global scale, will be utilized for fuel production and could, therefore, be used to supplement the world's

GTL plants to increase their liquid fuel output whilst regulating their consumption of natural gas resources. An alternative technology that could potentially utilize the technology of sonochemical partial oxidation of bacterial sludge is hydrogen energy fuel cells. Hydrogen fuel cells use proton exchange membranes to utilize hydrogen energy. The construction materials currently used in the gasification/reforming side of hydrogen fuel cells where the hydrocarbons are converted to hydrogen, carbon monoxide and carbon dioxide, presents a significant contribution to the overall cost of fuel cell technology. The utilization of ultrasound could potentially provide the hydrogen fuel cell industry with a bulk atmospheric solution to partial oxidation that would result in refractory materials not being required for construction.

The aim of this project is, therefore, to optimize the partial oxidation of bacterial sludge utilizing sonochemistry and to determine if the partial oxidation of bacterial sludge using ultrasound is a competitive alternative to the conventional steam gasification process. This will entail redesigning of the reactor, the optimization of the reactor conditions using a central composite design to determine a quadratic model to apply response surface methodology to optimize the process. The desirability approach will be used to optimize both the production of hydrogen and carbon monoxide simultaneously. This data will then be used to determine if the process is commercially feasible as an alternative to the conventional methods of sludge disposal and syngas production.

2. LITERATURE REVIEW

2.1 The role of the GTL industry in liquid fuels production

With an increased focus on the reduction of greenhouse gas emissions as well as the world's declining crude oil reserve, many of the major oil companies are shifting their focus to producing liquid fuels from Natural Gas, rather than from crude oil. With the world's total crude oil consumption in 2010 at 90 mil bbl/day (Administration, 2010) and the total equivalent fuels produced using the Gas-To-Liquids (GTL) process was 523 000 bbl/day (Adbel-Kreem, Bassyouni, Abdel-Hamid, & Abdel-Aal, 2009), GTL fuels contributed 0.5 % of the world's fuel requirements. The contributions of individual companies are seen in Table 1. The Pearl GTL plant in Qatar produces 140 000 bbl/day (Shell, 2011) and Sasol Iran at 110 000 bbl/day (Adbel-Kreem, Bassyouni, Abdel-Hamid, & Abdel-Aal, 2009).

Table 1: Estimates of GTL Contribution to overall liquid fuel generation (Adbel-Kreem, Bassyouni, Abdel-Hamid, & Abdel-Aal, 2009)

Name of Company	Location	Capacity (bbl/day)
Shell - Pearl	Qatar	120000
Sasol	Iran	110000
Shell	Iran	75000
Shell-OPC	Qatar	75000
ANGTL	USA	50000
Syntroleum	Peru	40000
Exxon Mobil	Qatar	34000
Sasol-OPC	Qatar	34000
NNPC	Nigeria	30400
PetroSA	South Africa	30000
Sasol	South Africa	17000
POVSA	Venezuela	15000
Shell	Malaysia	12500
Conoco (demonstration)	USA	400
BP (demonstration)	USA	300
Exxon Mobil (demonstration)	USA	200
JOGMEC (pilot)	Japan	7

The competitiveness of the GTL process is influenced mainly by the cost of the capital investment, the operating cost of the plant, the cost of the feedstock and the anticipated production rates (Adbel-Kreem, Bassyouni, Abdel-Hamid, & Abdel-Aal, 2009). The GTL production process from natural gas consists of a natural gas retrieval step, followed by syngas production from the natural gas, the Fischer-Tropsch conversion of CO/H_2 (syngas) to hydrocarbons and then, finally, the upgrading and hydro-processing to high purity liquid fuel products. Syngas is industrially produced from natural gas using steam reforming, catalytic partial oxidation, auto-thermal reforming or combined (two-step) reforming (Adbel-Kreem, Bassyouni, Abdel-Hamid, & Abdel-Aal, 2009). The steam reforming of natural gas uses methane and water to produce carbon monoxide, carbon dioxide and hydrogen. The GTL production process from coal requires the same downstream treatment process as when utilizing natural gas, but originates from coal mining operations, followed by the gasification of coal to produce syngas and is followed by the Fischer-Tropsch conversion of the syngas into hydrocarbons.

2.2 The production of syngas from biomass

With the world's natural gas resources diminishing, alternative feedstock for the production of syngas is widely being investigated (Li, Song, Ma, & Zhao, 2012). It was found by Li et al. (2010) that the cost of syngas production from biomass using steam gasification amounted to R 1.48/Nm^3 with the syngas yield at 0.67 Nm^3/kg. It was also reported by Li et al. (2010) that carbon dioxide and methane form a part of the product gas composition with a H_2/CO ratio of 2.3. An increase in the reaction temperature during steam gasification favours the production of hydrogen (Lucchesi & Stoppato, 1994). A process that yields more carbon monoxide than hydrogen can possibly be used to supplement traditional steam reforming that produces more than the desired ratio of hydrogen. A combination of the product streams from syngas production from biomass and steam reforming could be mixed to obtain a ratio closer to the desired Fischer-Tropsch ratio of hydrogen to carbon monoxide.

2.3 The production of syngas from bacterial sludge

Bacterial waste is generated widely in water treatment systems. This applies to commercial, domestic and industrial waste water treatment systems. The bacterial waste sludge can be generated by two different methods. Firstly, a waste water stream undergoes screening and is then passed to large settling tanks where solids will sink to the bottom of the tanks (Lux Research Inc, 2009). The solids are collected from the bottom of the tank and then become known as sewage sludge (Lux Research Inc, 2009).

The second alternative is when waste water undergoes anaerobic digestion. During anaerobic digestion, bacteria are used to consume organic matter in the water. The bacterial population grows exponentially and eventually reaches a point where the bacterial population growth starts to stabilize as not enough nutrients are available for the population to continue growing. At this point the bacteria would also stop consuming biodegradable matter in the water as respiration products start to poison the system. To avoid this situation and continuously have an active anaerobic digestive system, some of the bacteria are removed from the system on a continuous basis; therefore avoiding bacterial over-population. This system is referred to as an activated sludge system and can be seen in Figure 1.

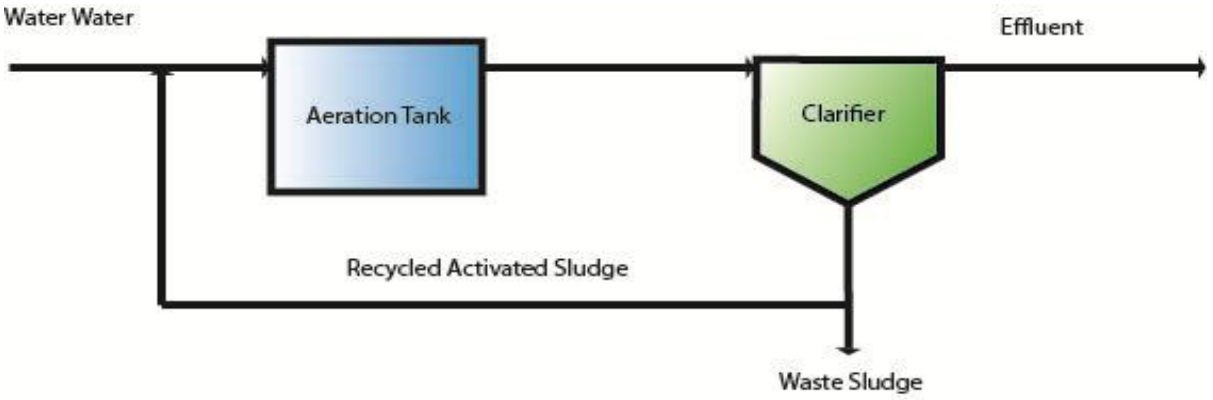

Redrawn from LennTech Water Treatment Solutions, Schematic Diagram of Activated Sludge Process

Figure 1: Schematic of Activated Sludge process (LennTech Water Treatment Solutions, 2003)

It was found that the amount of sludge produced annually is based on a country's wealth (Lux Research Inc, 2009). For high income countries the amount of sludge per person per day can be up to 250 grams. For developing countries this amount is a mere 6 grams per person per day (Lux Research Inc, 2009). As seen in Table 2, countries where complete treatment (zero discharge to rivers, lakes or sea, is allowed) the sewage sludge production rate per person is significantly higher as seen in the table below for the Netherlands, Finland, Germany, Hungary, Japan and the US (Lux Research Inc, 2009). For developing, poor countries, a large part of the population has no access to water treatment facilities and they therefore do not produce sewage sludge. As populations continue to grow, the amount of sludge produced will increase, but with economies becoming wealthier, more sludge will be produced per capita (Lux Research Inc, 2009).

In South Africa, with a population estimated at 50 million people, using an average of 60 grams of sewage sludge produced per person per day (Lux Research Inc, 2009), the total amounts to

3000 tons of sewage sludge per day. Currently this sludge is being placed into landfill sites, incinerated, piled in storage dams or dried and spread out on agricultural soil at an average cost of R 400/ dry ton (Boyd, Deacon, & van Niekerk, 2009). Using these averages, the total annual cost of sewage sludge disposal is estimated to be R 450 million per year. This total refers to the cost of disposing of sewage sludge and not utilizing the energy that is potentially available in this carbon rich source. The utilization of this sludge to potentially unlock a source of energy that could support the production of liquid fuels could potentially be feasible if only marginally less expensive as an environmental threat is also eliminated. If syngas is produced from this sewage sludge, natural gas and coal resources could be spared, reducing the carbon footprint of the organizations involved as their utilization of fossil fuels are reduced, whilst eliminating an environmental threat.

Table 2: Annual Sewage Sludge Production by Country (Lux Research Inc, 2009)

Country	Income Level	Population (2009)	Sewage Sludge Production rate (grams per person per day)
Netherlands	High Income	16,491,000	249.20
Denmark	High Income	5,500,510	99.60
Finland	High Income	5,231,000	78.60
Slovenia	High Income	2,010,000	77.70
Spain	High Income	40,525,002	72.30
United Kingdom	High Income	60,609,000	67.80
Germany	High Income	82,422,000	66.50
Austria	High Income	8,210,281	65.40
Portugal	High Income	10,606,000	61.10
United States	High Income	298,444,000	59.80
Russia	Middle Income	140,702,096	58.40
Czech Republic	High Income	10,235,000	53.50
Norway	High Income	4,611,000	51.40
Italy	High Income	58,134,000	47.10
Australia	High Income	21,007,310	47.00
Canada	High Income	33,100,000	45.50
Japan	High Income	127,464,000	43.00
France	High Income	64,057,792	37.60
Belgium	High Income	10,414,336	29.70
Slovakia	High Income	5,439,000	27.70
Turkey	Middle Income	70,414,000	22.60
Jordan	Middle Income	3,400,000	11.30
China	Middle Income	1,313,974,000	6.20
Brazil	Middle Income	188,078,000	5.40
Egypt	Low Income	78, 323, 000	3.06

2.4 The difference between biomass gasification and partial oxidation

2.4.1 Gasification:

Commercial gasification technologies were compared by Ciferno and Marano (2002) by compiling data from over 40 separate sources. This research compared information regarding different

feedstock compositions, operating conditions, gasification setup design, product syngas composition, undesired emissions, capital costs involved as well as the cost of any supporting equipment. At temperature between 1200 °C and 1300 °C, very little methane is expected to be produced during biomass gasification (Ciferno & Marano, 2002). A reduced amount of methane would lead to an increase in the amount of carbon monoxide and hydrogen produced (Reed & Siddhartha, 2001). The ratio of H_2/CO in the product gas required for downstream processing could be adjusted by looking at the ratios of air, oxygen and steam that were being fed to the gasifier (Ciferno & Marano, 2002).

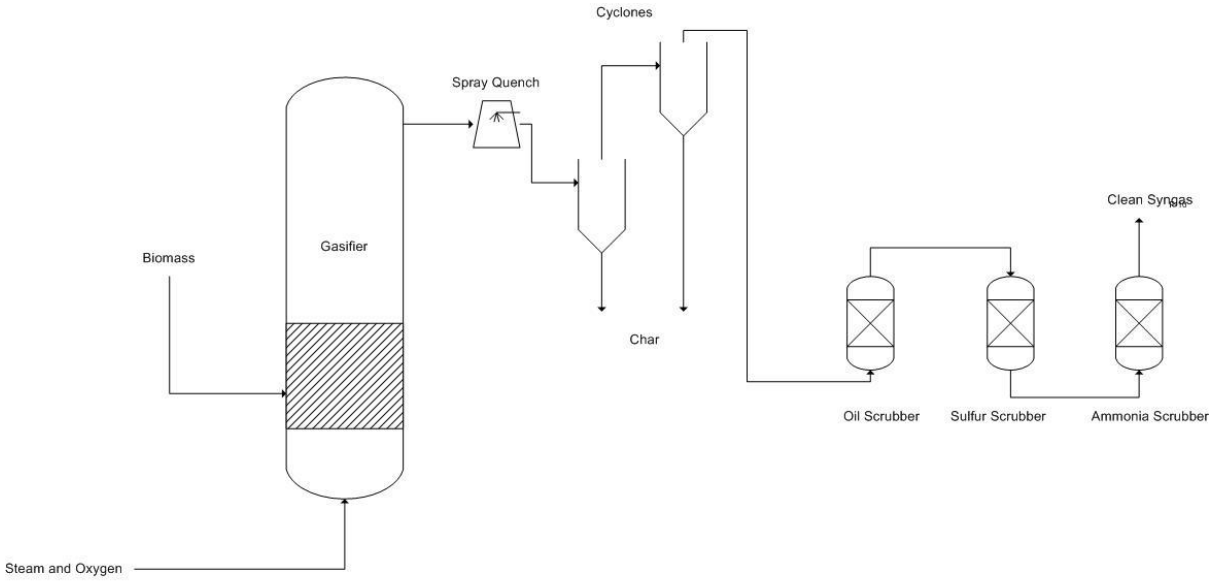

Redrawn from A Biomass to Biofuel Watershed Event, New Energy and Fuel.com

Figure 2: Schematic of normal Biomass Gasification (Fuel.com, 2008)

The research conducted by Ciferno and Marano (2002) concluded that the optimum gasification temperature range is between 500 °C and 1400 °C, with pressure ranging from atmospheric to 33 bar. Air, pure oxygen, steam and a combination of these were investigated as oxidants. It was found that using air, not pure oxygen, resulted in a product gas with an overall lower heating value (Ciferno & Marano, 2002). The gas product contained carbon monoxide, carbon dioxide, hydrogen, methane, nitrogen and water vapour. It was also found that using pure oxygen and steam as feed, the product gas would have a higher ultimate heating value in the range of 10 MJ/m^3 to 20 MJ/m^3 and a high concentration of hydrogen and carbon monoxide (Mann, 1995). When using pure oxygen instead of air, the product gas mixture is expected to consist of carbon monoxide, carbon dioxide, hydrogen and methane (Ciferno & Marano, 2002). To use pure oxygen as a reactant, an air separation unit would be required to separate nitrogen and air. Due to the expense of such a plant

and the associated energy consumption, very few applications actually use pure oxygen in their applications (Ciferno & Marano, 2002).

2.4.2 Partial Oxidation:

The difference between partial oxidation and gasification is that less than the required stoichiometric amount of oxygen is added to the system to promote the production of carbon monoxide rather than carbon dioxide (Gautam, Adhikari, & Bhavnani, 2012). When using syngas as a feed for the Fischer-Tropsch process to produce liquid fuels, a high concentration of hydrogen and carbon dioxide would be required with a H_2/CO ratio of less than or equal to 2 (Marda, 2009). During partial oxidation, steam is consumed in the endothermic Steam-Carbon reaction (Marda, 2009). Please refer to reaction 2 in Table 3 where it can be seen that an increase in the amount of steam added would increase the amount of hydrogen and carbon monoxide in the product gas. On the other hand, the addition of more steam would also promote reaction 9, the water-gas shift reaction. This would result in more carbon dioxide and hydrogen in the product but as the reaction is exothermic, it would provide energy for the endothermic Boudard reaction (Reaction 1 in Table 3) to take place (Rennard, 2010).

When considering the heats of reaction as stipulated in Table 3, the predicted effect of temperature could be determined. To calculate the heat of reaction for biomass samples with varying compositions, equilibrium modelling was used (Gautam, Adhikari, & Bhavnani, 2012).

2.5 Partial Oxidation Reactions

The reactions stipulated in Table 3 are expected to take place at temperatures above 1000 °C. The enthalpy for each reaction is reported at 25 °C based on the literature reported (Probstein & Hicks, 1982).

Table 3: Heats of Reaction @ 298 K (Probstein and Hicks, 1982)

Type of Reaction	Rxn Number	Reaction	Literature Enthaply (kJ/mol) @25 °C	Description
Carbon	Rxn 1	$C + CO_2 \leftrightarrow 2CO$	172	Boudouard
	Rxn 2	$C + H_2O \leftrightarrow CO + H_2$	131	water-gas or steam
	Rxn 3	$C + 2H_2 \leftrightarrow CH_4$	-74.8	Hydro -gasification
	Rxn 4	$C + 0.5\ O_2 \rightarrow CO$	-111	
Oxidation	Rxn 5	$C + O_2 \rightarrow CO_2$	-394	
	Rxn 6	$CO + 0.5O_2 \rightarrow CO_2$	-284	
	Rxn 7	$CH_4 + 2O_2 \leftrightarrow CO_2 + 2H_2O$	-803	
	Rxn 8	$H_2 + 0.5\ O_2 \rightarrow H_2O$	-242	
Shift	Rxn 9	$CO + H_2O \leftrightarrow CO_2 + H_2$	-41.2	
Methanation	Rxn 10	$2CO + 2H_2 \rightarrow CH_4 + CO_2$	-247	
	Rxn 11	$CO + 3H_2 \leftrightarrow CH_4 + H_2O$	-206	
	Rxn 14	$CO_2 + 4H_2 \rightarrow CH_4 + 2H_2O$	-165	
Steam Reforming	Rxn 12	$CH_4 + H_2O \leftrightarrow CO + 3H_2$	206	
	Rxn 13	$CH_4 + 0.5\ O_2 \rightarrow CO + 2H_2$	-36	

The endothermic reactions (1, 2 & 12) are supported by the other, exothermic, reactions as seen in Table 3. Gautam et al. (2012) explain that an increase in temperature would minimize the production of methane and carbon dioxide. As a result, it is expected that at temperatures between 1200 and 1800 °C, the amount of carbon dioxide and methane in the product gas is expected to be negligible (Mabizela, Meyer, & Mamphweli, 2006). This experimental work did not take the addition of steam into account and the addition of steam would promote reaction 2 in Table 3 which would increase the amount of carbon monoxide and hydrogen in the product gas (Zhu, 2010).

2.6 Sonolysis of water using Ultrasound

Sonolysis is the process during which water molecules are split into hydrogen and hydrogen peroxide. The effect of sonolysis is produced when mechanical waves sets cavitation into motion (Colussi, Weavers, & Hoffmann, 1998). It is said that sonolysis of water can be described by the following reactions (Miller, 1950):

1. $H_2O \rightarrow H\cdot + OH\cdot$
2. $H\cdot + H\cdot \rightarrow H_2$
3. $OH\cdot + OH\cdot \rightarrow H_2O_2$
4. $H_2O_2 \rightarrow H_2O + \frac{1}{2}O_2$
5. $H\cdot + OH\cdot \rightarrow H_2O$

The hydrogen peroxide, hydrogen and oxygen products are produced during the dimerization of their radicals as seen in Reaction 2 and Reaction 3 above (Miller, 1950). Another suggested reaction mechanism is described by Mason et al. (1988):

6. $H_2O \rightarrow H\cdot + OH\cdot$
7. $H\cdot + O_2 \rightarrow HO_2\cdot$
8. $HO_2\cdot + HO_2\cdot \rightarrow H_2O_2 + O_2$
9. $OH\cdot + OH\cdot \rightarrow H_2O_2$

2.7 Thermal Decomposition of Lime

When calcium oxide (lime) is mixed with water, calcium hydroxide is formed. When exposed to extreme temperatures, thermal decomposition of lime occurs in an aqueous medium (RSCI, 2008). Calcium hydroxide would form calcium oxide and carbon dioxide during ultrasonic cavitation as extreme temperatures are experienced (RSCI, 2008). Carbon dioxide is said to dissociate into carbon monoxide and oxygen when carbon dioxide is dissolved in water. According to Chendke and Fogler (1974), the thermal dissociation of carbon dioxide occurs during cavitation that results in carbon monoxide and oxygen. Therefore, as a result of the decomposition of the lime into carbon dioxide, it is possible to produce carbon monoxide during cavitation without partial oxidation occurring.

2.8 Sonochemical Reactor

To represent the conditions on a local scale at which gasification conditions are present, a sonochemical reactor was investigated. It was established in previous work (Suslick, Mdleleni, & Reis, 1997) that it is possible to experience extreme localized conditions using a sonochemical reactor to provide the required energy for partial oxidation to occur. It is expected that the use of a sonochemical system would be more efficient on a laboratory scale than when using it on an industrial scale as adequate information regarding the scale-up of such systems are still unavailable (Gogate & Pandit, 2003; Adewuyi, 2001). The oxidation of waste water at ambient conditions was investigated by Gogate and Pandit (2003) and it was found that ultrasonic cavitation could prove to be a viable solution for wastewater treatment in a laboratory scale. Under atmospheric conditions, the expense of exotic materials of construction, due to the application's high temperature and exothermic nature (Shah, 1999), could be avoided.

Cavitation can be described as the formation, the sequential growth and implosive collapse of cavities that occur in infinitesimal time intervals (Lorimer, 1987 ; Mason and Lorimer 1988; Suslick, 1990; Shah et al., 1999). The amount of cavities in the reactor at a given time is described by Naidu et al. (1994) using theoretical modelling of bubble dynamic equations. The content of the cavitation bubble is heated and the extremely high local temperatures and pressures, could serve as a driving force for chemical reactions that require extreme reaction conditions (Suslick, Mdleleni, & Reis, 1997). The rapid cooling rate to which these localized hotspots are exposed to, means that the bulk fluid is at atmospheric conditions.

The cavitation events occur in confined areas that could provide reactions conditions as a result of the “hot spots” generated. The production of highly reactive free radicals as well as the improved mass transfer rates due to the increase in the degree of turbulence as a result of the acoustic cavitation would aid in the development of the expected reaction conditions (Gogate & Pandit, 2003). It was also mentioned that the sonochemical reactor’s operating conditions influences the degree of cavitation intensity (Gogate & Pandit, 2003).

Cavitation results in the collapse of the bubbles, which supplies intense localized heating and high pressures with a very short life span (Suslick, Mdleleni, & Reis, 1997). In combination with the extreme cooling rates estimated to be in the region of 10^{10}K/s, a unique chemical and physical environment is generated in a liquid that is a bulk atmospheric conditions (Naidu, 1994).It was also found by Suslick et al. (1990) that the path of the chemical reaction is determined by the properties of the energy source. Sonochemical reactors also provide an improved application for solid-liquid systems as it plays a major role in increasing the reactivity of the system by enabling near perfect mixing conditions. The surface morphology of a particular particle can be dramatically be changed by the inter-particle collisions as a result of ultrasound application, increasing the reactivity of the system (Suslick and Doktycz, 1990).

2.8.1 The sonochemical reactivity two-site model

It has been found by kinetic studies that there are two reaction sites in a sonochemical system (Suslick, Schubert, & Goodale, 1981)and that the first, dominant reaction site is the bubble’s interior gas-phase. The second phase is a primarily liquid phase where a liquid surrounding a collapsing bubble is heated. The initial site’s effective temperature was estimated to be 5200 K and that of the secondary site to be around 1900 K (Suslick, Mdleleni, & Reis, 1997) and can be seen in Figure 3.

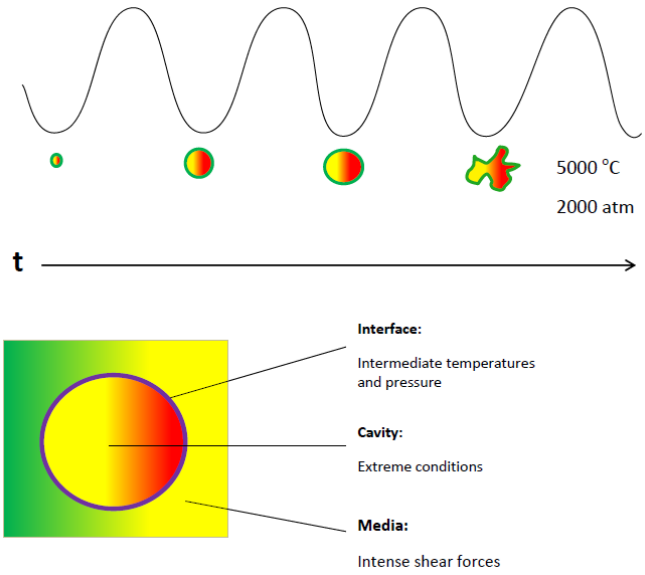

Figure 3: Cavitational growth and collapse of bubble (Timothy J. Mason, Dietmar Peters, 2003)

Cavitation in the liquid phase can be described as an instant during which mechanical stimulation is the cause for the destruction of attractive forces between molecules (Peters, 2003). In an ultrasonic application, the liquid is compressed and then followed by expansion. In this sudden pressure drop, a small, oscillating bubble of gaseous substance is formed (Beyers, 2011). These bubbles will expand and with each cycle of applied ultrasound, they will grow until they reach an unstable size. At this point they either crash or collapse violently (Mason et al. 2003).

2.8.2 Sonochemical reactor considerations

It has been found by Horst et al. (1996) that when reactions have long induction times , slow reaction rates and extreme exothermic behaviour, sonochemical reaction conditions could provide a plausible alternative. The reactor consisted of a cooling jacket around the reactor and the gases leave the system through a pressurized valve. They investigated a 70 W sonotrode as well as a 200 W sonotrode to determine the effects on the reactions. The sonotrodes were both used at an intensity of 25 W/m^2 and it was found by Horst et al. (1996) that the lowest power sonotrode behaviour was unstable. It was also found that an increase in static pressure would result in the bubble being smaller and therefore they would collide more violently (Horst, Chen, Kunz, & Hoffman, 1996). The reaction rates were accelerated as a result of an increased amount of destruction to the solid surface.

A cylindrical sonochemical reactor was studied by Asakura et al. (2005) and it was found that the key factor to control was the acoustic field. The acoustic field is influenced by the frequency setting, the intensity of the probe, the reactor shape, -size, -configuration as well as the physical properties of the fluids involved (Asakura, Maebayashi, & Koda, 2005). These physical properties include viscosity, vapour pressure, surface tension, and temperature and dissolved gasses (Chivate and Pandit, 1995; Entezari, 1997; Mason and Lorimer, 2002; Gogate et al., 2003). Asakura et al. (2005) looked at the dissociation of water molecules that produces OH radicals which was used to study the sonochemcial activity using the oxidation reaction. Due the the temperature being concentrated in specified zones within the system, it was found that sonochemical efficiency is dependent on the distance from the transducer (Entezari, 1997). The reactor should therefore be a similar length as the transducer probe and different reactor widths could be investigated (Horst et al., 2005).

It was found by Cravotto et al. (2005) that reaction rates and yields are mainly a characteristic of the reactor and transducer configuration. They used a transducer probe that moved upwards and downwards whilst the reactor was made to rotate eccentrically around the transducer probe at a predetermined speed (Cravotto, Omicciolo, & Stevanato, 2005). The transducer temperature was measured by using a thermocouple in various positions and the transducer frequency was adjusted between 15 – 50 kHz and a maximum power intensity of 1000W.

An increase in the reaction temperature can allow for cavitation to be accomplished at a lower acoustic intensity (Mason & Lorimer, 1988). This is as a result of the vapour pressure increase due to the heating of water. According to equation (1) and (2), T_{max} and P_{max} will fall due to a decrease in Pv and Pm. To gain the maximum sonochemical benefit, it is therefore suggested that all experiments should be conducted at as low a temperature as is feasible (Mason & Lorimer, 1988).

It was found by Miller (1950) that reproducible results are influenced by the position of the cavitation event. Ultrasonic waves are reflected on solid surfaces and if an external source of ultrasound is employed the available acoustic power will be a function of the geometry of the reactor. A round bottom flask when using a cup horn was found by Suslick et al. (1984) show complex interference patterns with the sonochemical yield as a function of the reaction vessel height. They also found no interference patterns for a flat bottomed flask, and concluded that a round and flat bottom flask reactor design, regardless of the reactor diameter, has an optimal solution height for maximum sonochemical effects.

It has also been reported that the operation frequency as well as the irradiation intensity (W/m^2) has an effect on the degree to which sonochemical effects are observed. Typical intensity results for low frequency operations, less than 100 kHz, was found to be between 1 and 10 W/m^2 (Mason & Lorimer, 1988). The available equipment, Hielsher UP400S Ultrasonic Processor, has a frequency of 24 kHz. As a result, studies will be focused on low frequency observations.

According to Mason et al. (1988), the use of a submersed probe in a sonochemical reactor is advantageous as high levels of power availability and that probes can me moved to give the optimum performance at different power delivery requirements. The disadvantages of a probe design is that the frequency is fixed, temperature control poses a problem, radical species may be generated at the tip of the probe and tip erosion could occur that would contaminate the sample.

The intensity of the vibrational amplitude of the tip and the intensity of sonication, can be adjusted by altering the power input to the transducer. It was found by Mason et al. (1988) that submersed probe systems are undeniably the most efficient method to transfer ultrasonic energy to a reaction mixture. The design of the ultrasonic horn forms a significant part of the success of sonochemical reaction studies. The piezoelectrical crystal emits a vibrational amplitude that is so small that an increased sonication intensity is only achieved by the direct coupling of the transducer. The horn would serve as an amplifier for the vibration of the transducer (Mason & Lorimer, 1988). The length and shape of the horn is dependent on the wavelength of the ultrasound in the specific material of construction. The wavelength is a function of the material as well as the frequency of the sound wave. Titanium alloys are mostly employed due to their high dynamic fatigue strength, resistance to cavitation erosion, low acoustic losses and chemical inertness. The ultrasonic horn is normally designed in multiples of half wavelengths. A stepped horn will be utilized to facilitate ultrasonic vibrations of around 20 kHz at the tip of the horn. With the step design, there will be no vibration at the midpoint of the cylinder shape as this would be the nodal point of the wave (Mason & Lorimer, 1988).

2.9 Reaction mechanism involving OH radicals

When intense ultrasound caused by ultrasonic cavitation is used to irradiate water, the gas phase bubbles are heated and the water vapour in the bubble is expected to be dissociated into OH radicals (Mason, 1999). When aqueous media and oxygen are exposed to irradiation using acoustic cavitation, Trabelsi et al. (1996) found that $OH\cdot$, $HO_2\cdot$ and $O\cdot$ radicals are formed. Due to the highly reactive nature of radicals formed, an enhancement in the physical mechanisms for the destruction

of hazardous waste is expected. The frequency at which the ultrasound is emitted was found to be a key parameter in the activation mechanism of the system. When a mechanical mechanism is required, a low frequency is said to favour this mechanism. Higher frequency operation is said to favour radical formation that would support chemical mechanisms (Trabelsi, Ratsimba, Wilheml, Delmas, Fabre, & Berlan, 1996).It was found that a reduction in bubble size would significantly improve the efficiency of the sonochemical process and can be influenced by an increase in static pressure of the system as well as the increased frequency of the ultrasound (Entezari et al., 1994).

2.10 Partial Oxidation of bacterial sludge using a sonochemical reactor

As it was found in literature that high temperatures and pressures are experienced on a localized scale during ultrasonic cavitation, it was investigated by Beyers (2011) and found to be an environment that would sustain partial oxidation of bacterial sludge. The collapse of the bubble generated localized hot spots with effective temperatures up to 5000 K and pressure up to 101324kPa (Suslick et al., 1999). It can therefore be assumed that the reaction takes place between the solid biomass, the steam and the oxygen at high temperatures and pressures (Horst et al., 1996). Actual partial oxidation reactions would occur at 1300-1500 K and 3500 kPa absolute (Ciferno & Marano, 2002) and therefore a sonochemical reactor can be used for partial oxidation whilst using construction materials for ambient conditions.

Gautum et al. (2010) found that hydrogen and carbon monoxide concentrations in the product gases where increased at elevated temperatures whilst the formation of methane and carbon dioxide is reduced. This finding is supported by the overall heats of reactions stipulated in Table 3. From the enthalpy values in this table, it is shown that the reactions that produce hydrogen require large amounts of energy that can therefore be provided by the sonochemcial system. This would then produce a maximum yield of hydrogen and carbon monoxide (Piga & Verykios, 2000)due to the extreme conditions experienced on a localized scale.

It was found by Beyers (2011) that for the sludge used, which contained 3.5 mass % volatile matter, and a maximum of 0.05 mole% hydrogen, 0.16 mole% carbon monoxide and 0.22 mole % methane in the gas phase were produced under the predetermined experimental conditions. This work proved that partial oxidation of bacterial sludge under atmospheric conditions is possible using ultrasound. It was therefore concluded that a cavitational reactor system provides the extreme conditions that are required for the partial oxidation of bacterial sludge when exposed to the cavitational reaction zones.

Due to the limited amount of carbonaceous matter in the available sludge at the time, limited amounts of product gas was produced during this process (Beyers, 2011). It was recommended by Beyers (2011) that an increase in the system pressure could possibly increase the reactivity of the process due to a decreased bubble size. It was also recommended that a cooling water bath is used to regulate the reactor contents to 0°C to ensure all possible energy is available for cavitation and that energy is not wasted on heating the bulk fluid. Beyers (2011) also found that it would be necessary to introduce a liquid trap to the system to protect gas analysis equipment from possible moisture break through. The possibility of using other abundantly available feedstock can be investigated if an increase amount of volatile matter is present.

2.11 Effect of Pressure on Sonochemistry

An increase in applied external pressure (P_h) would result in an increase in the intensity of the bubble collapse as well as the cavitation threshold (Mason & Lorimer, 1988). The pressure in the bubble at the moment of collapse is approximately $P_h + P_a$. An increase in the value of P_h would lead to a more rapid and violent collapse (Mason & Lorimer, 1988), when looking at equation (3).

The maximum expected temperature and pressure in a bubble under adiabatic conditions can be calculated using equations (1) and (2). According to equations (1), (2) and (3), utilizing gases with a large ɣ-value, like monoatomic Argon (ɣ=1.666), would provide for larger sonochemical effects from gas-filled bubbles. For this reason, monoatomic gases are used in preference to diatomic gases like nitrogen, air and oxygen (Mason & Lorimer, 1988).

$$T_{max} = T_0 \left\{ \frac{P_m (K-1)}{P} \right\} \qquad eq\ (1)$$

$$P_{max} = P \left\{ \frac{P_m (K-1)}{P} \right\}^{K/(K-1)} \qquad eq\ (2)$$

$$\frac{T_0}{T_{max}} = \left\{ 1 + Q \left[\left(\frac{P_h}{P_m} \right)^{1/3\gamma} - 1 \right] - 1 \right\}^{3(\gamma-1)} \qquad eq\ (3)$$

3. THEORETICAL FRAMEWORK

3.1 Response Surface Methodology - Rotatable CCD

Screening experiments were conducted to establish the settings for the factors used in the central composite design. These screening experiments included testing different reaction times and different amplitudes of operation whilst using mid-range pressures to determine the extreme upper- and lower-bound level settings. Based on the results from these experiments, the factors were selected for the central composite design.

A rotatable central composite design (CCD) tests five levels for each factor: -1, 0, -1, -α, α. The central composite design also provides information with regards to the linear and two-factor interaction effects as well as estimating the curvature effects. An included benefit of using a CCD is that it provides information on the overall experimental error and on experiment variable effects in a minimum number of required experiments (Montgomery, 1997).

Rotatability was used in a CCD to investigate all points at a given distance from the centre point in all directions as it was uncertain where the location of the optimum point will occur within a given region (Montgomery, 1997). Rotatability also has the effect that all points in any direction will have the same magnitude of prediction error (Montgomery, 1997). Due to the fact that the rotatable design added two extra levels of testing (-α, α), the increased amount of tests required provided an enhanced possibility for sources of experimental error that is associated with the operation and the setup (Montgomery, 1997).

To explain how the coded values were established for the CCD, the schematic of the un-coded level settings can be seen in Figure 4. The two circles represent a sphere in three dimensional space with the vertical axis representing time.

For a system to satisfy the Rotatability requirement, the prediction variance can only be dependent on the distance from the origin, in any direction (Montgomery, 1997) regardless of the orientation to the coordinate axis. The Rotatability requirement is described by:

$$\alpha = 2^{\frac{n}{4}} \qquad eq\ (4)$$

For the study at hand, n=3 (pressure, time and amplitude %) and resulted in α=1.681792831.

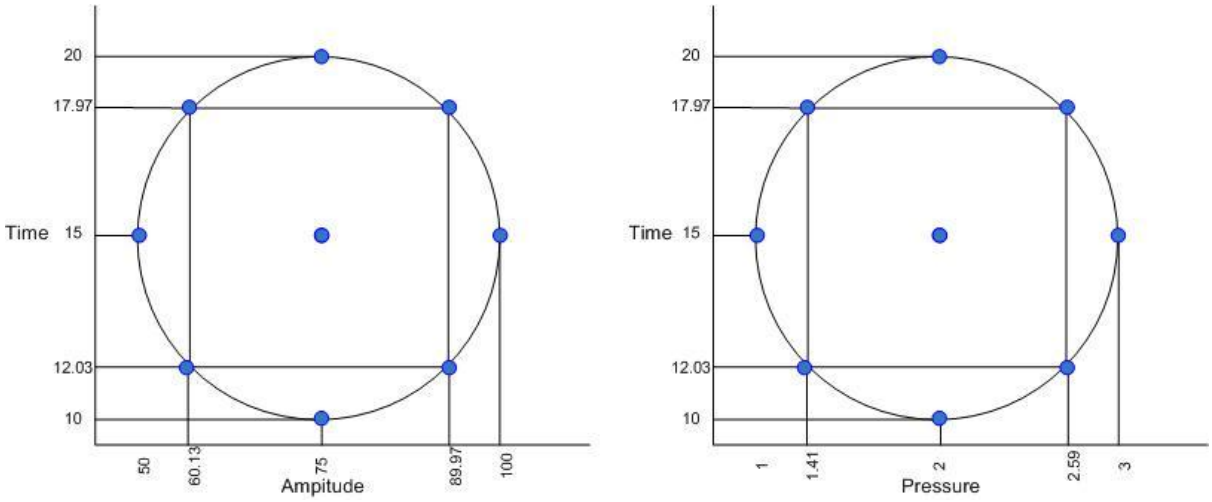

Figure 4: Schematic of Central Composite Design parameter settings

These level settings were tested incorporating repeatability for all points. The run order was also randomized to ensure that repeatability was maximized by excluding the possibility of a manually repeated experimental error and to eliminate the residual effects on treatments (Montgomery, 1997). The run order can be seen in Table 4.

The quadratic design with interaction was used and is accounted for in the last seven columns in Table 4.

Table 4: Coded CCD Design Matrix

Exp Num	x1	x2	x3	x1sq	x2sq	x3sq	x12	x13	x23	x123
11	-1	1	1	1	1	1	-1	-1	1	-1
2	1	-1	1	1	1	1	-1	1	-1	-1
27	-1.68179	0	0	2.828427	0	0	0	0	0	0
32	-1	1	1	1	1	1	-1	-1	1	-1
21	1	1	1	1	1	1	1	1	1	1
19	1	1	1	1	1	1	1	1	1	1
3	-1	1	-1	1	1	1	-1	1	-1	1
6	1	-1	1	1	1	1	-1	1	-1	-1
25	0	0	1.681793	0	0	2.828427	0	0	0	0
24	0	0	1.681793	0	0	2.828427	0	0	0	0
26	-1	-1	1	1	1	1	1	-1	-1	1
1	0	1.681793	0	0	2.828427	0	0	0	0	0
28	0	0	0	0	0	0	0	0	0	0
30	-1.68179	0	0	2.828427	0	0	0	0	0	0
33	0	1.681793	0	0	2.828427	0	0	0	0	0
31	1	1	-1	1	1	1	1	-1	-1	-1
29	-1	-1	1	1	1	1	1	-1	-1	1
23	1	1	-1	1	1	1	1	-1	-1	-1
8	0	0	0	0	0	0	0	0	0	0
5	0	0	0	0	0	0	0	0	0	0
22	0	0	-1.68179	0	0	2.828427	0	0	0	0
9	-1	1	-1	1	1	1	-1	1	-1	1
4	-1	-1	-1	1	1	1	1	1	1	-1
10	0	0	0	0	0	0	0	0	0	0
13	0	0	0	0	0	0	0	0	0	0
34	1	-1	-1	1	1	1	-1	-1	1	1
20	0	-1.68179	0	0	2.828427	0	0	0	0	0
16	0	0	-1.68179	0	0	2.828427	0	0	0	0
18	0	-1.68179	0	0	2.828427	0	0	0	0	0
15	-1	-1	-1	1	1	1	1	1	1	-1
7	1	-1	-1	1	1	1	-1	-1	1	1
12	1.681793	0	0	2.828427	0	0	0	0	0	0
14	1.681793	0	0	2.828427	0	0	0	0	0	0
17	0	0	0	0	0	0	0	0	0	0

3.1.1 Regression

To analyse the results obtained by the central composite design, the model under investigation was fitted by using the “Least Squares” method. During the least squares method, a model is optimized by minimizing the sum of squares of all the errors between the experimental and predicted values of the dependent variable (y) for each data point x (Edgar & Himmelblau, 2001). A non-linear model was considered based on the central composite design.

To illustrate, a generalized non-linear model is shown in equation 5.

$$y = f(x_1, x_2, x_3, \ldots\ldots, \beta_1, \beta_2, \beta_3 \ldots\ldots) \qquad eq\ (5)$$

The parameters are defined in the nomenclature of this study. The criterion to be minimized is described by equation 6:

$$\min_{\beta_j} \sum_{i=1}^{n} \left(Y_i - \hat{Y}_i\right)^2 \qquad eq\ (6)$$

3.1.2 Stationary Point

To determine the stationary points for the model determined by using the least squares method, the y-value where all x-values are equal to zero, was seen as the stationary point. To determine this value, each of the factors were partially differentiated with regard to the function y and set equal to zero. Considering the quadratic model determined by this study, the function can be written as:

$$y = \beta_0 + \beta_1 x_1 + \beta_2 x_2 + \beta_3 x_3 + \beta_4 {x_1}^2 + \beta_5 {x_2}^2 + \beta_6 {x_3}^2 + \beta_7 x_1 x_2 + \beta_8 x_1 x_3 + \beta_9 x_1 x_3 + \beta_{10} x_1 x_2 x_3 \qquad eq\ (7)$$

To determine the values for $x_1, x_2\ and\ x_3$ at the stationary point, this function needed to be partially differentiated with respects to each factor and set equal to zero.

$$\frac{\partial y}{\partial x_1} = 0\ to\ obtain\ x_1 \qquad eq\ (8)$$

$$\frac{\partial y}{\partial x_2} = 0\ to\ obtain\ x_2 \qquad eq\ (9)$$

$$\frac{\partial y}{\partial x_3} = 0\ to\ obtain\ x_3 \qquad eq\ (10)$$

These values were then used in equation 7 to obtain the local maximum or minimum value for the function. To determine if the stationary point was referring to a maximum or minimum local point, the raw data needed to be investigated, in conjunction with function optimization.

3.1.3 Generalized Reduced Gradient Method to obtain local maxima

To maximize the function obtained by the least squares method, the generalized reduced gradient method was used to obtain the local maxima. For this study, the generalized reduced gradient method was employed with inequality constraints. The values for the coded factor levels were used to constrain the algorithm utilizing MicroSoft Excel's Solver function. The values for the pressure (x_1),

time (x_2) and amplitude (x_3) were constrained within the region of -1 and 1. The sum of x_1^2, x_2^2 and x_3^2 was constrained to be less than or equal to 2.828427, the $\sqrt{\alpha}$. The maximum for the function was obtained and investigated by comparing the analysis described with a full analysis of the data using Design Expert software.

3.1.4 Desirability Approach

The desirability approach is employed to optimize multiple responses. The desirability approach estimates the conditions of x that will provide the most "desirable" response values for y (Multiple responses: The desirability approach). For each of the responses for the system $Y_i(x_1, x_2, x_3)$ the desirability function assigns a number between 0 and 1 to the possible values of the response $Y_i(x_1, x_2, x_3)$ where $d_i(Y_i) = 1$ represents a ideal response value and $d_i(Y_i) = 0$ a completely unacceptable response value (Rekab & Shaikh, 2005). The geometric mean is then employed to combine the individual desirabilities to provide the overall desirability:

$$D = (d_1(Y_1) \times d_2(Y_2) \times \dots\dots\dots \times d_k(Y_k))^{\frac{1}{k}} \qquad eq\ (11)$$

In this equation, k represents the number of responses.

3.2 Kinetic and Mechanistic Effects of Ultrasound

According to Mason et al. (1988), the expected reactions are a result of cavitation and this leads to either the reaction occurring within the cavitational bubble, where very high temperatures and pressures are experienced, the reaction occurring as a result of secondary possible reactions taking place at the gas-liquid interface of the bubble surface or the reaction possibly occurs as a result of enormous pressures released when the bubble collapses. It is also a possibility that a combination of these could give rise to the reaction enhancement effect experienced under ultrasonic treatment (Mason & Lorimer, 1988).

A mechanistic effect that could potentially have played a role in the sonochemistry, is the degassing of the liquid. It was found by Miller et al. (1950) that when a liquid is irradiated, then saturated with a gas again and irradiated, a non-linear concentration change time curve was observed. It was concluded that this non-linearity was as a result of degassing the solution (Miller, 1950). It is therefore suggested that argon is continuously bubbled through the system whilst studying the effect of using ultrasound. Due to the batch design of the sonochemical reactor in this study, argon

was bubbled through the liquid for 30 minutes prior to commencing an experiment. The system was then sealed under argon pressure to maintain the purge environment.

A radical scavenger can be used to determine the presence of the H· and OH· radicals during the sonolysis of water. It was found by Riesz (1983) that formate, thiocyanate, benzoate, methanol, ethanol 1-propanol, or acetone can be used to identify that H· and OH· radicals were formed during the sonolysis of water at 50 kHz, 23 °C, 600 W/m^2 and under continuous argon bubbling (Riesz, Makino, & Mossoba, 1983). Work was also done to determine the potential positive effect of utilizing monoatomic rather than diatomic gases. A comparison between argon, air and nitrogen achieved greater sonochemical yields. The work therefore indicated that dissolved amounts of gases of low thermal conductivity produced greater sonochemical yields.

Studies were also conducted by (Couppiss & Klinzing, 1974) to establish the effect of frequency on the reaction rate. Lower rate enhancements were observed when utilizing a high frequency apparatus. It was concluded that this is due to the fact that when the frequency is increased, the period of oscillation of the sound wave is decreased. This leads to a reduction in the possible time in which growth can occur to a maximum (Mason & Lorimer, 1988). It was concluded that an optimum exists for a specified volume and temperature at which the reaction rate would be at a maximum. The optimum power density was established to be 17 X 10^4 W m^{-2}kg^{-1} for all volumes at a frequency of 540 kHz and 298 K (Couppiss & Klinzing, 1974).

The design equation for an ideal batch reactor is (Roberts, 2009):

$$r_A = \frac{1}{V}.\frac{dN_A}{dt} = \frac{dC_A}{dt} \qquad eq\ (12)$$

With a simplistic rate equation being the power rate law:

$$-r_A = kC_A^{\propto} \qquad eq\ (13)$$

When assessing experimental data, a plot of the product formation or the change in reactant concentration versus time, would provide information with regard to what order of the integrated rate law would apply to the specific reaction.

For 0 order: $[A] = -kt + [A]_0$ where the rate = k *eq (14)*

For 1st order: $ln[A] = -kt + ln[A]_0$ where the rate = k[A] *eq (15)*

For 2nd Order: $\frac{1}{[A]} = 2kt + \frac{1}{[A]_0}$ where rate = k[A]^2 *eq (16)*

The data was then assessed based on the straight line plot that serves as the best fit to the data. A zero order rate would yield a straight line plot of [A] versus t. A first order rate would yield a straight line plot of ln[A] vs t and a second order rate would yield a straight line plot on 1/[A] versus t.

3.3 Compressibility for gas mixtures

The compressibility factor equation of state for gases is used to determine the degree to which a gaseous species deviates from ideal behaviour (Felder & Rousseau, 2005). For an ideal gas, z=1. The compressibility factor equation of state is:

$$z = \frac{P\hat{V}}{RT} \qquad eq\ (17)$$

where,

$$\hat{V} = \frac{V}{n} \qquad eq\ (18)$$

The law of corresponding states enables the calculation of z for a species at a given temperature and pressure by applying the critical temperature and pressure for that species.

The reduced temperature and pressure is said to be:

$$T_r = \frac{T}{T_c} \text{ and } P_r = \frac{P}{P_c} \qquad eq\ (19)$$

A z-value can then be looked up on generalized compressibility charts according to Felder and Rousseau (2005). The law of corresponding states can therefore states that the values of certain physical properties of a gas depend to a great extent on the proximity of the gas to its idea state (Felder & Rousseau, 2005).

For helium and hydrogen, the critical constants are adjusted according to Newton's corrections (Felder & Rousseau, 2005):

$$T_c^a = T_c + 8\ K \qquad eq\ (20)$$

$$P_c^a = P_c + 8\ atm \qquad eq\ (21)$$

For non-ideal gas mixtures, Kay's rule can be used to estimate the pseudo critical mixture properties as averages of pure component critical constants. The pseudo critical properties can be calculated as follows:

$$T_c' = y_A T_{cA} + y_B T_{cB} + \cdots \qquad eq\ (22)$$

$$P_c' = y_A P_{cA} + y_B P_{cB} + \cdots \qquad eq\ (23)$$

The reduced pseudo critical temperature and pressure can then be calculated using:

$$T_r' = \frac{T}{T_c} \text{ and } P_r' = \frac{P}{P_c} \qquad eq\ (24)$$

The reduced pseudo critical temperature and pressure can then be used on the generalized critical chart in the same manner as for a pure component. This method also enables the calculation of the compressibility of a gas mixture based on the composition, T and P, without knowledge of the total moles in the gas phase (Felder & Rousseau, 2005).

3.4 Solubility of gases in water

For a substance contained in a gas-liquid system in equilibrium at a temperature T and pressure P, Raoult's Law is used to describe the relationship between the fraction of that component in the gas phase and the fraction of that component in the liquid phase:

$$p_A = y_A P = x_A {p_A}^*(T) \qquad eq\ (25)$$

This approximation is valid when the value of x_A is close to 1 – when the liquid is also mostly substance A.

When very dilute solutions of substance A is in question, x_A is close to 0. In this case, Henry's law would apply provided that species A does not react, dissociate or ionize in the liquid phase.

$$p_A = y_A P = x_A H_A(T) \qquad eq(26)$$

Based on the process at hand, the amount of water vapour in the gas phase can be calculated using Raoult's law. This would serve as an indication as to whether the gas samples would be contaminated with water. This is required as the downstream gas analysis equipment could potentially be damaged. Due to the low temperature of the bulk liquid, it was found that no water vapour would be present at the given bulk liquid temperature and pressure.

The system was purged with argon to remove any residual air, but a complete purge was not feasible. The remaining nitrogen content was measured and the corresponding amount of oxygen in the air was calculated using 79% nitrogen and 21 % oxygen in air. It should be noted that the available gas chromatograph could not measure oxygen content. The amount of oxygen dissolved in the water was then calculated using Henry's law. This was required as the presence of excess oxygen would lead to the formation of carbon dioxide instead of the desired carbon monoxide. The amount of nitrogen at the end of the experiment was then used to calculate the amount of oxygen consumed by the reaction and compared with the amount of carbon dioxide formed.

3.5 Estimation of Biomass Synthesis Gas Composition using Equilibrium Modelling

A study conducted by Gautam et al. to establish a comparatively accurate mathematical expression to forecast the syngas composition produced by biomass gasification by conducting the ultimate analysis of the biomass. The following models were taken into consideration: thermodynamic equilibrium, steady-state, kinetics-free, semi-transient and transient. A system is said to be in thermodynamic equilibrium when that system is in chemical, thermodynamic and mechanical equilibrium. It was found that the thermodynamic model provided better results at a higher temperature (Reed, 1985). Even though it is not possible to have a process at perfect equilibrium, it can provide a relatively precise estimate of the expected composition of the syngas. The equilibrium model can therefore be used as a maximum limit on the syngas composition to compare experimental results with (Gautam et al., 2010).

The thermodynamic model derived by Gautam et al. was used to predict the syngas composition for the sludge biomass. This means that there will be discrepancies between the amounts of each component predicted. The addition of steam would result in more hydrogen development than CO formation. As the positive outcome would be a Ribblet ratio of 2, the aim is to conduct the experiments under conditions that would result in more hydrogen than carbon monoxide.
The Gautam et al. model used the following assumptions:

- All of the carbon found in the biomass is converted to product gas and the residence time in the reactor is long enough for the system to reach thermodynamic equilibrium.
- The ash in the feedstock (the non-volatile components) was assumed to be inert with regards to all the gasification reactions.
- All the gaseous products were assumed to behave ideally. This assumption normally holds true at elevated temperatures and low pressures.
- The reaction was auto-thermal and no additional heat source was applied.
- The amount of tar in the syngas is assumed to be negligible.

According to Gautam et al. the total enthalpy balance of the system can be written as follows:

$$\mathrm{H}^{\circ}_{\text{f-biomass}} = \mathrm{LHV} + \sum_{\mathrm{i}=1}^{\mathrm{n}} \mathrm{n_i p_i} \qquad eq\ (27)$$

$$LHV = 4.187\big(81C + 300H - 26(O - S) - 6(9G + m)\big)\frac{kJ}{kg} \qquad eq\ (28)$$

The formulas were derived using multiple regression analysis to obtain the relations. No relation was derived for CH_4 as it was found that under thermodynamic equilibrium the model predicted the methane concentration is <0.15% at a temperature of 800 °C.

$$CO(\%vol) = 0.71C - 1.35h + 0.4O - 22.43 \qquad eq\ (29)$$

$$H_2(\%vol) = 0.223C + 1.022H + 0.332O - 15.36 \qquad eq\ (30)$$

$$CO_2(\%vol) = -0.41C - 0.04O + 31.65 \qquad eq\ (31)$$

The moisture content of the biomass can be taken into account by using the following correlations:

$$C^* = \frac{C}{(1+0.01m_w)} \qquad eq\ (32)$$

$$O^* = \frac{O+0.889m_w}{(1+0.01m_w)} \qquad eq\ (33)$$

$$H^* = \frac{H+0.111m_w}{(1+0.01m_w)} \qquad eq\ (34)$$

These values were only used to form an estimate of the expected outcomes of the experiment and to perform a comparison between the predicted gasification results and the actual partial oxidation results.

4. PROBLEM STATEMENT

It was found by Beyers (2011) that it is possible to produce hydrogen and carbon monoxide using ultrasound to partially oxidise bacterial waste water sludge. No steam was added to the process and it was assumed that the aqueous sludge mixture would provide sufficient steam in the cavity of the gas bubble where the reaction would take place. During this study, limited amounts of hydrogen and carbon monoxide was produced and large quantities of carbon dioxide were produced.

It needs to be established if the production of syngas from bacterial sludge using ultrasound can be optimized to improve the hydrogen and carbon monoxide yield. The amount of carbon dioxide produced during the partial oxidation of biomass, needs to be reduced significantly. The yield of syngas produced per gram of biomass using ultrasonic cavitation needs to be established to determine if the ultrasonic cavitational process can be compare to conventional steam gasification processes.

5. HYPOTHESIS

The process developed by Beyers (2011) can be optimized by the reconstruction of the rector system as well as a detailed investigation into optimal operating conditions.

The hydrogen to carbon monoxide ratio can be optimized to 2 to support the Fischer-Tropsch process downstream.

The syngas production using ultrasonic cavitation is a feasible process based on the expected product gas yields.

Smaller cavitational bubbles will give rise to an increase in the production of hydrogen and carbon monoxide.

An argon-saturated environment will optimize the potential sonochemical effects experienced.

Maintaining the liquid contents of the reactor at 0 °C, less energy will be transferred to the bulk liquid and most of the available energy will be transferred to the cavitational occurrences – thereby optimizing the extent of reaction.

6. PROJECT SCOPE

A sonochemical reactor system will be redesigned and reconstructed based on the recommendations (Beyers, 2011). The reactor system will be designed to serve as a batch process with finite amounts of reactants present in the reactor. The system will be purged with argon to remove all air present in the reactor. Product gas samples will be collected by using a double needle valve system to ensure that the pressure inside the reactor is maintained during sampling. The product gases will be collected in a Tedlar bag and analysed using a GC with a sample loop. The gas chromatography (GC) with thermal conductivity detection (TCD) system uses Argon as carrier gas as an alternative to helium. The thermal conductivity of helium and hydrogen are too close to each other to establish separation. The TCD can detect hydrogen, methane and nitrogen. The Tedlar sample bags are also fitted with a septum that enables the extraction of a representative gas sample using a syringe. This syringe will then be injected to a secondary column connected to a Flame Ionization (FID) detector fitted with a methanizer. The methanizer is employed to detect low levels of carbon monoxide, carbon dioxide and residual methane.

Representative sludge samples will be used to estimate the water and ash content of the sample batch. After the process has been optimized and the longest reaction time tested, the remaining sludge after the experiment will be analysed to establish the extent to which the reactant has been consumed.

A central composite design will be used as an experimental design to determine a quadratic model. The quadratic model will be used to apply response surface methodology and to investigate the effect of the parameters on each other. The central composite design will have three factors and two replicates for the factorial and axial points to ensure that repeatability is tested extensively.

The optimum operation conditions will be determined and kinetic studies will be conducted at these specified conditions. At the optimum amplitude and pressure setting, the time will be varied up to a maximum of 40 minutes. The molar percentages of carbon monoxide and hydrogen in the product gas will be used to fit a trend to the kinetic data to establish if the reaction that produces hydrogen and carbon monoxide, respectively, is first, second or third order.

7. PROJECT OBJECTIVES

The aim of this project is to optimize the partial oxidation of bacterial sludge utilizing sonochemistry and to determine if the partial oxidation of bacterial sludge using ultrasound is a competitive alternative to the conventional steam gasification process. This will entail redesigning and construction of the reactor, the optimization of the reactor conditions using a central composite design to determine a quadratic model to apply response surface methodology to optimize the process. The desirability approach will be used to optimize both the production of hydrogen and carbon monoxide simultaneously.

This data will then be used to determine if the process is commercially feasible as an alternative to the conventional methods of sludge disposal.

The objectives can be summarized as follows:

- Redesigning and reconstruction of the equipment, including the construction of a stainless steel reactor with a cooling jacket as well as a controlled sampling section
- Setting up and calibration of a gas chromatograph(GC) with thermal conductivity detection(TCD) with a sample loop and a FID with a methanizer
- The characterization of the sludge before and after experimental runs
- Determining optimal reaction conditions by an extensive literature study on sonochemistry
- Determining rate constants from the experimental data
- Determining the nature of the chemical reactions involved in the production of hydrogen, carbon monoxide and carbon dioxide which includes partial oxidation, sonolysis of water and the decomposition of lime
- Reproducibility studies
- An energy input feasibility study based on the energy inputs required

SECTION II – PRELIMINARY STUDIES

8. Biomass Sample Preparation

Bacterial sludge was collected at Unit 45 and Unit 18 at the PetroSA GTL facility where raw water is treated to remove humic acids from the water and reaction water is neutralized. The GTL plant's raw water consumption is roughly 600 m^3/h. The activated sludge treatment process produces bacterial sludge as an unwanted by-product. This sludge is a rich source of biomass due to the nature of the treatment plant it originates from. To concentrate the presence of sludge in the aqueous mixture, the container was left for the solids to settle to the bottom. Once separate layers where visible, some of the water was removed. The process was repeated several times at the GTL plant's sample point and resulted in a more concentrated sludge whilst the required amount of water to serve as transport medium for the ultrasonic waves, was still present. The sludge was received at the laboratory in a 25 litre container in its concentrated form. No analysis of the decanted water was conducted by the parties that supplied the sludge and the possibility exists that valuable components were removed with the excess water.

After rigorous cleaning with distilled water, this aqueous sludge mixture was placed in an especially designed mixing vessel Figure 5.where continuous mixing was applied while sampling a specified amount of 70 ml. The mixing vessel was fitted with 4 equally spaced baffles and two sets of blades. The height of the blades was fixed between the three sampling valves. The rotation speed was adjusted to avoid foaming, whilst ensuring turbulent mixing is taking place within the vessel. The samples were randomly taken at varying times by utilizing either: Valve-1, Valve-2 or Valve-3, as seen in Figure 5. By weighing each of the 75 ml samples, a variation of no more than 4% in mass was encountered. The individual samples were expected to be representative of the entire batch based on the uniform mass distribution, but this assumption was later confirmed by elemental sample analysis. These samples where then numbered and placed in a fridge at 5 °C to preserve the biological matter for 4 months.

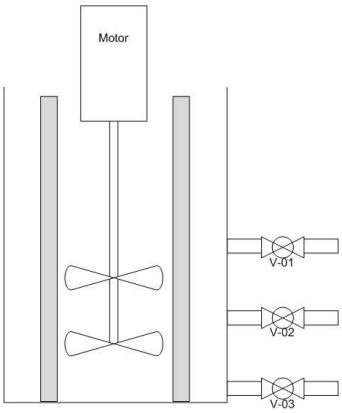

Figure 5: Sludge Mixing Vessel

The sample weight distribution can be seen in Figure 6. The average sample weight was found to be 72.9 grams with a standard deviation of 3.2 grams. It can be seen that an estimated increase of 5 grams can be seen in the weight of each sample from sample B-50 onwards. This can be as a result of the lighter fractions moving to the top of the mixing vessel and the heavier molecules settling in the bottom of the vessel, regardless of rigorous mixing. But based on a standard deviation of only 3.2 grams, the assumption was justified that near-perfect mixing was facilitated by the design of the mixing vessel and elemental analysis results in Figure 7 confirmed the assumption.

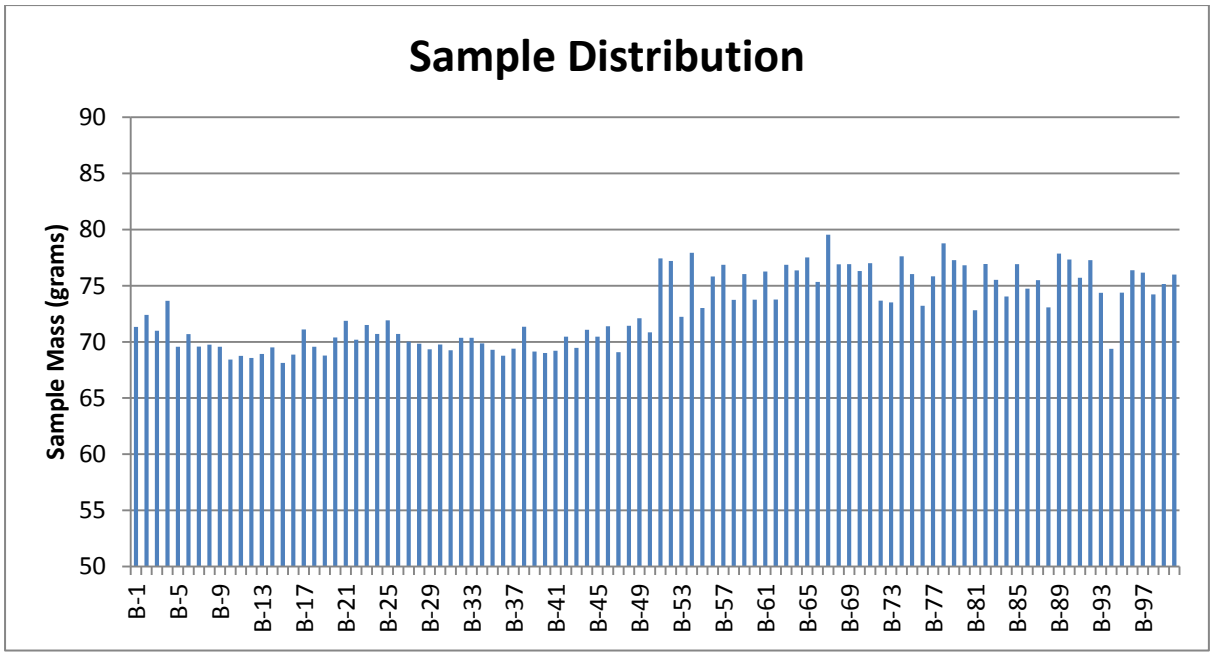

Figure 6: Sample Weight Distribution of sludge feed

9. Sludge Characteristics

Three representative sludge samples were randomly selected to be representative of the characteristics of the batch. These samples were B-33, B-6 and B-385. Samples starting with "A-" refer to the initial batch of sludge received from PetroSA. Based on the analysis of batch A, another sample was requested. The three representative samples were then dried at 105 °C overnight in a convection oven to remove most of the moisture from the sludge. This procedure was prescribed by the National Renewable Energy Laboratory method: NREL/TP-510-42622. The Oven Dry Weight (ODW) was then determined for the three samples and the water content of the samples calculated. The comparison between batch-A received initially and batch-B can be seen in Table 5.

Table 5: Sludge Properties

Sample Name	HHV (MJ/kg)	Bulk Density (g/mL)	Water Content (%)	Solids Content (%)	Initial Sample Weight (g)	Water Content (g)	Oven Dry Weight (g)
B-6-2013	9.82	0.94	98.0%	2.0%	70.69	69.3	1.39
B-33-2013	9.97	0.94	98.1%	1.9%	70.37	69.05	1.32
B-85-2013	9.84	1.03	97.5%	2.5%	76.42	75.52	1.92
Optimum Conditions	9.54						
A-3-1-2012	2.41	0.96	93.6%	6.4%	231.51	216.71	14.8
A-3-2-2012	2.22	0.84	95.4%	4.6%	198.3	189.21	9.09
A-3-3-2012	2.33	0.96	86.4%	13.6%	251.1	216.86	34.24

The Higher Heating Value (HHV) for each of the B samples was determined and compared with batch-A's calorific value. A bomb calorimeter was utilized for this test to determine the HHV – the available energy when the water is condensed out of the combustion products. Sensible and Latent heat is accounted for due to the condensation action. This procedure is described by Standard ANSI/ASABE S593.1 2011. As seen in Table 5, the HHV for batch-A was significantly less than for batch-B. After analysis of batch-A, a second batch was requested from the plant due to the evidently low HHV. The operations team at Unit 45 and Unit 18 on the GTL Plant then used this information to troubleshoot and identify the cause for this very low HHV. It was found that they were treating the pH of the unit with excessive amounts of lime. This action was then rectified and after stable operation was achieved, batch-B was sampled at the same sample point as batch-A and the significant improvement in the HHV can be seen in Table 5. The water content seen in Table 5 varied

between 86 and 98 weight %. The water content of sample batch-B was consistent at 98% due to the improved sampling method implemented for the preparation of batch-B.

Table 6: Experimental and Calculated HHV

CALORIFIC VALUE [MJ/kg]								
Property	**Sample B 85 2013**	**Sample B 6 2013**	**Sample B 33 2013**	**Sample A-3-3-2012**	**Sample A-3-1-2012**	**Sample A-3-2-2012**	**Average**	**Stdev**
Experimental HHV	9.84	9.82	9.97	2.33	2.22	2.41	6.06	3.47
Calculated HHV	10.82	10.72	10.58	2.84	2.71	2.73	6.73	3.68
Error	12.26%	9.21%	6.09%	21.91%	21.90%	13.31%	0.14	0.06

The measured HHV and a theoretical calculated HHV was compared in Table 6. The empirical correlation used to calculate this value, can be seen in eq (27):

$$HHV = 0.349x_C + 1.1783x_H - 0.1034x_O - 0.0151x_N + 0.1005x_S - 0.0211x_S \quad \text{eq (27)}$$

where x_i represents the mass fraction of each element in the analysed samples (Sokhansanj, 2011).

When comparing this correlation, it can be seen that a relatively small error applies for the samples from batch-B at an average value of 9.2%. When looking at samples from batch-A, an 11% increase in the error is observed on average. This larger than expected error could be due to the uncertainty in the oxygen content prediction in the Ultimate Analysis based on the form of the lime in the ash. Lime can either be present in form CaO or in the form $CaCO_3$, depending on the treatment it has undergone.

The ultimate analysis was conducted to determine the elemental composition of the sludge. These results can be observed in Figure 7. Light element analysis was conducted by means of a LECO Tru-Spec® micro-analyser. Conductivity and infrared techniques were employed to determine the composition of the samples.

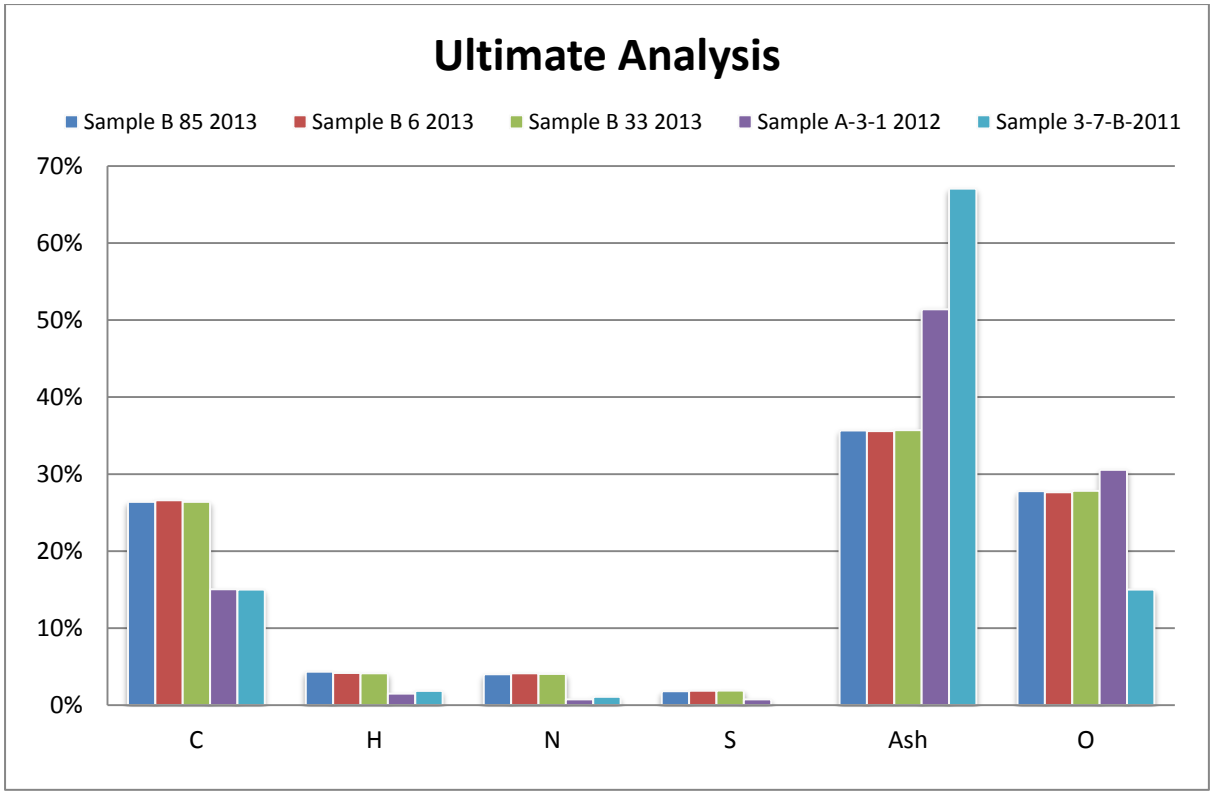

Figure 7: Sludge Ultimate Analysis

It can be seen that the ash content in samples from batch-A is 15% higher than of the samples from batch-B. This corresponds with the higher C, H, N, and S concentrations in sample B as seen in Figure 7. A sample from experimental work conducted by Beyers (2011) shows an even higher ash content and lower corresponding oxygen content. Due to the fact that the ash can either be in the form of CaO or $CaCO_3$, based on the treatment it has undergone, it shows a difference in the oxygen content. It is expected that the increased amount of oxygen present in sample batch-B should result in an increased value for Fixed carbon and Volatile carbon. Based on the elemental composition of the sludge, it was found that the theoretical maximum amount of hydrogen that can be produced is 4.07 mole % and carbon monoxide is 1.99 mole %.

Thermogravimetric analysis is used to determine the amount of moisture present in the sample once it has been dried overnight, the fixed carbon, the volatile carbon as well as the ash content. During Thermogravimetric analysis, the sample was continuously weighed whilst being exposed to different temperature and oxidative environments. The system operated under nitrogen gas flow and oxygen was added to the system to determine the mass of the fixed carbon towards the end of the experiment.

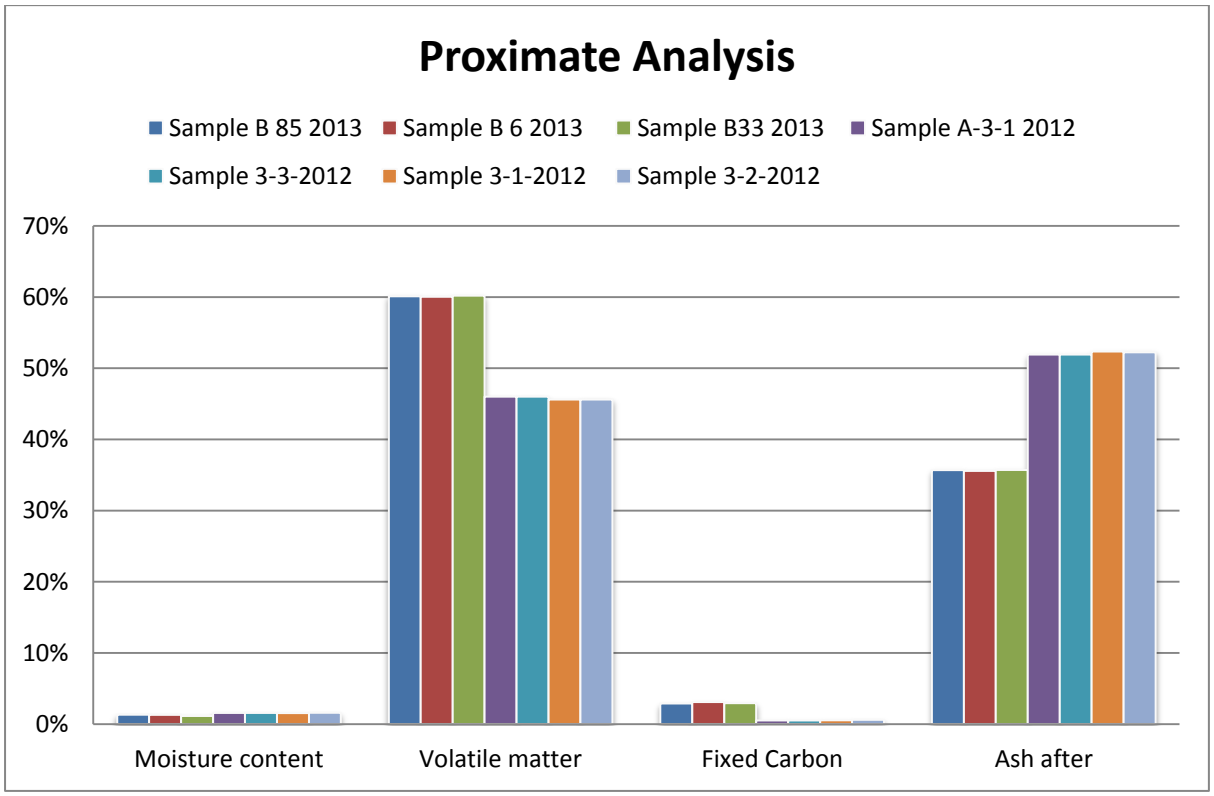

Figure 8: Sludge Proximate Analysis

The procedure started with 100% mass present at room temperature. The blue trend in Figure 9 illustrated the mass change behaviour during Thermogravimetric analysis. During step 1, the moisture still remaining in the sample after drying in a convection oven overnight for 105 °C, was evaporated whilst the reactor temperature is kept constant at 100 °C for 30 seconds. The temperature was then increased linearly at a rate of 100 °C/min. During this temperature increase, Step 2 indicates the change in mass due to the volatile carbon being released from the solid. The temperature was then held constant at 900 °C for 5 minutes after which, oxygen was introduced into the system. The oxidiseable content in the solid sample was then released as it is burnt off in the presence of oxygen. This step therefore defined the mass contribution of fixed carbon.

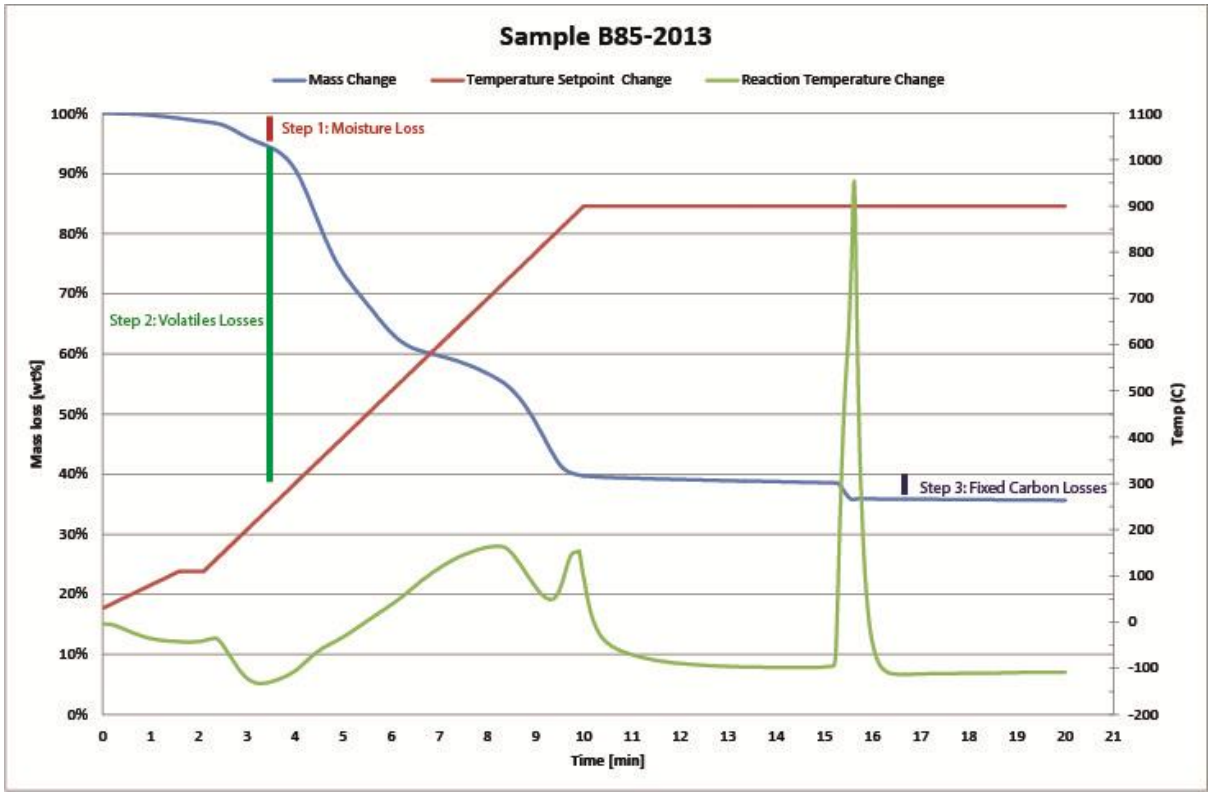

Figure 9: TGA Graph of Sample B85-2013

At the point where the mass change occurs due to the release of fixed carbon, the reactor internal temperature also increased significantly due to the exothermic oxidation reaction that occurred. This is indicated by the green line in Figure 9. The system was then kept at a constant temperature and in an oxidative environment for an additional 5 minutes to ensure all carboniferous matter has been released from the solid sample. The remaining mass after the experiment was defined as the mass of the ash present in the sample. From Figure 8 the results from the TGA testing indicate that the moisture contents of all the samples are nearly equal. This was expected as all the samples were pre-treated under the same conditions overnight at 105 °C in a convection oven and this water content refers to the ODW water content. The volatile matter was estimated at 15 % more for sample B and the fixed carbon was 4% higher than that of Sample Batch-A. This was confirmed by the decreased amount of ash present in Batch-B. According to the Ultimate analysis above, the high carbon mass percentages for Sample Batch-B was confirmed by the high fixed carbon and volatile carbon results for Batch-B. The overall correlation between the samples for batch-A showed a standard deviation of 0.13 mass % and an average of 26.47 mass %. For batch-B, the average and the standard deviation was 14.87 mass % and 0.13 mass %, respectively.

The particle size analysis of the samples were measured using a Saturn DigiSizer 5200 V1.10 utilizing the refractive index of 1.331 – that of Calcium Carbonate in water due to the high ash content of the samples. In Figure 10, three samples from 2011 are compared with a sample from batch-A and a sample from sample batch-B. It can be seen that the cumulative finer volume % of the latest sample (sample batch-B) increased significantly sooner than that of sample batch-A. This was an indication that the particle sizes in the latest samples are smaller than that of the original samples. Sample batch-A had a high ash content probably due to the presence of excessive amount of lime and it can be assumed that the particle size difference could potentially be due to the lesser presence of lime in the sludge from batch-B. The variation between the results from B-242-2013 and A-80-2013 was indicated by a standard deviation of 7.9 µm at the 50% midpoint. This could potentially be due to the difference in the composition of the different batches as illustrated by the ultimate and proximate analysis. The relatively small difference in the particle size, for the data for samples 3-7-A-2011, 3-1-A-2011 and 3-2-A-2011, indicated that the assumption that the refractive index of the sludge is the same as that of lime in water was justified. This assumption, however, led to a variation in data for the samples with 15% less ash.

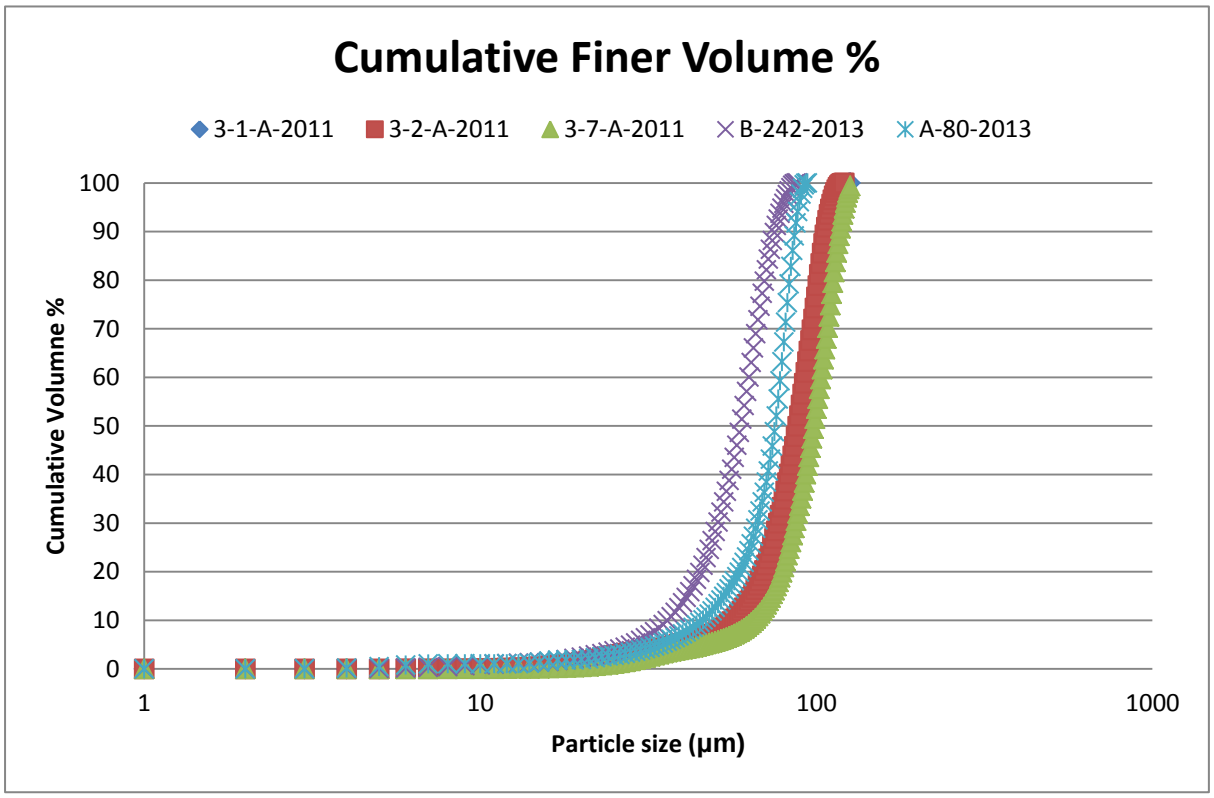

Figure 10: Sludge Cumulative Finer Volume % from Particle Size Analysis

At a particle size of 5.34 to 5.35 µm, the cumulative volume finer present of sample batch-A was estimated at 10%. At the same particle size, the plot in Figure 10 shows that 20% of sample A-80-2013 falls within that particle size. For sample B-242-2013, 60% of the sample falls into the particle size interval of 5.34 to 5.35 µm.

In Figure 11, the frequency at which each particle size appears, was shown for two samples from batch-B and three samples from batch-A. The results from samples 3-1-A and 3-2-A peaked at a frequency of 2.4 at a particle size of 59.92 to 59.93 µm. Sample 3-7-A was at a maximum frequency at a particle size of 84.65 to 84.66 µm. This maximum indicated that the particle size of sample 3-7-A is on average higher than that of samples 3-1-A and 3-2-A. This was confirmed by the green line on the right hand-side of Figure 11.

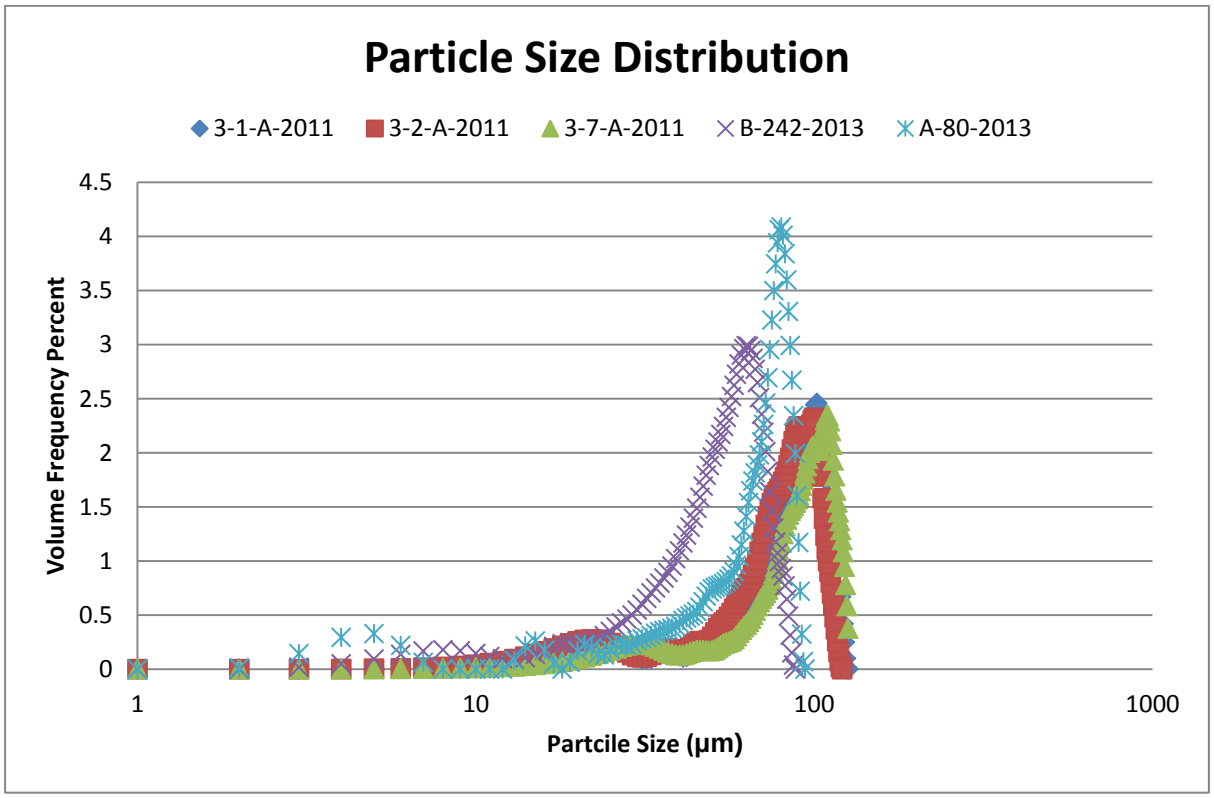

Figure 11: Sludge Particle Size Distribution

The particle size of sample B-242-2013 was concentrated around 5.34 to 5.35 µm and sample A-80-2012 around 15.05 to 15.06 µm. The mean sample size for batch-A was found to be 55.93 µm with a standard deviation of 3 µm. As expected from the analysis of the cumulative finer volume % plot, the average particle size of sample B-242-2013 was collectively smaller than that of sample A-80-2013. It can also be seen that the collective particle size of sample 3-7-A-2011 has the largest particle size large than 200 µm. The latter sample batch received, batch-B, had the smallest particle size

illustrated by the mean at 27.96 μm and a standard deviation of 3.65 μm. The Particle Size instrument output can be seen in Appendix E.

In heterogeneous reactions where solids are dispersed within the liquid sample, it is said that the overall reactivity of the system will depend on the maximum available reactive surface area of the solid (Mason & Lorimer, 1988). The smaller the particle size, the higher the available reactive surface of the biomass. It was therefore expected that the smaller overall particle size of sample batch-B, would potentially be a contributing factor to the expected improved extent of reaction.

10. Reactor set-up and supporting equipment

The reactor setup was designed based on the recommendations made by Beyers (2011). The reactor was reconstructed of stainless steel and process flow details are given in Figure 12. The bottom of the reactor has a rounded bottom to present as little interference with the spherical ultrasonic field at the bottom of the probe tip. The reactor walls are cooled using a cooling jacket with an upwards flowing mixture of 60 vol% glycol and 40 vol% water from a water bath.

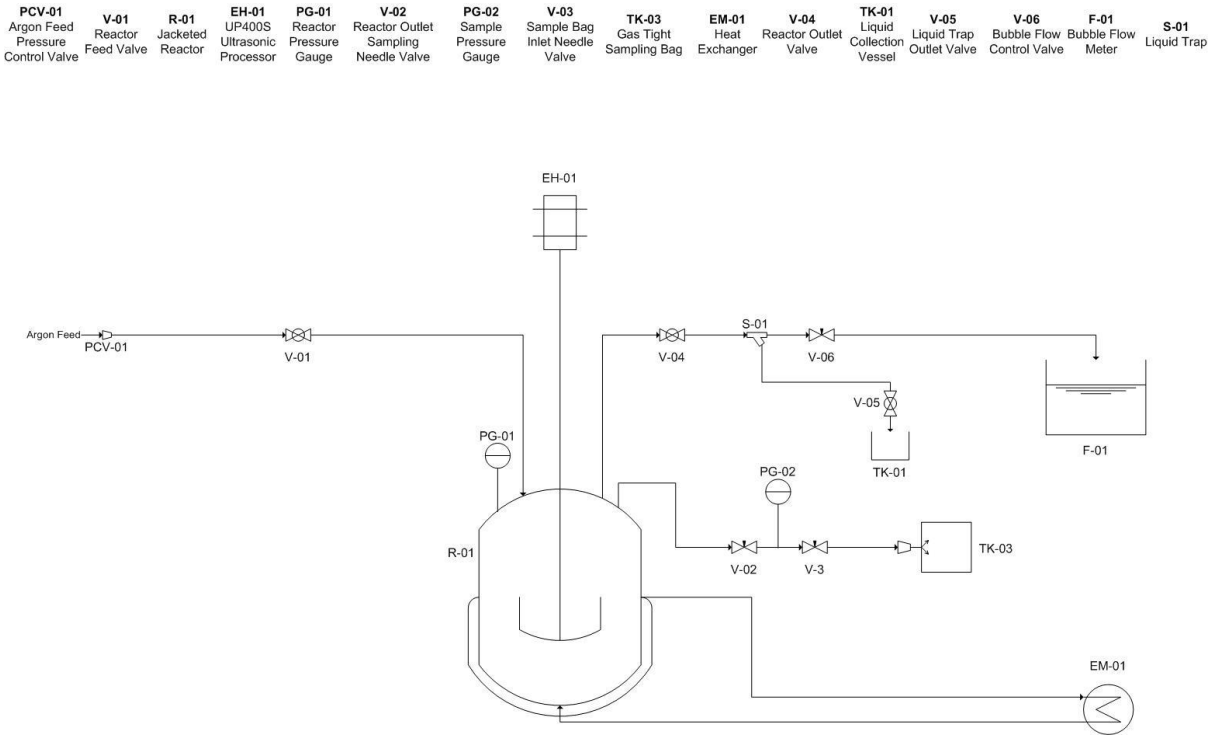

Figure 12: Partial Oxidation of bacterial sludge Process Flow Diagram

A detailed view of the setup can be seen in Figure 13. The argon gas feed entered the system via the pipe shown between the gas bottles and the reactor. The reactor consisted of the ultrasonic processor (the grey box) that is connected to the reactor and cooling water jacket. A pressure gauge was fitted to the reactor to monitor the reactor pressure. No thermocouple was available in the setup to monitor the reactor temperature and as a result, the cooling water bath temperature was monitored to estimate the reactor temperature. A second pressure gauge was fitted to the reactor sampling port to ensure that the Tedlar gas sampling bags are not exposed to excess pressure.

Figure 13: Experimental Setup for partial oxidation of bacterial sludge using ultrasound

The pressure was locked into the reactor by means of a rubber o-ring and valves on the gas inlet and outlet of the reactor. A rubber o-ring was fitted between the ultrasonic probe and the reactor flange. This o-ring absorbed the vibrations from the ultrasonic probe. The location of the o-ring was selected to be at the expected nodal point of the ultrasonic wave based on the probe design (Mason & Lorimer, 1988). It is expected that vibrations in the probe is at its minimum in the nodal point and this would result in an appropriate section to seal the probe into the reactor.

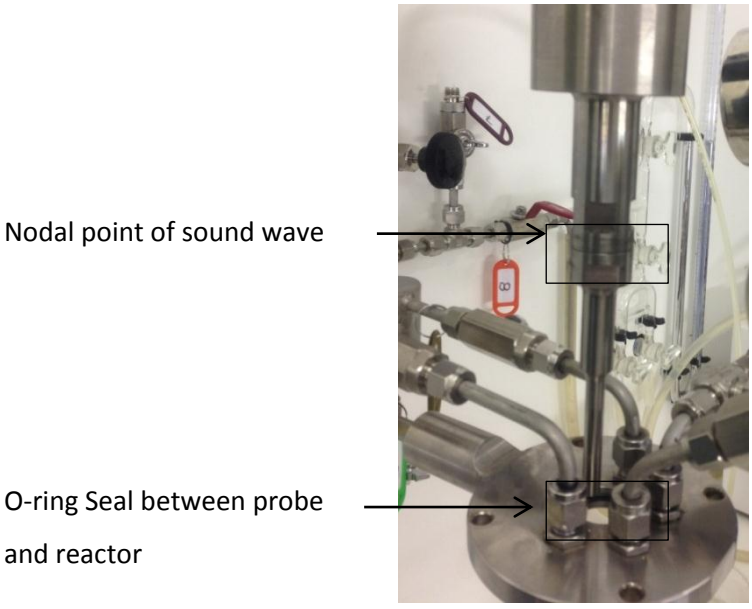

Figure 14: Reactor Probe

The second, larger o-ring was located horizontally between the stainless steel reactor vessel and cooling jacket and the reactor flange, as seen in Figure 15. The gas outlet inside the reactor had an angled plate to guide the flow of any liquids as a result of bubbling downwards (Figure 16).

Figure 15: Reactor Gas outlet

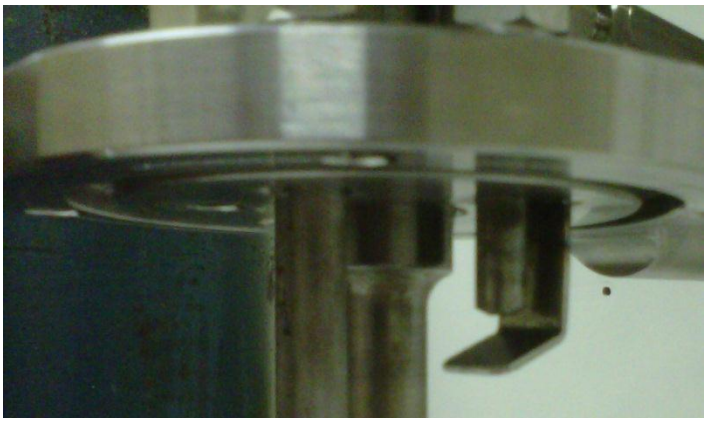

Figure 16: Reactor Flange at gas outlet

This angled plate was added to avoid the build-up of any liquid in the product gas stream. In the event of any additional moisture building up in the gas outlet line, a water tap was constructed by using an expanded volume in the pipeline with wire mesh on the inside as seen in Figure 17. Water can be drained from the water trap outlet via a Valve-5. The collected liquid at this point could be added to the mass balance to account for any losses.

Figure 17: Mesh Wire Water Trap

The reactor cooling bath was tested by placing water in the reactor and monitoring the temperature in the reactor with a glass thermometer and the cooling water bath over a time period of 2 hours. The results can be seen in Figure 18. During this trial, the reactor was not connected to the reactor flange and was rested on the setup table. A glass thermometer was inserted into the reactor cavity that contained distilled water. The reactor was connected to the cooling water bath as during a normal reaction run utilizing the same connecting tubing.

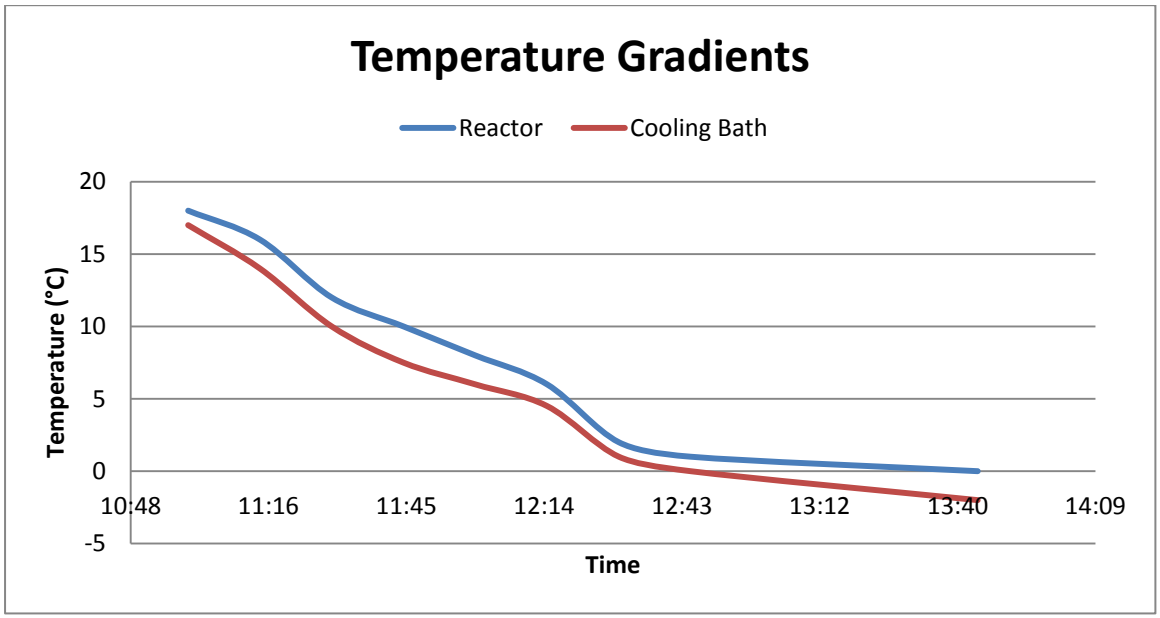

Figure 18: Reactor temperature gradients

A nearly constant temperature gradient of 1.7 °C can be seen in Figure 18, where the gradient refers to the difference between the water temperature in the reactor and the water temperature in the cooling water bath. Using the thermal conductivity of Stainless Steel 318, it was calculated that the average cooling supplied by the water bath is 5.6 W. As no thermo couple is present in the reactor to measure the bulk liquid temperatures during operation, it was assumed that this cooling rate was sufficient to avoid the water evaporating as a result of boiling. The temperature of the cooling water bath, which acts as a heat sink, was monitored to establish if any severe temperature changes were observed in the reactor during experiments.

The reactor was pressure tested to establish if safe operation is possible within the design specifications of the system. The reactor was filled with 100 ml of water. The reactor was sealed by tightening the bolts of the top of the reactor whilst taking care to not strip the bolts. All valves were checked to ensure the system is closed. In the event of the system not being able to contain 5 bar gauge pressure, the pressurizing gas (argon) and the water could spray from the reactor via the o-

ring seal. The argon bottle was opened and the pressure regulator set at 1 bar. Valve-1 to the reactor was opened and the pressure was left to equalize in the reactor. The water in the reactor stopped bubbling once the pressure had equalized. The ball valve (valve-1) into the reactor was closed and the pressure regulator was set to 2 bar. The ball valve into the reactor was carefully opened again and the reactor was left to equalize. This process was repeated and the pressure gradually increased to 5 bar (the limit of the pressure gauges) and it was determined that safe operation is possible at 5 bar gauge. The system was then left for 6 hours at a pressure of 5 bar to ensure no leaks were present.

A detailed sketch of the ultrasonic reactor, R-01, can be seen in Figure 19. The reactor design was based on the optimum intensity as discussed in the Literature Review section of this report for a 24 kHz ultrasonic processor. The Ultrasonic Processor used in this study was a Hielscher UP400S with an H7 tapered titanium horn. At the system frequency and under an average argon pressure of 2 bar, the optimum intensity was found to be 1.44 W/cm^2 (Mason & Lorimer, 1988). The maximum possible power available is 400 Watt and the corresponding exposed surface area was calculated to be 276 cm^2. The reactor length was restricted to 3 cm longer that the ultrasonic probe as the ultrasonic effects are concentrated in a spherical cloud surrounding the probe tip. The ID of the reactor was then found to be 6 cm. A detailed sketch of the reactor shows the location of the baffles in the cooling jacket that was designed to circulate the flow of cooling water in an upwards motion around the reactor to maximise possible heat transfer as the warmest section of the reactor is expected to be in contact with the incoming cooling liquid.

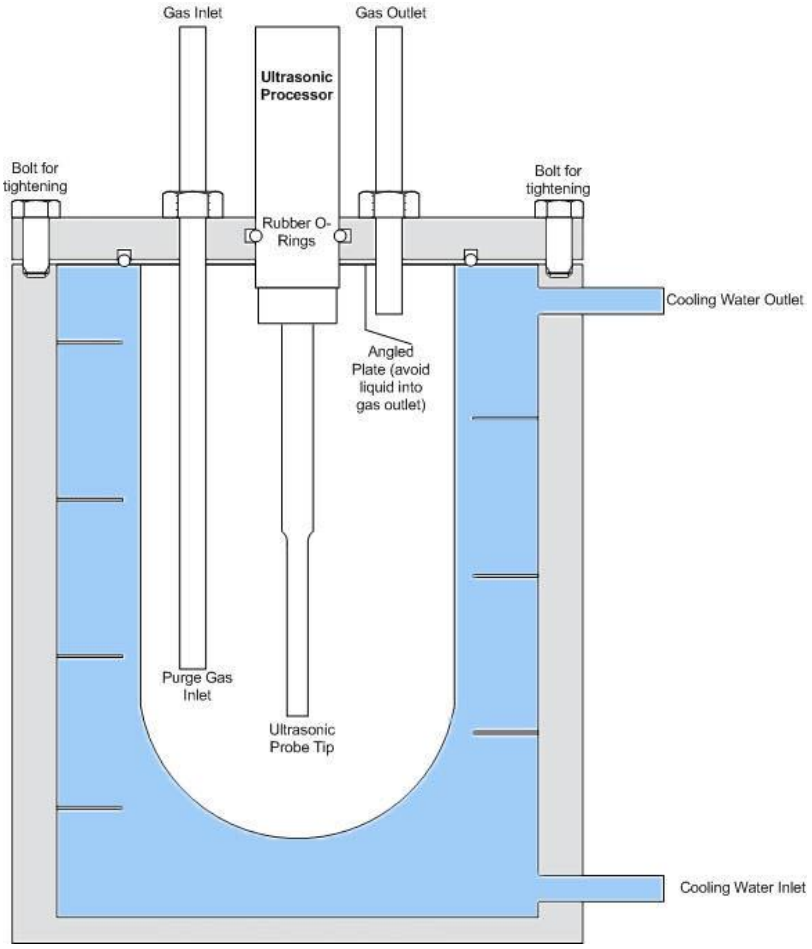

Figure 19: Detailed Sonochemical reactor drawing with cooling water jacket

To ensure batch operation, it was important that pressure losses due to sampling are avoided. The sampling procedure was tested at different reactor pressures to ensure that the pressure is maintained in the reactor during sampling. It was also necessary to check the pressure that the tedlar gas sampling bags can withstand. This testing was conducted by adding water to the reactor, sealing the reactor and starting with nitrogen pressure of 1 bar in the reactor. The stainless steel valve fitting on the reactor was opened after it was connected to the system with Teflon tubing. The first needle valve (V- 02) was opened and left to stabilize for a few seconds. Valve-02 was then closed and V-03 that is connected to the tedlar bag was slowly opened. Once the tedlar bag was full, the needle valve was slowly closed and the tedlar bag was weighed. The system pressure was then increased to 2 barg by opening V-01 and the argon bottle pressure regulator and setting the regulator to the required outlet pressure. This process was the repeated. It was established that the dual-needle valve system provides an effective manner for gas sampling up to 5 bar without causing pressure losses to the reactor.

11. Gas Chromatography

11.1 Overview

Gas chromatography was selected to analyse the different expected products from this study. Gas chromatography utilizes differences in physical properties to separate gas mixtures. These components in the gas mixture will then elude from the column at a component specific residence time and will be detected by the appropriate detection device utilizing either differences in thermal conductivity or the ability of a compound to form ions during the combustion of compounds utilizing a hydrogen flame (Gas Chromatography, 2009).

During gas chromatography for gas samples, the sample was injected, by the appropriate method, into the column. The column was heated under flow of an inert, called the carrier gas. The carrier gas used in a specific application depended on the compounds that need to be separated during the application. The gas was passed through the column and into the appropriate detector. The signal from the detector whilst only the carrier gas is present became the base line in the results. The gaseous components will relate to the carrier gas in different intensities and this difference was used as a means of quantifying the amount of a component that is present in the sample. Components were separated based on the molecular weight and vapour pressure of the components as well as the polarity difference between the stationary and the mobile phase (Kupiec, 2004). Components are, therefore, identified based on their unique elution time from the column at a specific temperature, pressure and type of carrier gas. Care needed to be taken as, depending on the operating conditions, some components may have the same residence time in the column. In such a case, the temperature program and/or the carrier gas flow rate needed to be changed to separate these compounds.

For this specific application, hydrogen, carbon monoxide, carbon dioxide, methane and nitrogen (to measure air) needed to be quantified. The available equipment consisted of a Varian GC fitted with a Carboxen 100 Packed Column. To enable the quantification of the gas sample, an internal standard could not be used due to experimental difficulties. An external standard was employed, but required a constant volume injection for each run. A gas sample loop was therefore added to the injection port to ensure that a set volume enters to Carboxen packed column for every test conducted.

11.2 Thermal Conductivity Detector

The principle used to detect different gasses in a TCD is based on the difference in the thermal conductivities of the carrier gas and the carrier gas with its sample contents. To determine this difference in thermal conductivity, the detector filament is heated to a temperature higher than that of the TCD oven. The filament acts as a resistor. Whilst maintaining a constant temperature, the carrier gas and the carrier gas containing the gas samples is passed over the filament. When the carrier gas with the sample is passed over the filament, more energy would be required to maintain the filament temperature. This required energy is measured five times per second and recorded (Kupiec, 2004). To rule out any effects on the detection that is not as a result of the gas sample, a second channel of resistors maintain a constant carrier gas flow. The voltage difference is then used to compare the output from the carrier gas with that of the carrier gas and the sample.

The system under investigation was originally set up using helium as carrier gas, but as the aim of the study was to determine the concentration of hydrogen specifically, it was decided to use argon as carrier gas. Due to the similarity on the thermal conductivities of helium and hydrogen, argon was suggested by the column manufacturer as an appropriate alternative.

11.3 Flame Ionization Detector with a methanizer

To determine very low concentrations of carbon monoxide and carbon dioxide, a FID with a methanizer was added to the system. This configuration was set up in parallel to the TCD. The FID used the fact that the ions produced when burning hydrocarbons are proportional to the concentration of the carboniferous species in the gas sample stream. To detect the ions produced during burning, a potential difference over two electrodes is used. At the nozzle head where the flame is produced, the positive electrode resides. The negative electrode is located at some distance above the flame.

The FID cannot detect carbon monoxide and carbon dioxide and therefore a methanizer was fitted to the FID. In the methanizer, hydrogen is mixed with the sample and carrier gas and then passed over an especially designed nickel catalyst. This methanizer section is operated at 380 °C to facilitate the conversion of CO and CO_2 into CH_4 – which is detectable by the FID (Gas Chromatography, 2009). The gas from the methanizer is then fed into the FID. The collector plate electrode in the FID attracts the ions to the plate and current is induced when the ions hits the plate (Kupiec, 2004). The current

produced is directly proportional to the amount of ions absorbed by the negative electrode. The current is therefore sent to an integrator that feeds the results to the software, taking the presence of the carrier gas into account.

11.4 Column Conditioning

Conditioning of a column was required to remove any volatile components from the column due to the manufacturing process or from contamination when the column is not in use. The aim was to obtain a stable baseline. The Carboxen 1000 packed column was pre-conditioned for 16 hours at 225 °C using argon gas at a flow rate of 25 mL/min. according to manufacturer's specifications. At the end of conditioning, it was found that the baseline had stabilized. The column on the FID channel was preconditioned according to manufacturer specifications before this study was commenced.

11.5 Column Operating Method Selection

The expected products in the gas samples were a mixture of oxygen, nitrogen, methane, carbon monoxide and carbon dioxide. These are purely present in the gas phase. The sample loop was not heated as no condensed species were present in the sample. The injection port on the FID was heated based on the Varian system design, but no condensable species were present. The argon gas flow rate on the TCD was set and maintained at 30 mL/min, according to manufacturer specifications. The TCD oven set at 160 °C and the TCD filament is set to 170 °C to avoid any condensation on the filament. The column oven was maintained at 120 °C and no step change in the column oven temperature was used due to the fact that the species in the sample were eluding within 8 minutes. A step up in the column temperature is only utilized to ensure species with high residence times elude sooner. By maintaining a constant column oven temperature, it was ensured that the operation between the TCD channel and the FID channel required no system changes.

The FID channel utilized helium as carrier gas and also required instrument grade air and hydrogen. The instrument grade air flow rate was maintained by ensuring the pressure regulator was set at an outlet pressure of 15 bar gauge. The FID column was also maintained at 120 °C. The FID oven was set to 280 °C and the methanizer oven was set to 380 °C to facilitate the reaction between carbon monoxide, carbon dioxide and hydrogen to form detectable methane. A summary of the equipment and the method can be found in Appendix A.

11.6 Calibration

The calibration of the TCD was relatively simple with the use of the constant volume sample loop. As a constant volume is injected with each run, the area change is directly related to only the change in composition of the gas. For the TCD, the calibration was initiated with 100% pure gas samples. The instrument grade gas samples were obtained from multiple sources and stored in Tedlar sample bags. Each of the 100% pure samples was injected between 3 to 8 times to obtain sample points for the calibration plots. The pure gas injections were also used to determine the unique residence time for each component. To obtain a second point on the calibration line, a gas standard was used. A gas standard was supplied by PetroSA along with a detailed chromatograph to show where each component was expected to elude as well as the detailed composition. The gas standard was originally purchased from Sigma Aldrich. This gas standard was transferred to a Tedlar bag and the same injection method used for the 100 % pure sample was used. The composition of the gas standard can be seen in Table 7.

Table 7: Gas standard Composition

Component	Mole%
Hydrogen	47.82
Oxygen	<0.01
Argon	1.64
Nitrogen	11.35
Carbon Monoxide	2.43
Carbon Dioxide	12.72
Methane	13.07
Ethane	1.45
Ethene	2.37
Propane	0.43
Propene	2.98
Iso-butane	0.03
N-butane	0.2
C4 total Alkanes	0.23
Butene-1	1.68
Trans-2-butene	0.04
Iso-Butene	0.15
Cis-2-butene	0.05
C4 Total Alkenes	1.92
Iso-pentane	0.03
N-pentane	0.07
Neo-pentane	<0.01
C5 total Alkanes	0.1
C5 total Alkenes	0.88
C6 +	0.61

For the TCD, a 2 point calibration was achieved for hydrogen and methane. For nitrogen, a three point calibration was achieved by injecting an instrument grade air sample. The calibration curve plots for the gases can be found in Appendix B.

For the FID, the calibration was conducted using a 100 µl gas tight syringe for inject the samples. As the methanizer cannot accurately quantify 100% pure samples of carbon monoxide and carbon dioxide, the 100 % pure gas samples were only injected to identify the unique residence time of the components and not as points on the calibration curve. The gas standard was used to calibrate the FID using the reduced concentrations present in the gas standard. After trial and error, the method to obtain as close as possible to a constant volume using the syringe injection, was established. The FID channel was calibrated using 2.43 mole% carbon monoxide and 12.72 mole % as a points of the respective calibration curves. After 6 injections achieved exactly the same area on the chromatogram, the calibration curves were saved. The results from the calibration can be seen in Appendix B.

Clarity Integration software:

The following calculations are performed by Clarity Integration software:

1. Determination of the Response Factor of each component, RF_i

$$RF_i = \frac{area\ of\ component\ i\ (std\ run)}{concentration\ of\ component\ i\ in\ the\ standard} \qquad eq\ (28)$$

2. Determination of Concentration of each component in the sample, C_i:

$$C_i = \frac{area\ of\ component\ i\ (sample\ run)}{RF_i} \qquad eq\ (29)$$

3. Determination of the reported Concentration of each component I in the sample, reported C_i:

$$reported\ C_i = \frac{C_i 100\%}{sum\ total\ of\ the\ GC\ Results} \qquad eq\ (30)$$

All components are reported with the units of mole%, to the nearest 0.01 mole %.

12. Variable Selection and Range Testing

In previous studies, Beyers (2011) tested the effect of changing the time, amplitude, oxygen pressure and concentration of the sludge initially loaded as reactant. It was found that the time, amplitude and amount of oxygen added plays a significant role on the degree of sonication. Based on these findings and recommendations by Beyers (2011), it was decided to base this study on changing the reactor diameter, removing all oxygen from the process due to excessive amounts of carbon dioxide that was produced, controlling the temperature of the reactor by means of utilizing a cooling jacket, operating at higher pressure to investigate the effect and varying the amplitude of operation. The amplitude of operation refers to the amplitude of the sound wave that is emitted by the ultrasonic processor. The maximum amplitude the system can experience is at a parameter setting of 100% and the minimum at 40% on the ultrasonic processor. The amplitude served as an indication of the electrical power into the ultrasonic transducer.

Statistical screening design experiments were conducted to determine the range of the factors that will be used in the statistical design of experiments. The planned range for the factors can be seen in Table 8. It was decided to take the mid-point pressure and amplitude to test time as the first factor.

Table 8: Factor Ranges for Screening Experiments

	Amplitude	Time	Pressure
Case 1	50%	10 min	1 barg
Case 2	70%	20 min	2 barg
Case 3	100%	40 min	3 barg

From Figure 20 it can be seen that a maximum amount of hydrogen is produced at the longest possible time period. The amount of carbon monoxide present reduced at 40 minutes. It was therefore decided that the optimum time range would be where both hydrogen and carbon monoxide were maximized. It was also noted at this stage that the temperature of the reactor flange increased due to vibration energy that is being transferred via the o-ring for the test that ran for 40 minutes. To protect the equipment but also optimize the hydrogen and carbon dioxide production, it was determined that the maximum reactor time to test should be 20 minutes. Kinetic studies at the optimum condition would again be tested for 40 minutes. The second test was conducted to see what the effect of low amplitude would be on the product formation. It was

decided to again use the mid-point pressure (2 barg) and low amplitude (50%), but run the experiment for 10 minutes and repeat for 20 minutes.

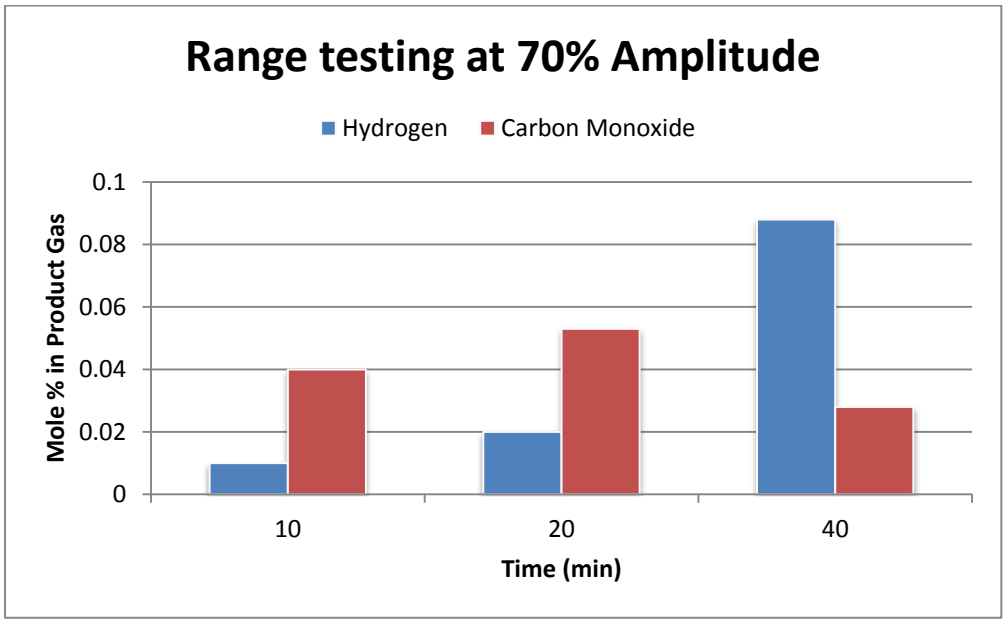

Figure 20: Hydrogen and Carbon Monoxide Production during Screening Experiments at 70%

It can be seen in Figure 20 and Figure 21 that the amount of desired gas produced at 50% amplitude is significantly less seeing as these plots are on the same scale.

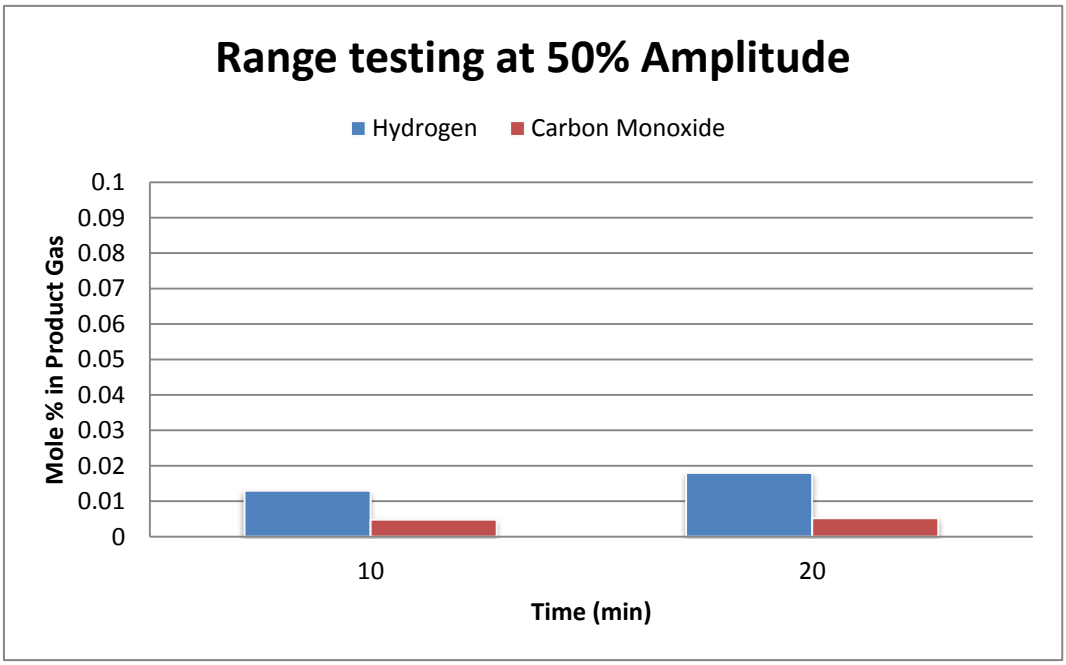

Figure 21: Hydrogen and Carbon Monoxide Production during Screening Experiments at 50%

13. Experimental Planning

13.1 Central Composite Experimental Design

A central composite design was used in the experimental design for this project. The central composite design was used to establish a quadratic model that was used in conjunction with response surface methodology to establish the optimal range for the experimental factors. The central composite design had 3 factors, namely: time, amplitude and pressure. There were two replicas for the factorial points as well as the axial points which resulted in a total number of experimental runs of 34. The two response variables, Y1 and Y2, was the molar percentage H_2 and molar percentage CO in the product gas. To optimize the two response variables simultaneously, the desirability approach was used. This would theoretically maximised both the hydrogen and carbon monoxide production simultaneously.

13.2 Introductory Experiments to establish variable ranges

The screening experiments were conducted to establish the settings for the factors used in the central composite design and can be found in Table 9. The discussion of these factors and their selection occurred in chapter 13.

Table 9: Factor Settings

Factors	-α	+α	Low	High	0
Time (minutes)	12.03	17.97	10	20	15
Amplitude (%)	60.13 (60%)	89.97 (90%)	50	100	75
Pressure (barg)	1.41	2.59	1	3	2

Due to the settings on the ultrasonic processor only being marked as 0, 20%, 30%, 45%, 60% and 70%, it was not possible to follow Table 9 accurately. It was assumed that all settings would be within 2% of the desired setting (eg. 60% instead of 60.13%). The pressure in Table 9 refers to the pressure at the beginning of the experiment after the system was pressurized with argon. The time coded value of 12.03 corresponds to a reaction time of 12 min and 1.8 seconds, which was rounded off to 12 minutes. A time of 17.97 corresponds to 18 minutes and 58 seconds. When applying the settings for the factors in Table 9, the planned experimental runs to complete the quadratic model can be found in Table 10. The amplitude settings were rounded to the closest possible setting on the ultrasonic processor.

Table 10: Experimental Design

Run Number	Pressure (barg)	Time (min)	Amplitude (%)	Response Y1 (H2 %)	Response Y2 (CO %)
1	2.00	20.00	75.00		
2	2.59	12.03	89.97 (90%)		
3	1.41	17.97	60.13 (60%)		
4	1.41	12.03	60.13 (60%)		
5	2.00	15.00	75.00		
6	2.59	12.03	89.97 (90%)		
7	2.59	12.03	60.13 (60%)		
8	2.00	15.00	75.00		
9	1.41	17.97	60.13 (60%)		
10	2.00	15.00	75.00		
11	1.41	17.97	89.97 (90%)		
12	3.00	15.00	75.00		
13	2.00	15.00	75.00		
14	3.00	15.00	75.00		
15	1.41	12.03	60.13 (60%)		
16	2.00	15.00	50.00		
17	2.00	15.00	75.00		
18	2.00	10.00	75.00		
19	2.59	17.97	89.97 (90%)		
20	2.00	10.00	75.00		
21	2.59	17.97	89.97 (90%)		
22	2.00	15.00	50.00		
23	2.59	17.97	60.13 (60%)		
24	2.00	15.00	100.00		
25	2.00	15.00	100.00		
26	1.41	12.03	89.97 (90%)		
27	1.00	15.00	75.00		
28	2.00	15.00	75.00		
29	1.41	12.03	89.97 (90%)		
30	1.00	15.00	75.00		
31	2.59	17.97	60.13 (60%)		
32	1.41	17.97	89.97 (90%)		
33	2.00	20.00	75.00		
34	2.59	12.03	60.13 (60%)		

After the quadratic model was established, response surface methodology was applied to determine the optimum range of the factor settings. Experiments would also be repeated to ensure that the results are reproducible prior to establishing the quadratic model. The optimum settings based of the desirability approach using response surface methodology was then tested. These optimization

experiments will be conducted for a range of factor settings within the optimum area on the response surface.

13.3 Sampling Techniques

To ensure that the batch system did not lose any pressure during sampling, a dual needle valve system was introduced with a pressure gauge on the outlet of the dual valve system. During normal operation, the dual needle valve system was closed. During the sampling process, a tedlar bag was connected to the second needle valve (V-03) and the tedlar bags valve was opened. The first needle valve (V-02) was opened slowly for a few seconds. V-02 was then closed again. After the first valve has been closed, the V-03 was slowly opened and the pressure on the gauge monitored to ensure that the tedlar bag was not exposed to more than 3 bar. V-03 was then closed and the tedlar bag valve as well. The tedlar bag was then carefully removed and analysed using gas chromatography. The the content of the tedlar bag was emptied by vacuum into a well-ventilated area after analysis. The tedlar bag was then purged with nitrogen to remove any residual gases from the last analysis and a vacuum will be drawn to ensure no gas entered the sample bag before use.

13.4 Experimental Procedure

The reactor was operated according to the following procedure:

1. The inside of the reactor is cleaned using acetone and dried.
2. Switch on the cooling water bath and pump and check that the cooling water is flowing from the top of the cooling jacket
3. Measure the cooling water bath temperature until it reaches 0 °C in the bath
4. Two 75 ml samples were added to the reactor and an additional 30 ml distilled water added to fill the reactor cavity to the desired height
5. The reactor is connected to the sonotrode using the 4 bolts at the top of the stainless steel gasket whilst ensuring the horizontal o-ring fits into the groove on the flange
6. Ensure all valves are closed around the reactor
7. Check that the dual needle valve system on the gas sampling point are closed
8. Open V-01 and check that the regulator on the argon bottle is closed
9. Open the argon bottle and slowly open the regulator while watching the pressure on the reactor pressure gauge
10. The system should now be allowed to build pressure up to 3 bar
11. Once the system reaches 3 bar, the inlet valve into the reactor should be closed
12. The pressure regulator and argon bottle should also be closed at this point
13. The reactor needs to maintain this pressure for 30 minutes to ensure that no gas leaks occur
14. Once the reactor passes the leak test, the pressure can slowly be released using the dual needle valve system until the system pressure is a 0 bar gauge and all valves should be closed

15. Open V-01
16. Open the n argon bottle and slowly open the regulator until the pressure on the reactor reaches 2 bar
17. Open the ball valve into the reactor carefully
18. Once the pressure has equalized, slowly open the gas outlet valve (V-04) and then slowly open the needle valve (V-06). This will cause bubbling inside the reactor and the water trap should be frequently checked to ensure water is not being bubbled into the gas outlet
19. The argon should now be flowing from the gas bottle, bubbling in the reactor and leaving the system through the ventilation system.
20. Gas samples should be taken after 30 minutes to establish if any oxygen is present in the system
21. If oxygen is still present in the system, repeat the 30 minutes of purging with argon
22. Once the oxygen test is passed, the outlet to the reactor should be closed
23. The system should be allowed to build up pressure to an operational pressure as set by the experimental design
24. Once the system reaches the desired pressure, the inlet valve can be closed on the reactor and the argon bottle and its regulator is closed
25. Check that the cooling water bath is still operational and check the temperature
26. Switch on the ultrasonic processor
27. Carefully set the ultrasonic processor to the required amplitude setting
28. This is the start of the experiment: note time, energy input, pressure and cooling water temperature
29. Let the experiment run for the desired amount of time
30. Once the experimental time has elapsed, switch off the ultrasonic processor
31. Let all product gas out into a tedlar bag by carefully sampling using the dual valve system in s stepwise manner until all pressure is released from the reactor
32. To remove any residual toxic gases from the system, open valve V-01 and slowly open the argon regulator. Some pressure should still be available without opening the argon bottle
33. Allow this pressure to enter the reactor until the needle on the regulator reaches 0 ml/min
34. The argon in the reactor would then have pushed the lighter gases to the top – open V-04 and V-06 to let the toxic gases purge from the reactor by the back pressure provided by the residual argon
35. Once all pressure has been released, it is safe to disconnect the bolts at the top of the reactor
36. Carefully remove all contents from the reactor and pour into a weighed porcelain bowl
37. Weigh wet sample before placing in over to dry at 90 °C overnight
38. Once dry, weigh the dry sample and empty the dry contents into a sample container for analysis.
39. Switch off the cooling water bath and pump
40. Clean reactor using firstly distilled water and then using acetone

13.5 Solid and Gas Sample Analysis

The collected product gas in the Tedlar bags was analysed using gas chromatography using a TCD and an FID fitted with a methanizer.

13.5.1 GC Start-up Procedure:

Before the samples can be analysed, it is important to correctly start-up the GC to avoid any possible damage to the sensitive detection equipment or column packing.

Firstly ensure that no hydrogen is leaking by turning the hydrogen valve on the GC clockwise. At this stage, open the argon and helium gas bottles and check the flow regulators to ensure that there is still gas in the bottles. Check with a pipette if there is flow through the TCD column by checking for bubbles at the TCD outlets. Check that no gas is leaking from the injection ports. Once it has been established that there is flow in the columns and no gas leaks, the computer can be switched on. Login into the Clarity software as username “Admin” and click on the “Method” icon. Under “ Data Acquisition”, enable the TCD and disable the FID. Select the column oven on the GC interface and set the oven temperature to 120 °C. Select the detector on the GC interface and set the TCD oven to 160 °C and the TCD itself to 170 °C. Ensure the TCD electronics are switched off at this stage. Scroll to the next screen and ensure that the polarity is set to negative, and that autozero is switched on. Once the TCD oven has reached the desired temperature, the TCD electronics can be switched on after the bubble test on the TCD outlet confirms gas flow through the column.

13.5.2 GC Operating Procedure:

The Tedlar bag can now be connected to the gas inlet on the TCD side. The gas sample loop dial should be in the “load” position – turned to a maximum in the clockwise direction. The valve on the Tedlar bag can now be opened. Apply a small amount of pressure by hand on the gas bag and bubbles should be observed at the TCD gas outlet that is submersed in water. This is a sign that the gas loop is being purged. Continue this applied pressure for 2 minutes to ensure that all the air and residual gasses has been displaced from the gas loop.

The system is now ready to run the analysis. After stopping the applied pressure on the gas sample bag, turn the gas loop dial anti-clockwise and immediately press “Run” on the GC interface. Start the run on the Clarity software at this point manually. The Tedlar bag can be closed to minimize losses while the analysis is running.

After 10 minutes, all possible compounds that can be present in the sample would have eluded. The system should stop the run automatically at this point. The peaks will then be visible on the software interface and the integrated area value is shown in mV.s. This file is then saved and closed.
Each sample was repeated to confirm the results, but if there was a significant difference between the first two analysis, it was repeated for a third time. The Tedlar bag valve was closed and the TCD gas inlet valve was also closed. The Tedlar bag was removed from the Teflon tube fitting.

On the Clarity software, under Data Acquisition, switch the channel to FID and deactivate the TCD. Use the 100 µl syringe and push the needle carefully through the septum in the Tedlar bag valve. Open the fitting on the front of the syringe and draw the desired amount of gas sample from the bag contents. Ensure that the exact amount is drawn for each experiment. Close the fitting on the front of the syringe to lock the gas inside the syringe and then pull the syringe needle from the septum. Place the needle in the sample port as far as possible. Open the fitting on the front of the syringe and press the plunger section of the syringe down. Ensure all gas is injected in one motion. This activates a "Run" on the GC. The Clarity software should be started simultaneously. The run time was set to 5 minutes of the FID after which the system would stop the run automatically. The peaks will then be visible on the software interface and the integrated area value is shown in mV.s. This file is then saved and closed.

This process was repeated and if significant deviations were observed between analysis 1 and 2, then a third analysis would be conducted to confirm the results.

After the analysis on a sample has been completed on the TCD and the FID, the bag content was evacuated in a fume cupboard and a vacuum was drawn on the bag. The bag was the flushed with compressed air and a vacuum was drawn again. The bags were sealed and the vacuum conditions maintained until the next sample was taken on the reactor.

13.5.3 GC Shut-down Procedure:

After analysis for a specific day was completed, the electronics on the TCD was switched off. The FID electronics were switched off. The next step was to simultaneously close the air and hydrogen valves and immediately after close the corresponding gas bottles. Switch the TCD oven, FID oven and methanizer off. Switch the column oven to 30 °C – this action would activate the oven fan. Wait until the column oven reaches 30 °C and then switch off the column oven after opening the column oven

door. After all the components have cooled down to room temperature, the helium and argon gas bottles can be closed and the computer switched off.

13.5.4 Solid sample analysis:

Three representative samples of the bacterial sludge were analysed prior to commencing the experiments to obtain the characteristics of the untreated samples. Firstly, the water content of the three samples was established by first weighing the samples and then drying the samples at 105 °C for 24 hours. The dried sample was then weighed and the difference in mass is the water content of the sample.

The dried samples were used for elemental analysis and the average composition of the three samples was used as the composition prior to treatment. This process was repeated for all dried samples after each experimental analysis.

The three dried samples were also sent for TGA (Thermo Gravimetric Analysis) with mass spectrometry to establish the fixed carbon, the amount of volatile matter as well as the ash content.

The Higher Heating Value (HHV) of the samples was determined by use of a bomb calorimeter. This process is discussed in detail in chapter 10 of this report. The average value for the three samples was used. This process was repeated for the optimized kinetic test run that was conducted for the longest period of time. This would indicate the maximum change in the HHV for this study.

SECTION III – REACTOR COMMISSIONING AND TESTING

14. Physical behaviour in the sonochemical reactor

In Figure 22, the differences in the final temperature and pressure for each run can be seen. These changes were based on the initial conditions specified in Table 12. It was found that the average temperature change in the cooling water bath for the 34 runs was 2.15 °C with a standard deviation of 0.89 °C. The maximum temperature change was observed during run 24 – when the system was operated for a maximum time of 15 minutes, 2 bar gauge and an amplitude of 100%. The minimum temperature change was observed for run 4. Run 4 was conducted for 12 minutes, at 1.41 barg and at a amplitude of 60%. Run 26 was conducted at the same amplitude and pressure, but at a amplitude of 90%. During run 4, the temperature increase was 0.5 °C, but during run 16 the temperature increase was 0.7 °C. This indicates that increasing the amplitude by 30%, only caused a 0.2 °C difference in the temperature rise of the cooling water bath.

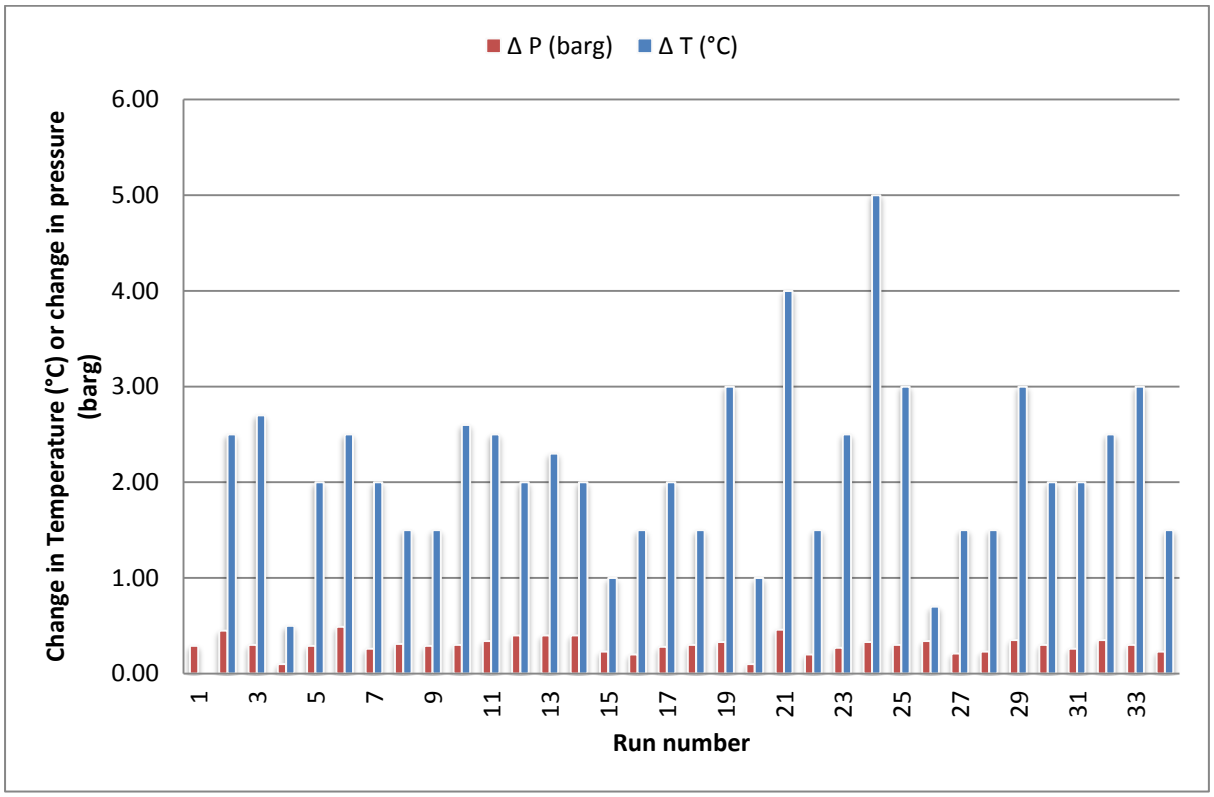

Figure 22: Pressure and Temperature Changes during Sonochemical Experimental Runs

The pressure increase in the system was suggested to be as a result of degassing of the liquid as well as the formation of gaseous oxidation products. The average pressure increase for the 34 experiments conducted was 0.3 barg with a standard deviation of 0.08 barg. This effect is observed

in Figure 22. It is also noted that the smallest pressure change corresponded with the smallest temperature change for run 4. This was expected when considering the ideal gas law.

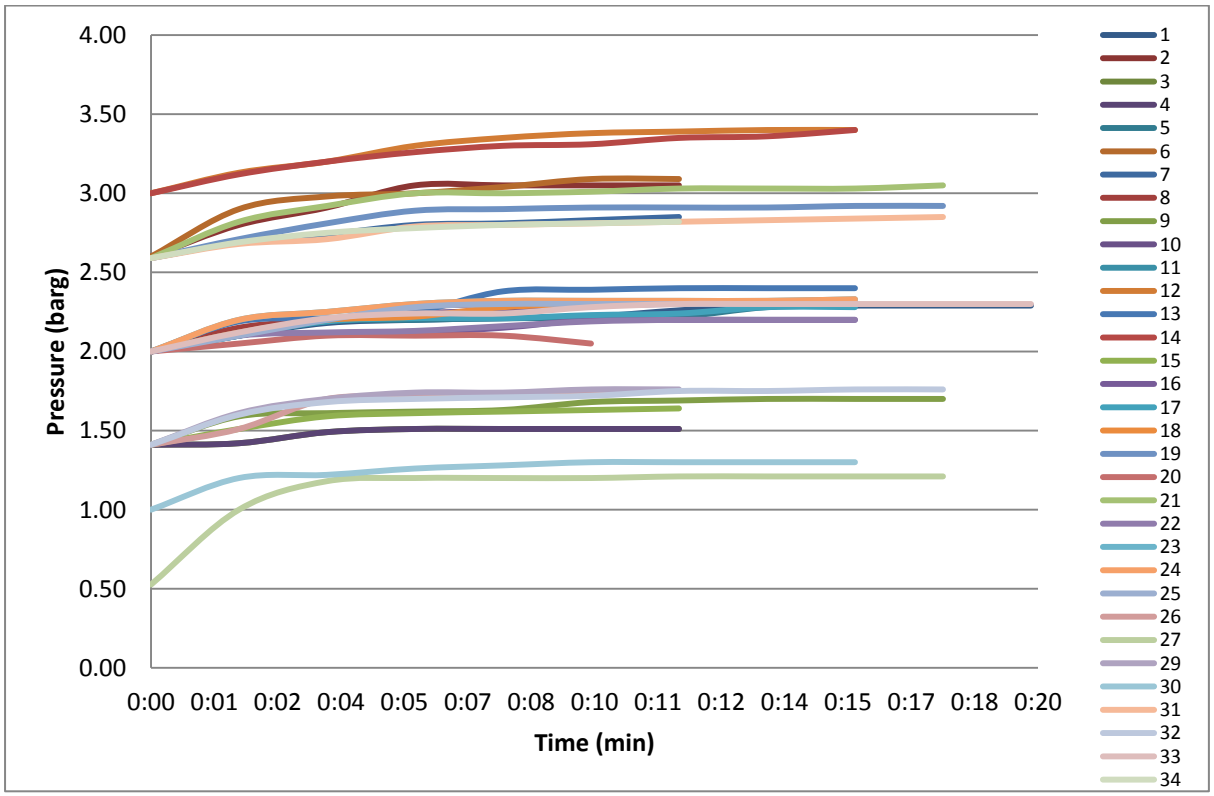

Figure 23: Pressure changes over time during Sonochemical Experimental Runs

The pressure changes for all the experiments over time can be seen in Figure 23. The initial pressure increase can be due to the partial oxidation of biomass that forms gaseous products or it can be due to the degassing of the liquid by the initial application of ultrasound.

For the runs started at 3 barg, the slope of the line continuously increased with time without reaching a plateau. This could potentially be an indication that degassing is affected by the pressure in the reactor and that higher pressure would delay the degassing process. Dissolved gasses in a liquid medium can act as the nuclei for cavitation bubble formation and as a result, these bubbles or dissolved gases do not collapse easily during the compression cycle of the wave as they the already contain gas. They will therefore grow and continue to grow until they coalesce and eventually float to the liquid surface (Mason, 2009). If the pressure on the liquid surface (static pressure) is greater, the bubble will experience more resistance and would take longer to break through to the liquid surface. It could also be an indication that the reaction takes place for the entire duration of the run if the pressure increase is due to the formation of oxidation products.

The cooling water bath was set to a constant temperature of -5 °C with a cooling liquid flow rate of 300 L/min. The cooling water bath effective temperature was not controlled by the measured temperature of the bath, but rather by the set point of the equipment. No thermocouple was present inside the cooling bath and all readings were taken using a thermometer. Due to reactor design limitations, the temperature in the reactor could not be measured and the cooling water bath's temperature was used to estimate the reactor temperature. The temperature change in the cooling water bath was therefore directly correlated to the temperature change in the reactor as no feed-back control was implemented on the cooling water bath. When assuming a constant heat transfer coefficient between the cooling water and the exposed reactor surface, the change in temperature in the reactor is directly proportional to the change in cooling water temperature.

The temperature increase observed in the cooling water can therefore be as a result of the exothermic reactions taking place due to sonication. This was investigated in the kinetics section of this study. It was expected that the same hydrogen production trend observed over time should be linked to the temperature increase for the kinetic runs. It was also noted that the vibrations caused by the probe were not completely absorbed by the o-ring and the reactor flange temperature increased as a result. The headspace in the reactor was exposed to this increased flange temperature, but also exposed to the flowing cooling water fluid. The combined effect of the exothermic reaction as well as the vibration energy that caused the heating of the flange, resulted in the temperature change in the cooling water temperature. It can, however, be assumed that the the flange temperature increase was constant at a set amplitude and time. This therefore resulted in a representative temperature effect due to flange heating being observed for all runs. An increase in the cooling water temperature was therefore an indication of the reactor temperature increasing. An increase in the reactor temperature, in turn, was an indication of the extent of the exothermic reaction that took place under the experimental conditions.

The observed pressure increase in the first minute of sonication followed a similar slope regardless of the initial starting pressure. It was therefore expected that the liquid was degassed rapidly during the first 90 seconds of the experiment and that pressure increases past this time frame is due to the formation of oxidation products. Due to the cooling bath liquid set point being maintained below 10 °C and the observed temperature of the sludge after the reaction being negligible, it is assumed that the pressure increase is not due to the formation of water vapour. This assumption was confirmed as no condensation products were observed in the gas sample bags for any experiment. The slopes of the experiments conducted at 3 bar indicate that the system pressure continuously

increased. This can either be as a result of a delay in degassing at high headspace pressures or it can be an indication that the oxidation of the biomass occurred and produced gaseous products for the duration of the experiment.

15. Product Gases

The production of hydrogen in mole % of the gas phase can be observed in Figure 24. The minimum hydrogen produced, occurred during runs 12 and 14 at a value of 0.014 mole % hydrogen. The maximum amount of hydrogen produced can be seen in run 2 with a value of 0.14 – exactly 10 times more than the minimum value. The experiments that produced more than 0.1 mole % hydrogen were all conducted at an amplitude of 90%, apart from run 27 which was conducted at 75%.

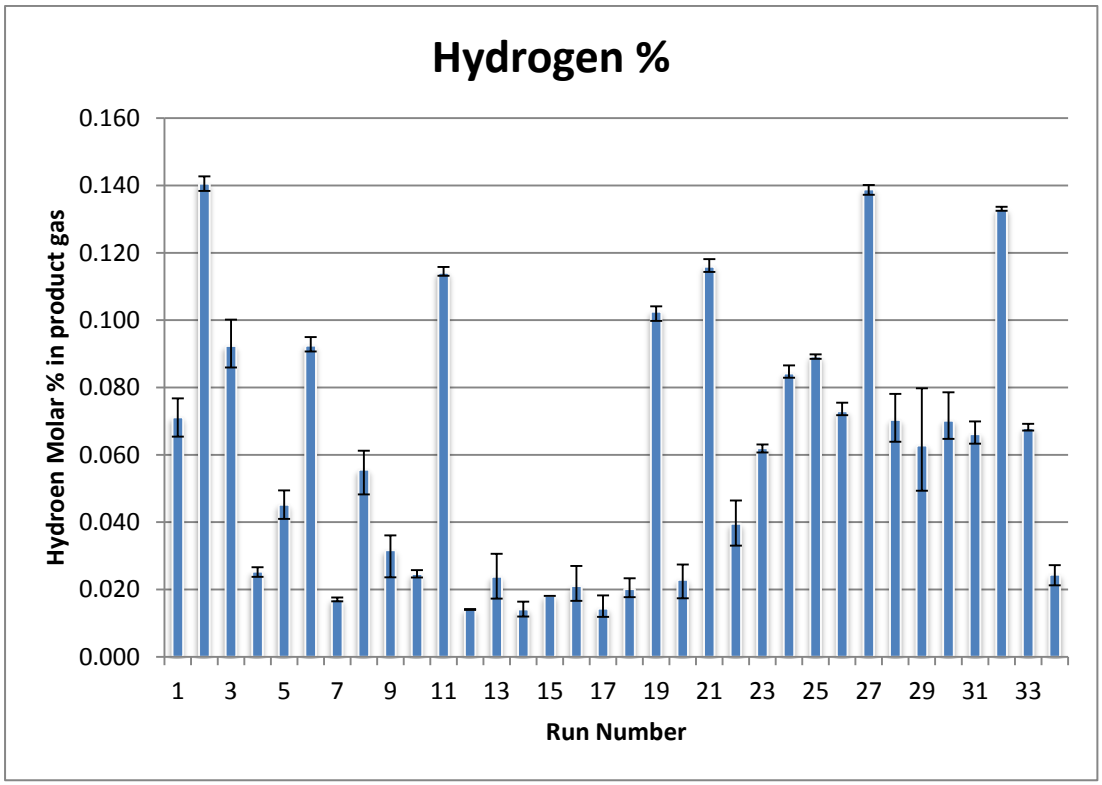

Figure 24: Hydrogen Mole % formed during Sonochemical Experimental Runs

In Figure 24 the error bars on the plot indicates the minimum and maximum values that were observed during the analysis. Each experiment was analysed on the TCD three times and the average plotted as the blue bars. The variation in the error size is due to the uncertainty involved with the analysis of low concentrations of hydrogen. On the calibration curve, a 100% point as well as a point at 47.85% was used to obtain the slope of the calibration curve. A calibration point at a lower concentration could have minimized the errors. On average for the 34 experiments, 0.06 mole %

hydrogen was produced with the minimum hydrogen production at 0.014 mole % and the maximum hydrogen production at 0.14 mole %.

The carbon monoxide in the product gas was measured using the FID Methanizer on the GC. The maximum amount of carbon monoxide was 1.90 mole % during run 27. This mole % includes the inert argon that is present in the system. Run 27 also produced a large amount of hydrogen, as seen in Figure 24. The conditions under which run 27 was conducted were 1 barg pressure, 15 minutes and amplitude of 75%. The initial screening experiments indicated an optimum at this experimental range and the central composite design was designed to investigate this operational point and points in its proximity.

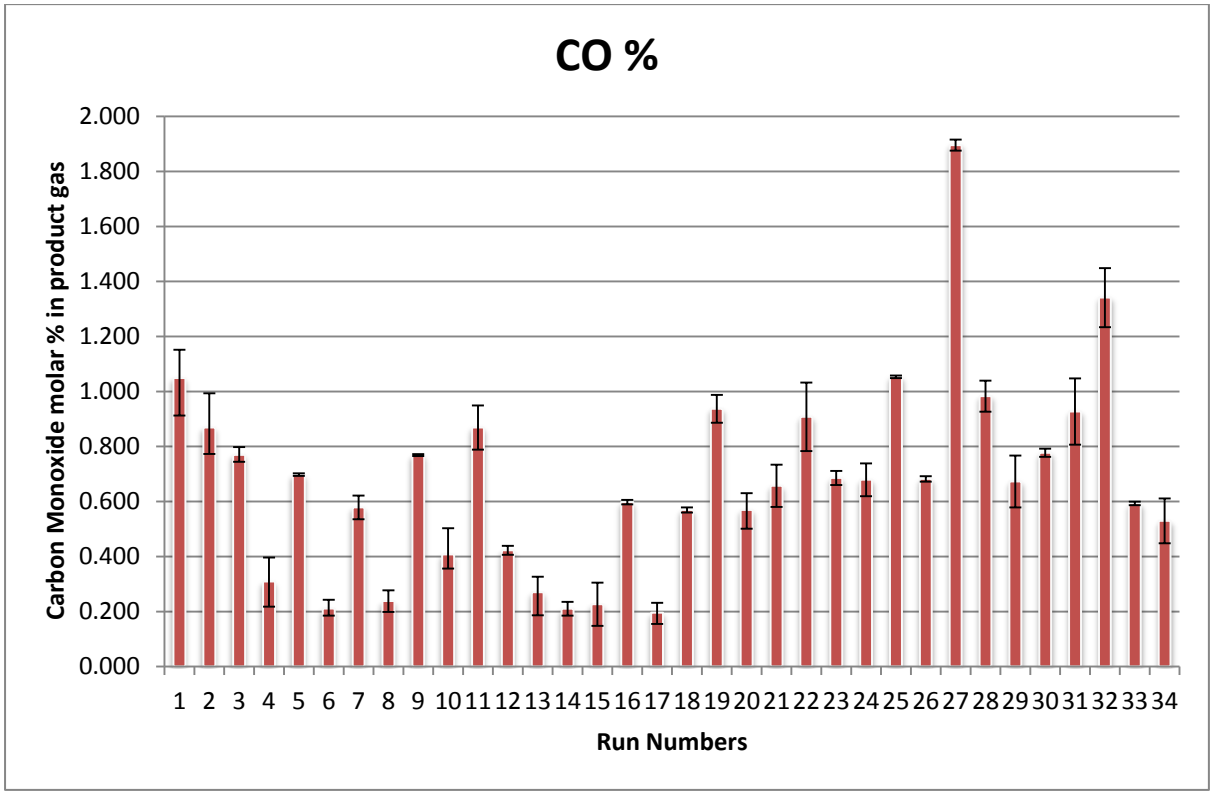

Figure 25: Carbon Monoxide Mole % Formed during Sonochemical Experimental Runs

When utilizing the FID with methanizer, the system was fitted with an inlet syringe injection port. Due to the gaseous nature of the product, care was taken to draw exactly 50 µl for each test as an increase in the amount of gas injected would lead to an increase in the peak area. This would then mask if the area increase was as a result of increased carbon monoxide production or if it was due to an error in the injection method. The error bars on Figure 25 indicated acceptable reproducibility of the FID analysis. Each injection was repeated three times on the FID and the relatively large errors

for run 1, 2,4,22 and 32 were as a result of a difference in the injection volume. The average carbon monoxide concentration for all the runs was found to be 0.66 mole % with the maximum value at 1.9 mole % and the minimum at 0.2 mole %. This corresponds to the 10 times more product gas observed between the maximum and the minimum in the hydrogen production.

To compare the contribution of each of the desired products, Figure 26 shows the weighted contribution of the hydrogen and carbon monoxide that was produced for all 34 runs. It can be seen that an increase in carbon monoxide coincides with an increase in hydrogen production. This was expected due to the partial oxidation reaction mechanism as discussed in the theory section of this study.

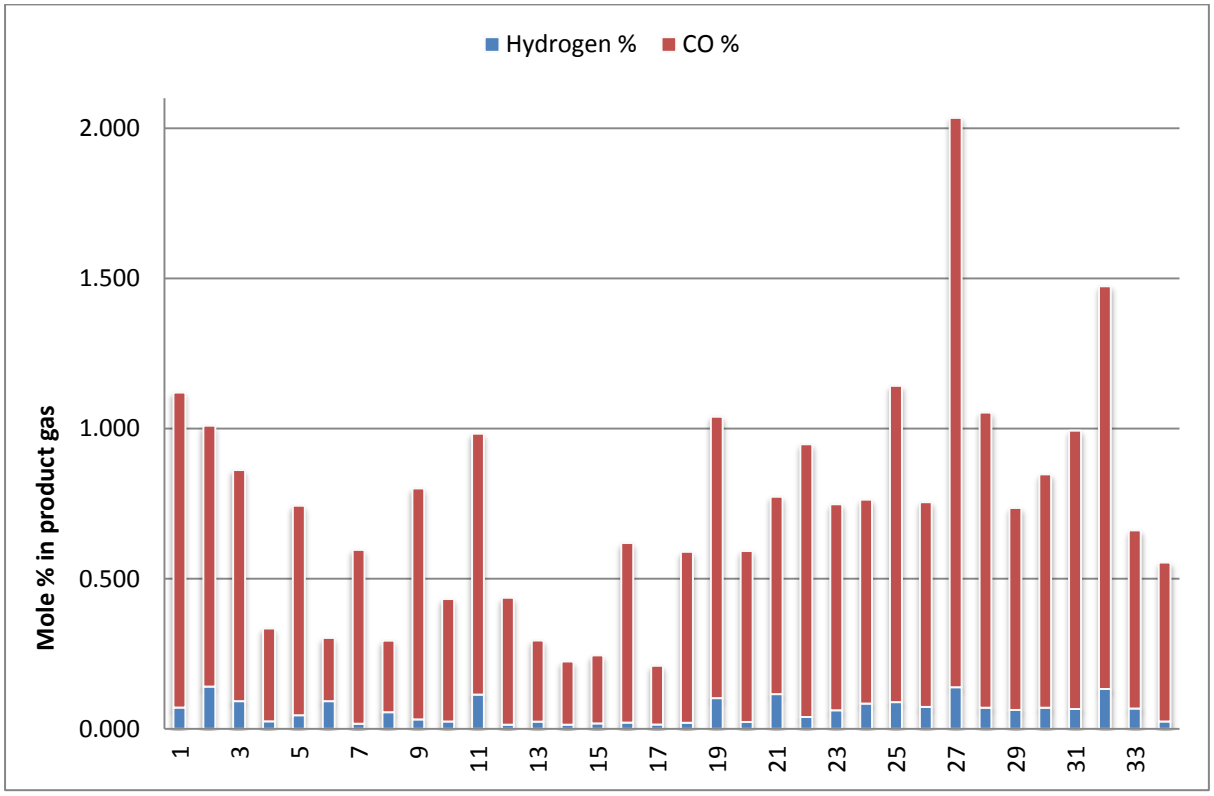

Figure 26: Product Gas Contributions during Sonochemical Experimental Runs

The average ratio of H_2/CO was found to be 0.09 with a minimum ratio at 0.03 and maximum at 0.44. The desired ratio is between 1 and 2, depending on the required products (Li, Song, Ma, & Zhao, 2012). At a solubility of 0.002 g hydrogen/gram of water at 0 °C (Fuel.com, 2008), it is unlikely that the produced hydrogen was dissolved in the water content of the sludge due to the fact that sonication also induces degassing of the liquid. Hydrogen molecules also have a tendency to escape from systems due to the small molecule size. The Tedlar bags used are said to have a low hydrogen permeability of 150 cc/(100in^2)(24hrs). Carbon dioxide in tedlar bags has a permeability of

11.1 cc/(100in^2)(24hrs)and nitrogen has a permeability of 0.25 cc/(100in^2)(24hrs) (Peters, 2003). Based on the gas spending 1 hour in the Tedlar bags before it is analysed, 1.94 ml of the hydrogen would have escaped the bag based on the bags size of 10 by 10 cm. Using the same exposure conditions, 0.144 mL of the carbon monoxide could have escaped based on the permeability of carbon monoxide in the Tedlar bag. As a result, it is expected that more of the hydrogen permeated out of the bag than the carbon monoxide. After multiple uses, the septum on the syringe also posed a potential area where the gas sampling bag could leak from.

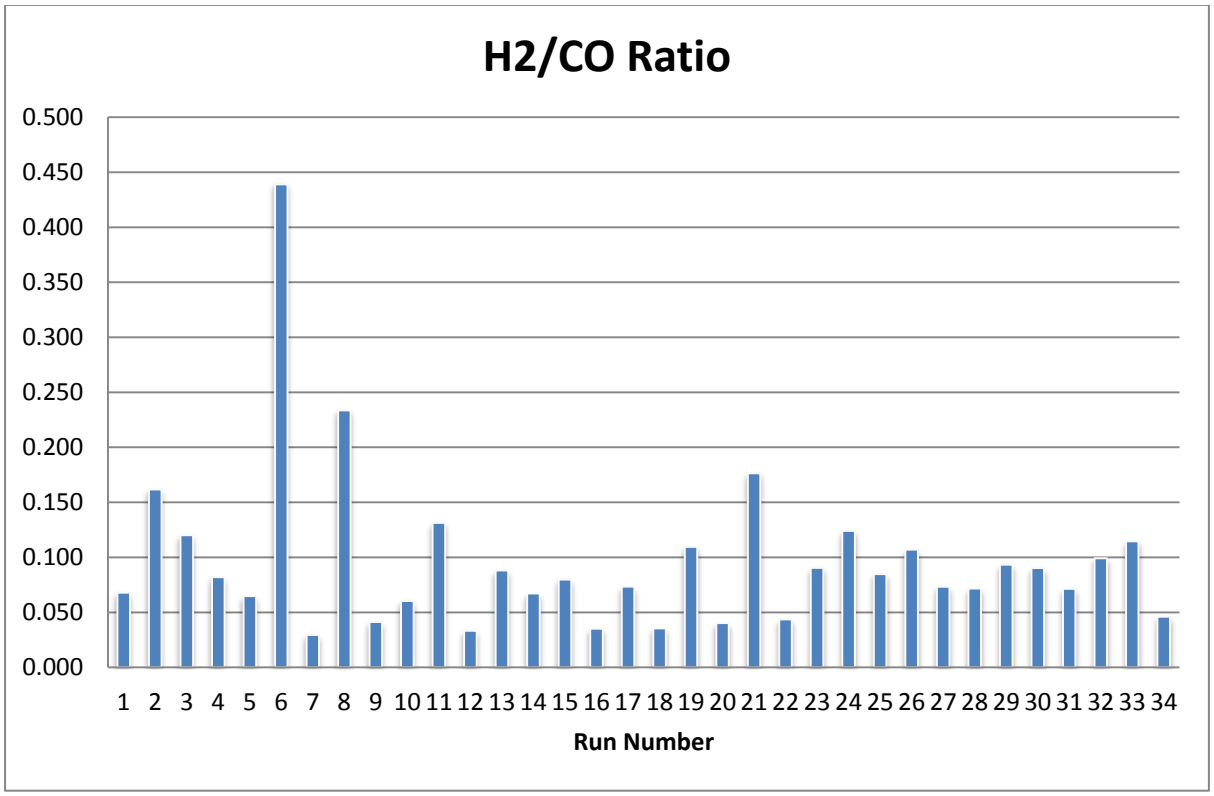

Figure 27: Hydrogen to Carbon Monoxide Ratio for Sonochemical Experimental Runs

The presence of the inert purging gas, argon, was excluded from Figure 28 to show the distribution of oxidation product gases. During purging of the reactor, an acceptable limit for the presence of air was set 4.84 mole % nitrogen that would correspond to less than 1.3 mole % oxygen in the system.

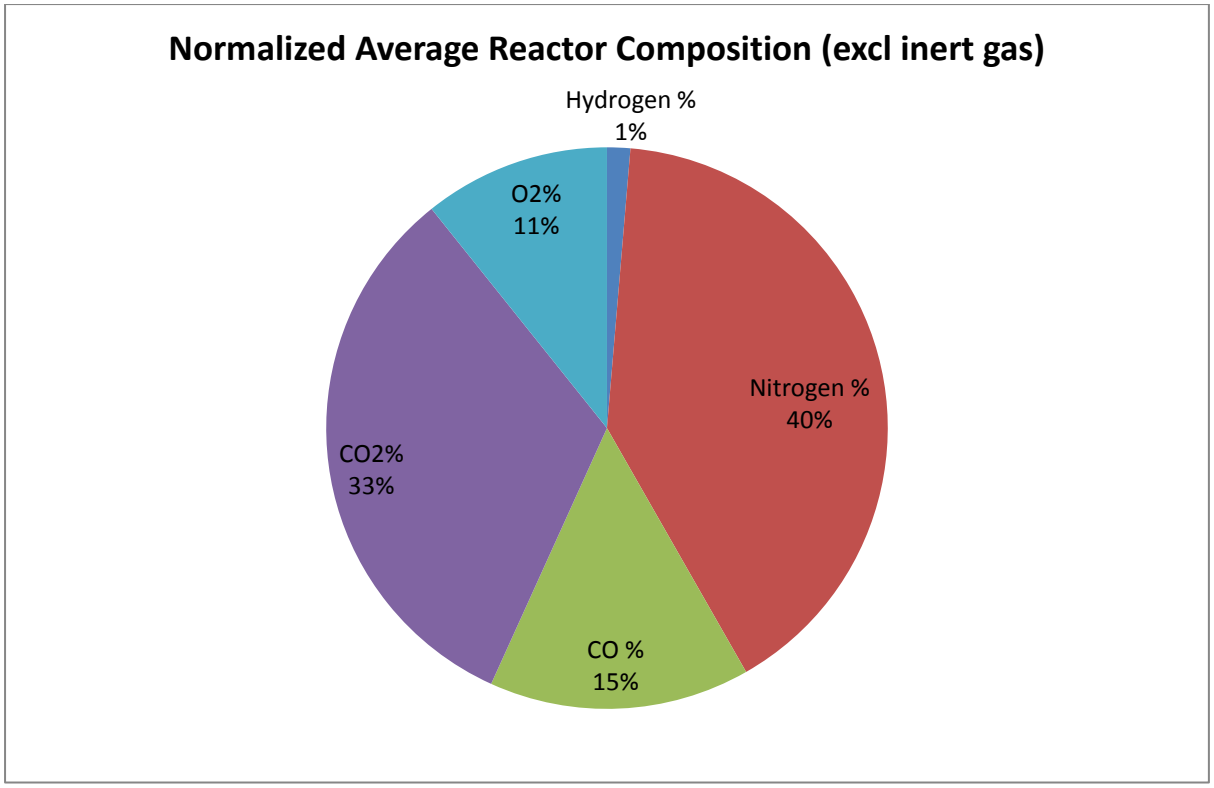

Figure 28: Normalized Average Reactor Composition after Sonochemical experiments excluding Argon as inert gas

Due to the extensive argon bubbling prior to commencing the experiment and the solubility of oxygen in water being 0.28 g/kg water at 2 bar, it was assumed that no oxygen was dissolved in the sludge water fraction. Oxygen is present in air at 21% and the presence of nitrogen in the reactor cavity above the liquid therefore confirms the presence of oxygen in the same ratio as air. The oxygen present in the system due to the air impurity would be used to sustain partial oxidation.

Table 11: Gas Composition Errors and Standard Deviations

	Hydrogen %	Nitrogen %	CO %	CO_2%	O_2%	Argon%
Average	**0.06**	1.72	0.66	1.34	0.46	92.82
Std Dev	**0.037**	1.0	0.36	1.52	0.27	16.63

As discussed in chapter 11, the reactor system was designed to emit an ultrasonic intensity per area of be 1.44 W/cm^2. To determine if the system was reaching the designed intensity, the power reading on the UP400S equipment was measured and divided by the internal exposed surface area of the reactor. In Figure 29, the calculated intensity is plotted at the experimental pressure. The average intensity for each run was taken and divided by the internal area of the reactor. In Figure 29 five sets of points can be seen against each of the investigated pressures. The slope between the

point at a pressure of 1 bar and the point at a pressure of 3 bar, increases slightly. This therefore indicated that the pressure, at which the system is operated, influenced the intensity that is delivered to the reactant to a very small degree. The line at a y-value of 1.44 represents the designed intensity of the system.

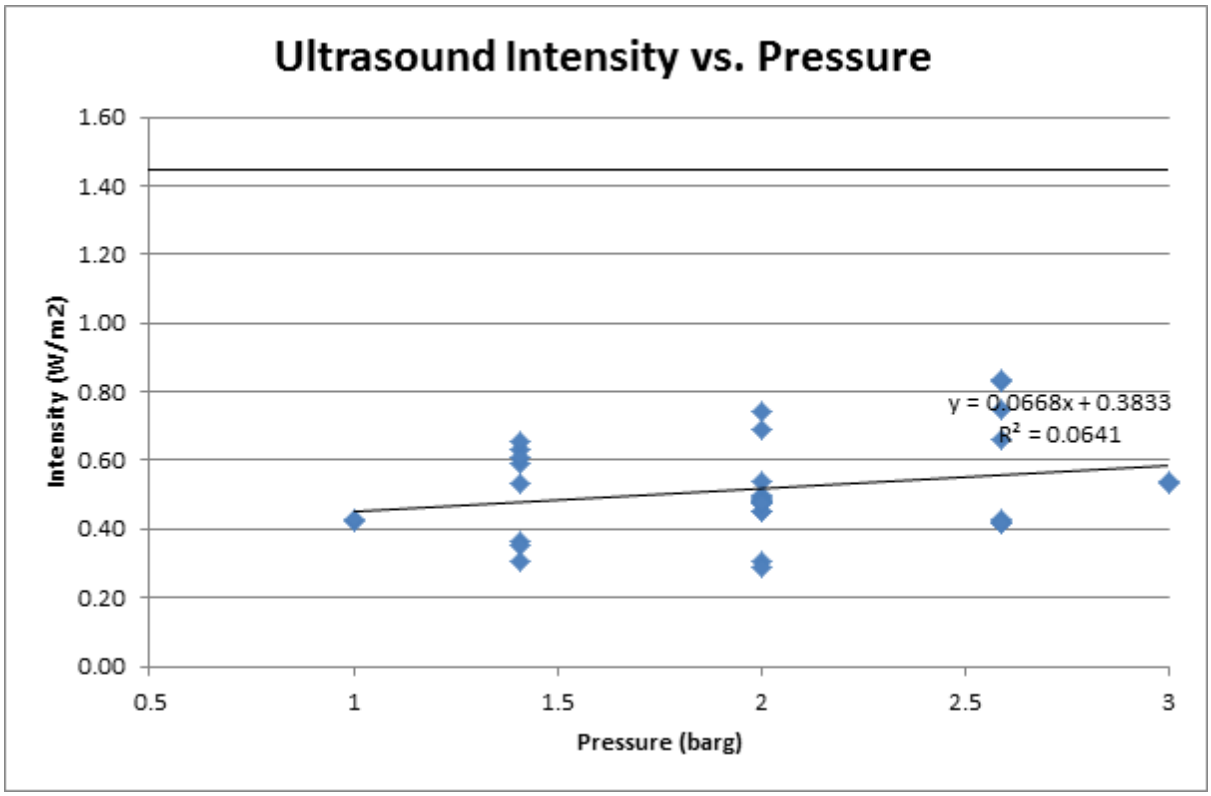

Figure 29: Ultrasound delivered Intensity and Pressure correlation during Sonochemical Experimental Runs

Due to the variation in intensity at a specific pressure, it was determined that pressure is not the most significant factor that affects the intensity delivered to the system. The amplitude of operation was an indication of the height of the sound wave that is being emitted. As a result, it is directly proportional to the power supplied to the system.

In Figure 30, the intensity is plotted against the amplitude settings for all the runs. It can be seen that there are still some outliers above the trend line, but an increasing trend is observed for all amplitudes. The amplitude of operation therefore influenced the ultrasound intensity emitted to the reactants. Another factor that could potentially affect the intensity is that when vibrations are transferred to the reactor flange, energy is transferred into the reactor flange and not into the probe

tip. This could potentially explain the large discrepancy between the design intensity and the actually intensity of the system.

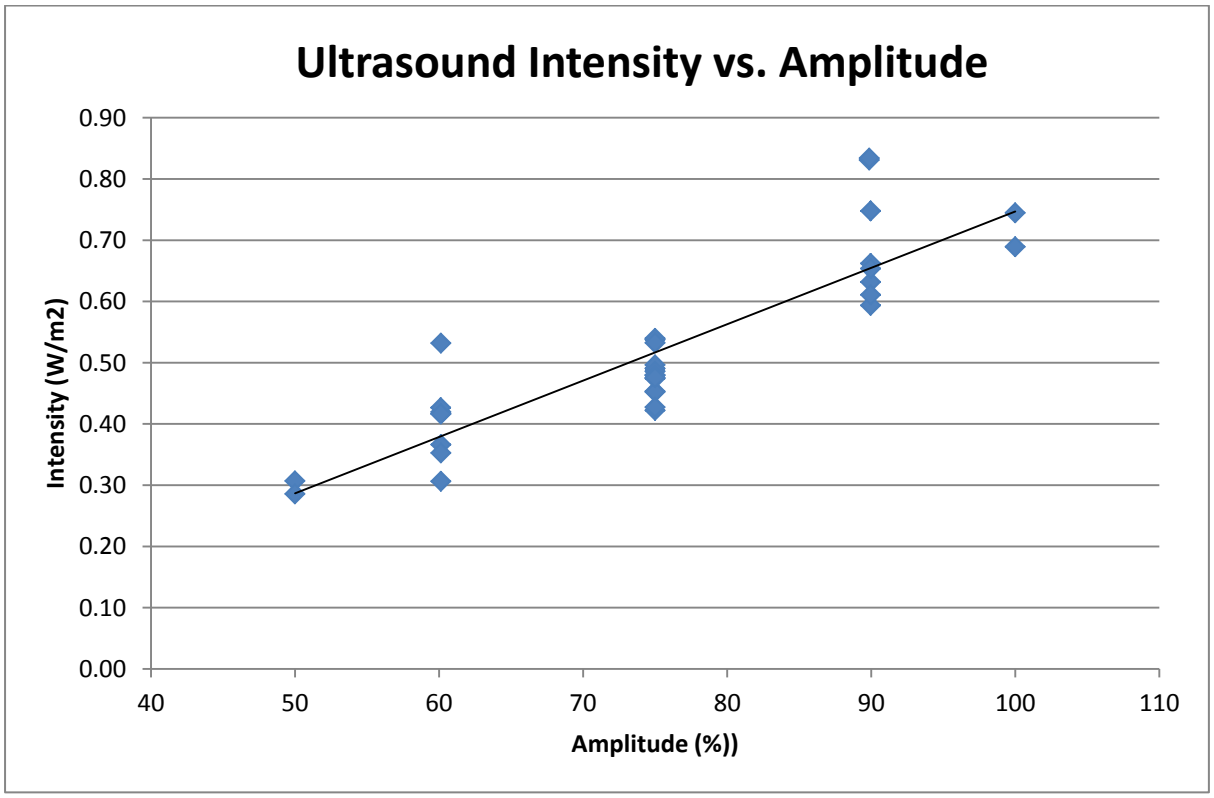

Figure 30: Ultrasound Delivered Intensity and Amplitude Pressure correlation during Sonochemical Experimental Runs

A summary of the results obtained during the experiments conducted can be found in Table 12. The experiments were sorted according to the central composite design order to illustrate which experiments were conducted at the same conditions. It can be seen that all experiments were conducted at least twice according to Table 12. The run number that has been used in the discussion of this study refers to the Experiment number in Table 12. The gas composition inside the reactor was indicated as well as the change in pressure and temperature for each run. The last six experiments were conducted at the central point of the central composite design and shows acceptable repeatability with an average hydrogen production of 0.04 mole% and the average carbon monoxide production was 0.47 mole %.

Table 12: Summary of results

Experimental Run Design							Reactor Contents after experiment							
DE Order	Experiment Number	Date	Pressure (barg)	Time (min)	Amplitude	Concentration	Hydrogen %	Nitrogen %	CO %	CO2%	O2%	Argon%	Δ T (°C)	Δ P (barg)
1	4	3/10/2013	1.41	12.03	60.13	2/3	0.025	1.390	0.309	1.142	0.369	96.765	0.5	0.1
2	15	10/10/2013	1.41	12.03	60.13	2/3	0.018	4.302	0.227	0.351	1.144	93.959	1	0.23
3	34	21/10/2013	2.59	12.03	60.13	2/3	0.024	0.814	0.530	0.323	0.216	98.092	1.5	0.23
4	7.1	23/10/2013	2.59	12.03	60.13	2/3	0.017	0.971	0.579	0.236	0.258	97.939	2	0.26
5	9.1	23/10/2013	1.41	17.97	60.13	2/3	0.032	1.436	0.769	0.220	0.382	97.163	1.5	0.29
6	3	2/10/2013	1.41	17.97	60.13	2/3	0.092	6.156	0.770	2.606	1.636	88.741	2.7	0.3
7	23	19/10/2013	2.59	17.98	60.12	2/3	0.062	0.963	0.686	4.259	0.256	93.775	2.5	0.27
8	31	20/10/2013	2.59	17.97	60.13	2/3	0.066	0.931	0.927	0.992	0.248	96.836	2	0.26
9	29	20/10/2013	1.41	12.03	89.97	2/3	0.063	1.233	0.673	1.558	0.328	96.145	3	0.35
10	26	20/10/2013	1.41	12.03	89.97	2/3	0.073	1.773	0.682	2.450	0.471	94.551	0.7	0.34
11	6	3/10/2013	2.59	12.03	89.87	2/3	0.092	3.015	0.211	0.770	0.801	95.111	2.5	0.49
12	2	2/10/2013	2.59	12.03	89.87	2/3	0.141	0.780	0.869	5.810	0.207	92.194	2.5	0.45
13	32	21/10/2013	1.41	17.97	89.97	2/3	0.133	2.179	1.341	0.912	0.579	94.855	2.5	0.35
14	11.1	23/10/2013	1.41	17.97	89.97	2/3	0.114	1.052	0.869	0.156	0.280	97.529	2.5	0.34
15	19.1	11/10/2013	2.59	17.97	89.97	2/3	0.103	1.339	0.937	0.191	0.356	97.074	3	0.33
16	21	19/10/2013	2.59	17.97	89.97	2/3	0.116	1.915	0.657	5.240	0.509	91.562	4	0.46
17	30	20/10/2013	1	15.00	75	2/3	0.070	4.372	0.777	1.360	1.162	92.259	2	0.3
18	27	20/10/2013	1	15.00	75	2/3	0.139	2.214	1.896	2.011	0.588	93.152	1.5	0.21
19	14	9/10/2013	3	15.00	75	2/3	0.014	2.245	0.210	1.062	0.597	95.872	2	0.4
20	12	9/10/2013	3	15.00	75	2/3	0.014	1.105	0.422	1.812	0.294	96.352	2	0.4
21	18.1	10/10/2013	2	10.00	75	2/3	0.020	1.007	0.569	0.065	0.268	98.072	1.5	0.3
22	20	11/10/2013	2	10.00	75	2/3	0.023	1.012	0.569	0.000	0.269	98.127	1	0.1
23	1.2	23/10/2013	2	20.00	75	2/3	0.071	1.857	1.049	0.765	0.494	95.765	0	0.29
24	33	21/10/2013	2	20.00	75	2/3	0.068	1.408	0.593	0.438	0.374	97.119	3	0.3
25	16.1	23/10/2013	2	15.00	50	2/3	0.021	1.130	0.598	0.000	0.300	97.951	1.5	0.2
26	22	19/10/2013	2	15.00	50	2/3	0.040	1.058	0.908	3.757	0.281	93.957	1.5	0.2
27	24	19/10/2013	2	15.00	100	2/3	0.084	0.766	0.679	6.010	0.204	92.258	5	0.33
27	25	24/10/2013	2	15.00	100	2/3	0.089	2.498	1.053	0.193	0.664	95.504	3	0.3
29	28	20/10/2013	2	15.00	75	2/3	0.070	1.285	0.983	1.664	0.341	95.656	1.5	0.23
30	5.1	23/10/2013	2	15.00	75	2/3	0.045	1.178	0.698	0.349	0.313	97.417	2	0.29
31	17	10/10/2013	2	15.00	75	2/3	0.014	3.137	0.196	0.093	0.834	95.726	2	0.28
32	13	9/10/2013	2	15.00	75	2/3	0.024	3.731	0.270	0.889	0.992	94.095	2.3	0.4
33	10	7/10/2013	2	15.00	75	2/3	0.025	1.117	0.408	1.509	0.297	96.646	2.6	0.3
34	8	4/10/2013	2	15.00	75	2/3	0.056	0.910	0.238	0.881	0.242	97.674	1.5	0.31

16. Mass- and Energy Balance

Mass Balance

A mass balance was conducted on the system utilizing the conditions and results from the maximum time experiment at the optimum reaction conditions. This was selected as the basis for the mass balance as the most significant change in the reactant would be observed under these conditions.

The system was operated as a batch system and the mass balance was conducted accordingly. The analysis from the representative samples used in the sludge characterization tests were used as the initial conditions for the batch system. Ideally the analysis would have been repeated on all product samples, but due to certain constraints this testing was only conducted on the experimental run at the maximum possible time and optimum reactor conditions to serve as an indication of the maximum possible change.

The following analyses were required for the initial and final conditions:

1. Elemental Analysis
2. Higher Heating Value
3. Oven Dry Weight

Initial conditions:

The initial composition of the gas was measured by TCD and FID with methanizer on the GC after purging of the system using argon gas. The elemental composition of the solid was measured using light elemental analysis. The higher heating value was determined using a bomb calorimeter. The ash content was determined using Thermogravimetric analysis (TGA).

The composition of the gas phase at initial reaction conditions was calculated using the generalized compressibility chart for non-ideal gas mixtures. Kay's rule was used to calculate the pseudo-critical temperature and pressure for the gas mixture. It was assumed that the reactor contents was at a temperature of 10 °C at the start of the experiment and the reactor was at a pressure of 3.543 atm absolute. The assumption for the temperature for the reactor contents is based on the measured water temperature inside the reactor during the initial trial experiments to establish the gradient between the reactor temperature and the cooling batch temperature. Refer to Figure 18 where it can be seen that the estimated reactor temperature is at 10 °C after cooling for 30 minutes (during the purging process).

The compressibility factor of the vapour phase was calculated to be 0.88. This value was used to calculate the total moles of gas present in the beginning of the experiment.

Final conditions:

As no elemental analysis was conducted on the solid after the 40 minutes kinetic run, the elemental analysis data from Van Baarsel (2013) at optimum conditions was used. This assumption was validated by comparing the actual measured HHV during the experiment with that of the theoretical calculated HHV based on the elemental composition by Van Baarsel (2013).

By utilizing the theoretical correlation by Sokhansanj (2011), the HHV was calculated using the elemental composition as suggested in Table 13.

$$HHV = 0.349x_C + 1.1783x_H - 0.1034x_O - 0.0151x_N + 0.1005x_S - 0.0211x_S \quad \text{eq (28)}$$

$$HHV_{calc} = 0.349(0.2490) + 1.1783(0.0331) - 0.1034(0.2584) - 0.0151(0.0291) + 0.1005(0.0056) - 0.0211(0.4248) = \mathbf{9.43\ MJ/kg}$$

The measured actual HHV for the 40 minute kinetic run was **9.54 mJ/kg**. This represents a 1.27% error which was deemed acceptable for mass balance calculations.

The reactor temperature was estimated using the temperature change in the cooling water bath as reference. This temperature change was added to the initial estimate of 10 °C which resulted in the reactor temperature being 16.5 °C at the end of the experiment. The measured final reactor pressure of 3.95 atm absolute was used as a basis for the calculations.

Kay's rule was used to calculate the pseudo-critical temperature and pressure of the gas mixture. Newton's correction was used to calculate the critical temperature and pressure of hydrogen. The calculations resulted in a compressibility factor of 0.82 at the end of the experiment.

Using the compressibility factor of 0.82, the total number of moles in the gas phase could be calculated. With the gas composition known, the amount of moles of each gas could be calculated. For the detailed calculations, please see Table 13.

Assumptions:

- No water vapour was generated during the experiment

- Only argon, oxygen and nitrogen were present in the vapour phase at the beginning of the experiment.
- The average C, H, N, O, S values from the representative samples were valid for this specific experiment
- The average HHV values from the representative samples were valid for this specific experiment
- As no elemental analysis was conducted for the 40 minute kinetic run, it was assumed that the elemental analysis from the work conducted by Van Baarsel (2013) at the same conditions would be representative of the elemental composition of the conducted experiment. This assumption was validated by calculating the theoretical HHV using Van Baarsel's (2013) elemental and comparing with the measured HHV.

Table 13: Mass Balance – 40 minute kinetic run as basis

Before Experiment			Volume	Mass (g)	Mw (g/mol)	Moles
Gas						0.02
Liquid				196.06		10.88
Solid				4.21		0.38
N2	2%	Gas			28.01	0.00
O2	0%	Gas			32	0.00
Argon	98%	Gas			39.95	0.02
C	26.47%	Solid		1.11	12.01	0.09
H	4.22%	Solid		0.18	1.01	0.18
N	4.06%	Solid		0.17	14.01	0.01
O	27.75%	Solid		1.17	16	0.07
S	1.85%	Solid		0.08	32.07	0.002
Ash	35.65%	Solid		1.50	56.08	0.03
Water		Liquid		196.06	18.02	10.88
After Experiment			Volume	Mass (g)	Mw (g/mol)	Moles
Gas						0.02
Liquid				196.06		10.88
Solid				3.56		0.28
N2	3.68%	Gas			28.01	0.00
O2	2.60%	Gas			32	0.00
Argon	85.07%	Gas			39.95	0.02
C	24.90%	Solid		0.89	12.01	0.07
H	3.31%	Solid		0.12	1.0	0.12
N	2.91%	Solid		0.1	14.0	0.01
O	25.84%	Solid		0.92	16	0.06
S	0.56%	Solid		0.02	32.07	0.00
Ash	42.48%	Solid		1.51	56.08	0.03
CO	1.65%	Gas			28.01	0.000
CO2	0.32%	Gas			44.01	0.000
H2	0.57%	Gas			2.02	0.000
Water		Liquid		196.06	18.02	10.88
Reactor Total Volume	330.17	ml				
Gas Volume (incl pipes)	120.17	ml				

Energy Balance

The energy balance on the system was conducted to establish the energy required per specific amount of syngas produced. Due to the fact that very little is known regarding the exact reactions taking place, a simplified energy balance was conducted taking the energy supplied to the system from ultrasound and the cooling supplied to the system into account. The difference between these values indicated the internal energy of the system.

In Figure 31, the average ultrasound power input per amplitude setting is illustrated. A general decrease was observed in the power supplied to the system over time. This could potentially be due to the increase in pressure over time as the biomass reacts. The higher the pressure in the system, the more energy is required to achieve cavitation (Santos, Lodeiro, & Capelo-Martinez, 2009). Due to the fact that the amplitude was fixed for each run, the supplied power decreased as pressure increased.

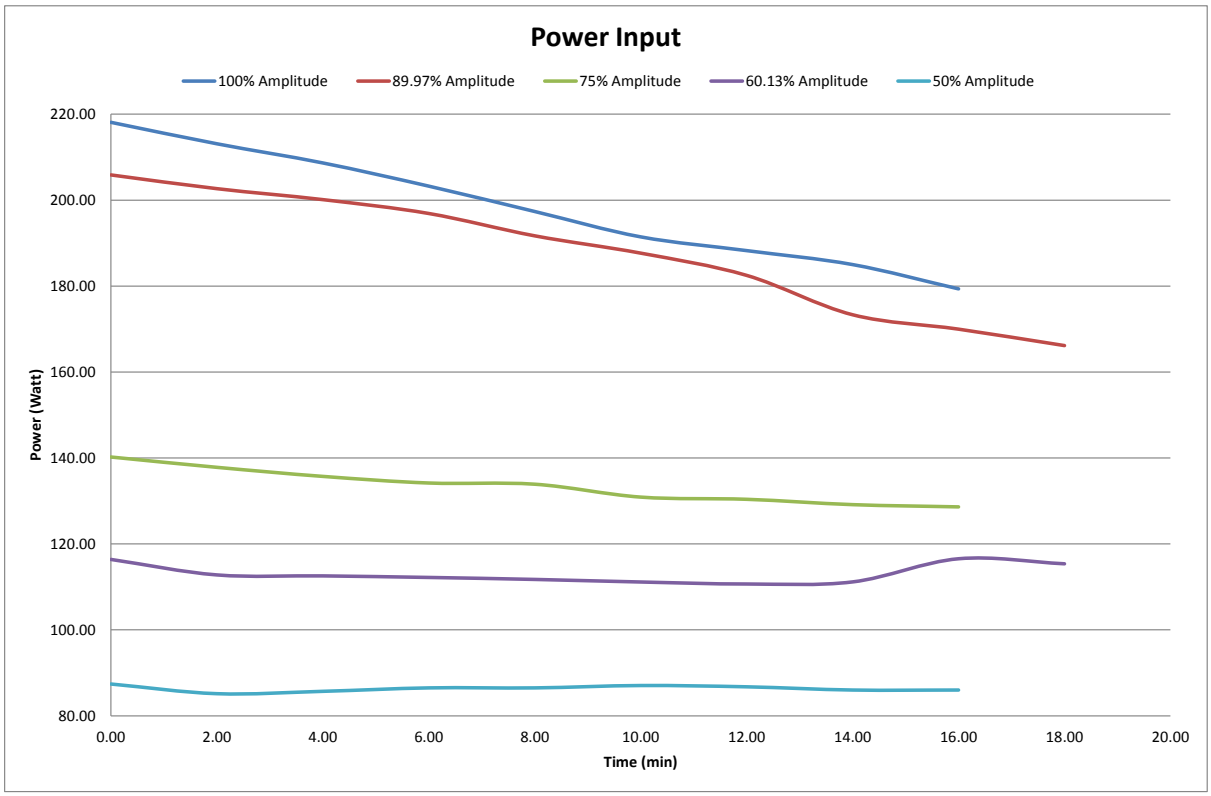

Figure 31: Ultrasound power input during 40 minutes kinetic run at optimum conditions

To conduct and energy balance on the system, the 40 minute kinetic run was utilized to combine the mass balance production values with the energy balance to obtain the cost of syngas in R/Nm^3.

After considering the system, it was found that the general energy balance equation could be reduced to eq (29) as no kinetic or potential energy is involved in the system.

$$\Delta U = Q - W \qquad eq\ (29)$$

Utilizing this definition, heat was defined as positive when it is transferred to the system and work was defined as positive when it is done by the system on the surroundings (Felder & Rousseau, 2005).

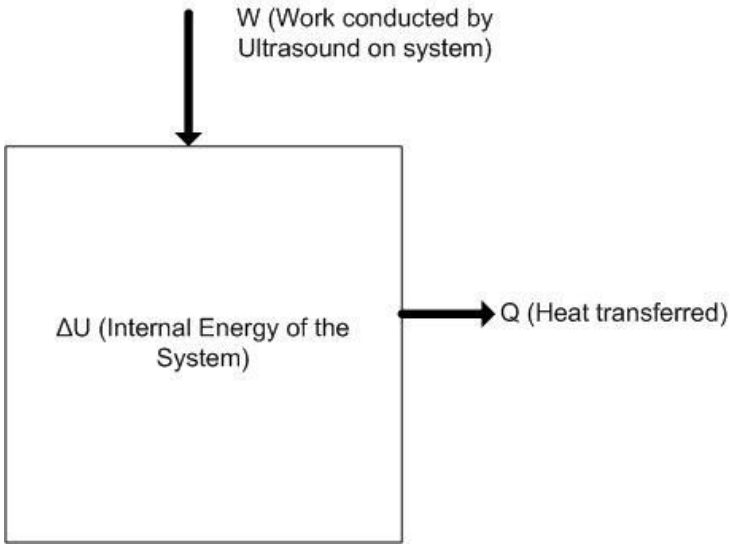

Figure 32: Energy Flow of Sonochemical Reactor System with Cooling

To calculate the cumulative energy over a 40 minute time period as illustrated by Figure 33, the area under the graph was integrated. It was found that the integral area was 71478 W.s, which relates to 0.002 kWh.

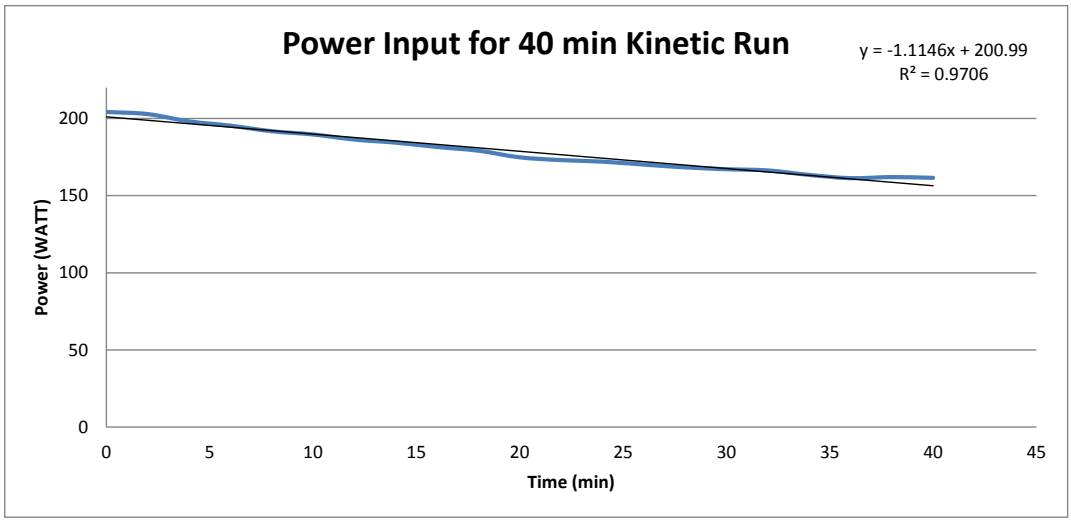

Figure 33: 40 min Kinetic Run Power Input at optimum conditions

The energy removed by the cooling water bath was calculated and an average cooling rate was determined as the cooling liquid flow rate remained constant. The energy supplied to the cooling water bath also remained constant. This average cooling rate was then also integrated over the 40 minute time period to obtain a kWh value for the cooling system. The calculation can be seen in Table 14. The data from Figure 18 was used to determine the temperature difference when no

reaction is taking place and only water is present in the reactor. Nine different temperature measurements were taken and the energy removed was calculated for each temperature measurement. The average was then calculated and can be seen in Table 14 as Qave. The straight line equation in Figure 33 was then used to integrate over time to obtain $\dot{Q}ave$ as a rate.

Table 14: Energy Removed by Cooling Water

Q=kA(T1-T2)/L		Units
A - constant	0.00251	m^2
K - constant	13.4	W/m.K
Q1	3.37	W
Q2	6.74	W
Q3	6.74	W
Q4	8.42	W
Q5	6.73	W
Q6	5.05	W
Q7	3.37	W
Q8	3.37	W
Q9	6.74	W
Qave	**5.61**	**W**
$\dot{Qave}$	**0.000062**	**kWh**

The internal energy calculation results can be seen in Table 15 to have a negative value. This is consistent with the fact that energy is transferred from the system to the surroundings in the form of heat.

Table 15: Internal Energy Calculation

$\dot{Qave}$	0.000062	kWh
W	0.002	kWh
ΔU	-0.002	kWh

$$Cost\ of\ syngas = \frac{Energy\ into\ reaction\ \times cost\ of\ electricity}{volume\ of\ syngas\ produced} \qquad eq\ (30)$$

The volume of syngas produced during the 40 minute kinetic run, was calculated using the ideal gas law and the corresponding z-factor. The volume of gas produced during the 40 minute kinetic run was 0.0001 Nm^3. If the cost of electricity is taken as R1.21/kWh (Mid Year Pricing Determination, 2013) and the total energy required from work and cooling into the system is 0.002 kWh, the cost of syngas production equates to R 19.98/Nm^3. This cost only takes operational costs in the form of

energy required into account and does not account for initial capital investment for the construction or the cost of any additional downstream processing into account. The downstream processing equipment could CO and CO_2 treatment as well as a compressor to attain the downstream required process pressure.

17. Kinetics

The maximum hydrogen and carbon monoxide molar percentages in the product gas were investigated. The maximum value for hydrogen was 0.114 mole % in the product gas at a pressure of 1.41 barg, 17.97 minutes and 90% amplitude. These pressure, temperature and amplitude settings are a function of the original central composite design. The maximum production of carbon monoxide was found to be at 1 barg, 15 minutes and 75 % amplitude with a value of 1.9 mole % in the product gas. The second highest value for carbon monoxide was found to be 1.3 mole % at a pressure of 1.41 barg, 17.97 minutes and 90% amplitude – corresponding directly to the maximum yield of hydrogen in the product gas. These values can be seen in Table 12. The optimum conditions to maximize the production of hydrogen and carbon monoxide simultaneously were found to be 2.59 barg, 17.89 minutes and 90% amplitude. These conditions were used to determine the change in the composition of the products over time. Four separate experiments were conducted at 5 minutes, 10 minutes, 20 minutes and 40 minutes. The gas products were analysed to investigate the system kinetics.

In Figure 34, the molar hydrogen percentage in the product gas was plotted over time. As no hydrogen is present before the start of the experiment, it was decided to use the concentration of hydrogen at the end of the experiment as the basis for the empirical correlation.

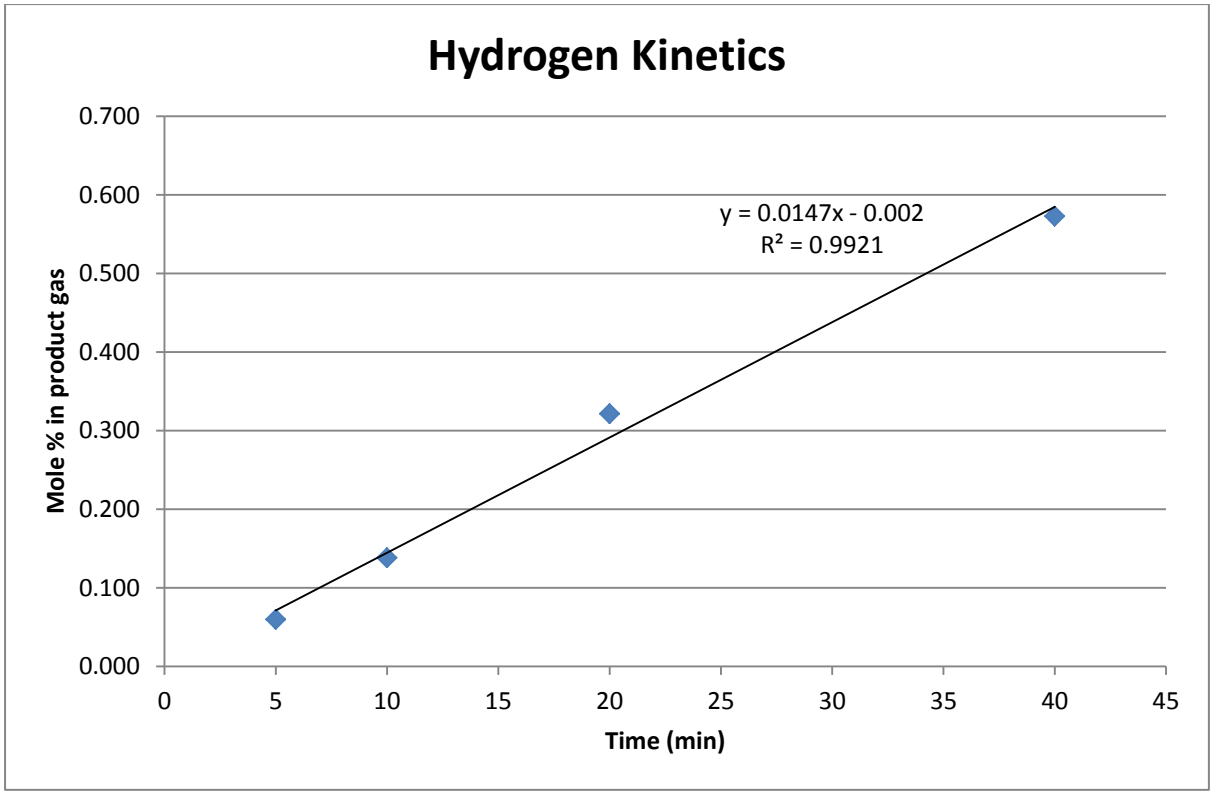

Figure 34: Hydrogen zero order Kinetics at optimum conditions

The straight line correlation in Figure 34 was an indication that zero-order kinetics governs this reaction system. The slope of the straight line is therefore the rate constant. An R^2 equal to 0.9921 indicates that this empirical correlation presents a good prediction of the system kinetics:

$$[A] = -kt + [A]_O \qquad eq\ (31)$$

Empirical correlation to describe hydrogen production:

$$\left[C_{H_2}\right] = k_{H_2} t + \left[C_{H_2}\right]_O \qquad eq\ (32)$$

$$\left[C_{H_2}\right] = 0.0146t \qquad eq\ (33)$$

where $\left[C_{H_2}\right]$ is in mole % and t in minutes and the slope is equal to the rate constant.

The intercept of the line was at a value zero mole % hydrogen. This is an indication that no hydrogen is present in the beginning of the experiment. This is confirmed by the lack of a hydrogen peak in the analysis of the final purge gas composition that is conducted before each experiment.

The same analysis was conducted for the production of carbon monoxide and the results can be seen in Figure 25. The carbon monoxide concentration was analysed using the FID with methanizer on the GC. This resulted in some deviation in the amount of gas injected for each analysis. An outlier is observed at 20 minutes and this was expected to be due to an injection error. The experiment could not be repeated as no sludge was available as feed.

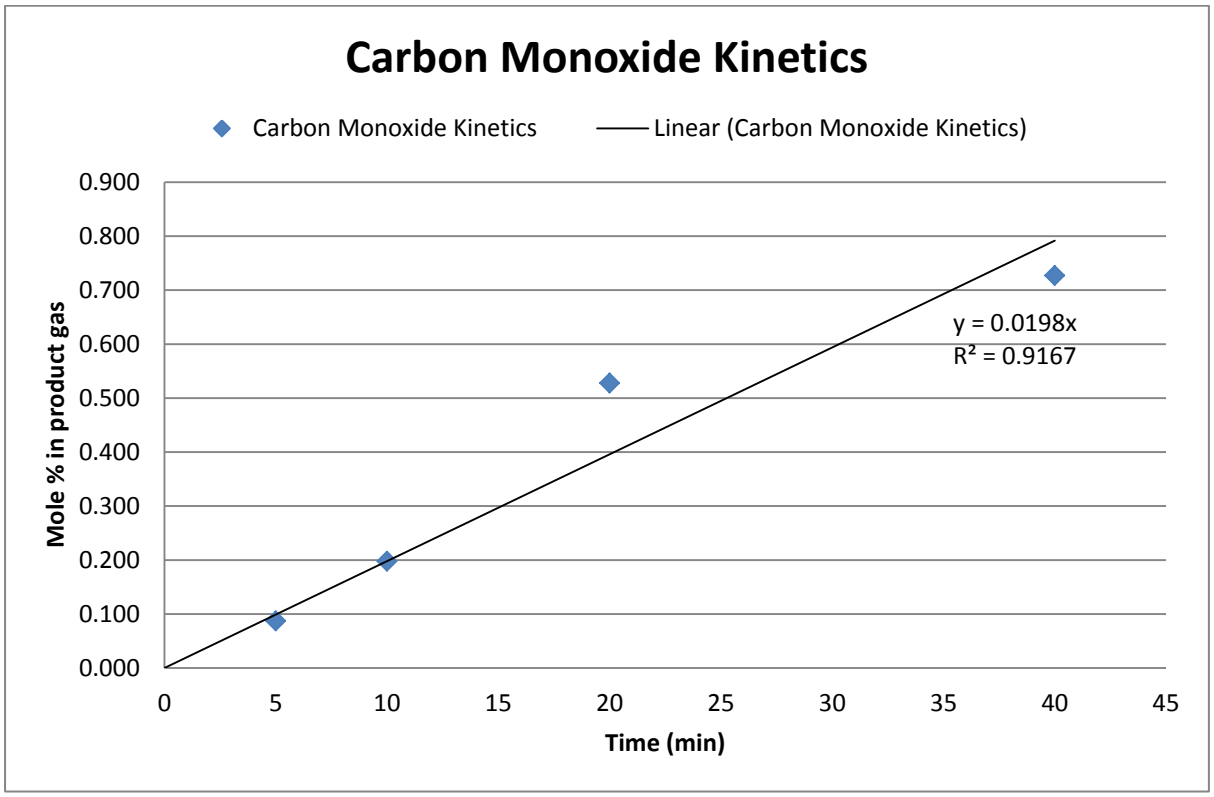

Figure 35: Carbon Monoxide zero order Kinetics at optimum conditions

Even with the outlier present, a relatively good match was still obtained using the 3 data points in Figure 35. An R^2 value of 0.92 was observed. The intercept is zero as no carbon monoxide was present initially in the reactor.

The system kinetics can therefore be described as:

$$[A] = -kt + [A]_O \qquad eq\ (34)$$

Empirical correlation to describe carbon monoxide production:

$$[C_{CO}] = k_{CO}t + [C_{CO}]_O \qquad eq\ (35)$$

$$[C_{CO}] = 0.0198t \qquad eq\ (36)$$

where $[C_{CO}]$ is in mole % and t in minutes and the slope is equal to the rate constant.

Due to the trend observed in Figure 35, it was decided to also investigate first and second order reactions. When a reaction is considered first order, a plot of ln[CO] against time would yield a straight line with the intercept on the y-axis equal to $\ln[CO]_0$. For a second order reaction, a plot of 1/[CO] against time would yield a straight line with the intercept on the y-axis equal to $1/[CO]_0$.

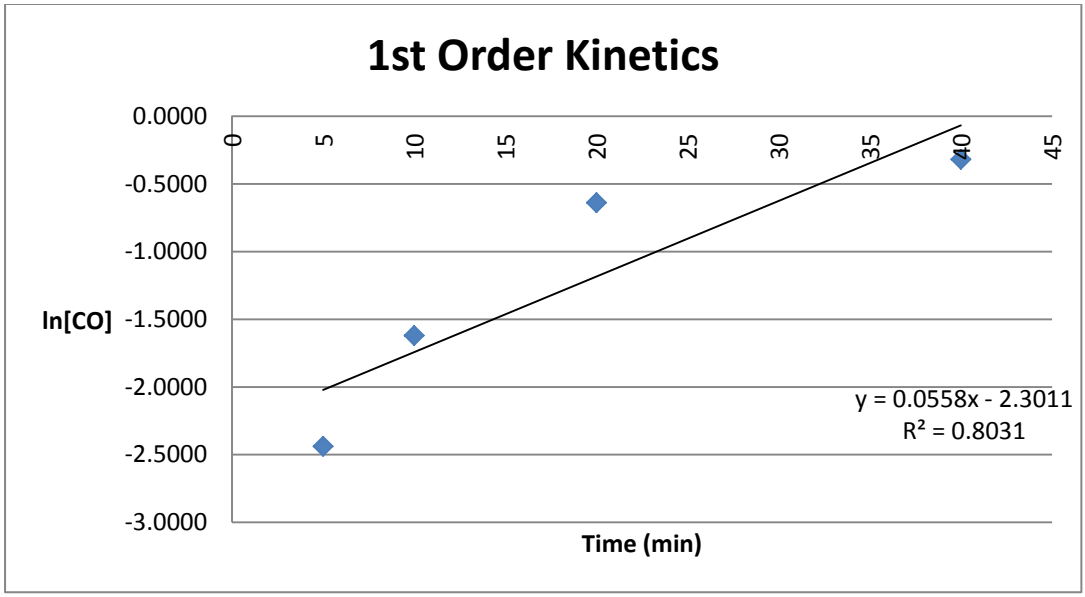

Figure 36: Carbon Monoxide 1st Order Kinetics at optimum conditions

In Figure 36 it can be seen that a plot of ln[CO] against time does not result in a straight line. An R^2 value of 0.8031 shows that there is significant scatter present in the results and that the approximation in equation (36) presents a more accurate presentation of the experimental data.

As the reaction was found to not be governed by first order kinetics, a second order model was investigated. In Figure 37 a plot of 1/[CO] against time shows that a linear trend was also not applicable. As the data is scattered and resulted in an R^2 value of 0.63, it can be concluded that the system was not governed by second order kinetics.

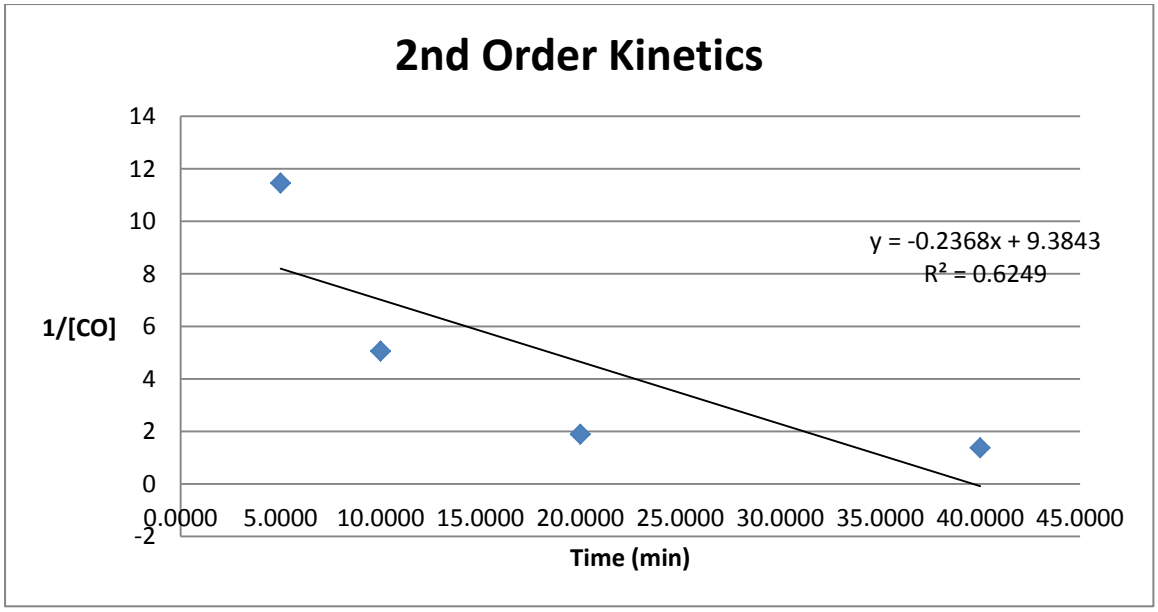

Figure 37: Carbon Monoxide 2nd Order Kinetics at optimum conditions

As it was found that neither first nor second order reactions are taking place after investigating Figure 36 and Figure 37, it can be concluded that the production of carbon monoxide is a zero order reaction and has a rate constant of 0.02 mole % CO/time.

18. Control Experiments

At the optimum conditions determined by the central composite design, it was decided to conduct some experiments to determine if the product gas composition is influenced by any external factors. It was decided to test distilled water as a control experiment and to test the product composition when sludge that had a zero HHV value is used as feed. This is termed “Old Sludge” in Figure 38. The results from these control tests were then compared with the product composition of the optimized factors of the current study. The reactor system was repeatedly flushed with distilled water; all residues was scrubbed off and pipes where flushed with argon. The reactor was then washed with acetone and dried using compressed air to ensure all impurities were removed from the reactor surface. This process was repeated between each experiment run in the set of control experiments. The student ensured, to the best of her ability, that the system was free from any residual sludge from the experiment conducted with sludge from sample batch-B. “New sludge optimum” refers to the maximum sludge production using sludge from sample batch-B.

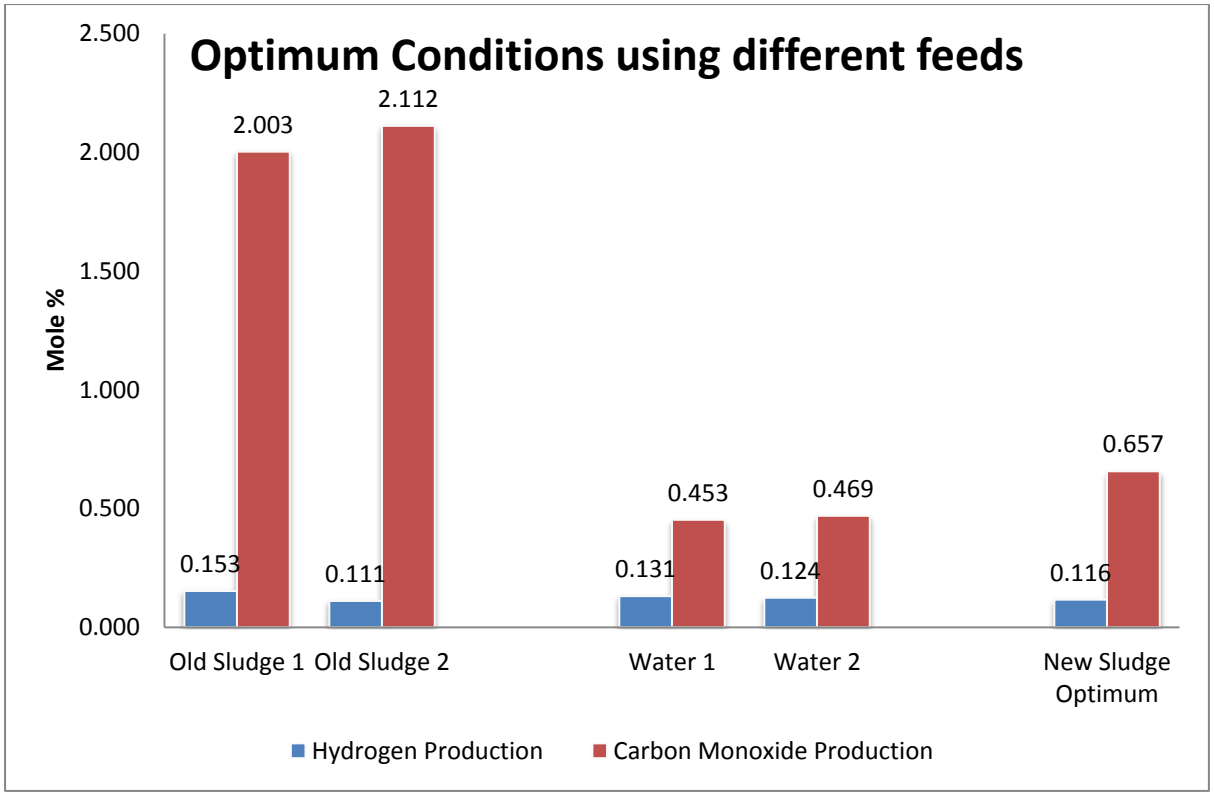

Figure 38: Results from Control Experiments using distilled water, previously sampled sludge as well as new sludge at optimum conditions

The "inactive" sludge was tested in two separate experiments to test repeatability. The product gas was found to contain 0.15 mole % hydrogen in the first experimental run and 0.11 mole % hydrogen in the second experiment. It can be seen in Figure 38 that the carbon monoxide production from the "inactive" sludge experiments was found to be 2.0 and 2.11 mole %. This value is more than double the result obtained during treatment of sludge from sample batch-B, as seen on the right hand side of Figure 38.

The distilled water run was repeated to test repeatability. The hydrogen mole % in the product gas was found to be 0.13 and 0.12 mole % and that of carbon monoxide was found to be 0.45 and 0.47 mole %. The hydrogen production for the "inactive" sludge, distilled water and for the optimal run using the "active" sludge varied between 0.11 mole % to 0.15 mole %. The mean was 0.13 mole % with a standard deviation of only 0.02 mole %. This indicates that very similar amounts of hydrogen were formed during all experimental runs during these control tests. As discussed in the literature review section of this report, water exposed to high intensity ultrasound undergoes sonolysis. This would result in the production of hydrogen and hydrogen peroxide. As the sludge consisted of 98% water, it is expected that the sonolysis of water would take place. Due to no

significant difference in the hydrogen concentration of the product gas utilizing different feed material, it can be concluded that all hydrogen production is as a result of the sonolysis of water and not due to the partial oxidation of biomass.

The carbon monoxide produced during the control experiments ranged from 0.45 mole % and 2.11 mole %. The average carbon monoxide was found to be 1.14 mole %, but with standard deviation of 0.84 mole %. With such a large standard deviation, the effects of carbon monoxide production cannot be ascribed to a single source. When considering the "inactive" sludge experiments, it was found that the sludge mostly consisted of lime that is used in the unit for pH control. Lime can be in the form of CaO or $CaCO_3$, depending on the conditions the lime has been exposed to. Calcium carbonate undergoes thermal decomposition and forms calcium oxide and carbon dioxide (Thermal Decomposition of Calcium Carbonate, 2013). The carbon dioxide produced during the thermal decomposition of the lime then undergoes the endothermic Boudouard reaction where carbon dioxide reacts with carbon to form carbon monoxide. See equation reaction 1 in Table 3.

The presence of carbon monoxide during the experiments using the "inactive" sludge is therefore not due to the partial oxidation of biomass, but the due to the thermal degradation of calcium carbonate and consequent Boudouard reaction at the extreme localized reaction conditions.

The amount of carbon monoxide produced using the "active" sludge is 0.2 mole % more than when only using water. Due to the relatively high HHV of the "active" sludge, it confirmed that the carbon monoxide formed was due to the partial oxidation of biomass. The presence of carbon monoxide at the end of the experiment using only distilled water can possibly be ascribed to an impurity analytical error due to exposing the methanizer to high carbon monoxide concentration. Some residual carbon monoxide from previous experiments could potentially remain in the system. Air also has a carbon monoxide level of 0.5-3 ppm and as a result, when the water was exposed to air, carbon monoxide could have dissolved in the water. The solubility of carbon monoxide in water is 0.044 g/kg water at 0 °C and 0.03 g/kg water at 18 °C. The temperature change in the reactor due to the cavitational events could have potentially allowed for the dissolved carbon monoxide to be released from the liquid phase as a result of the different solubilities at different temperatures. Another possible cause for the larger than expected result for carbon monoxide in the distilled water run, is the presence of organic carbon in the water. The total organic carbon (TOC) was not measured and as a result, could potentially be the cause for the presence of carbon monoxide in the

product gas after exposure to ultrasound. Tap water is expected to have a TOC up to 10mg/L. Distilled water was used in the experiments, but as no TOC measurement was taken, it cannot be ruled out as a possible cause. When the TOC is higher than 10 mg/L, it would result in a brownish tint to water, but it is not uncommon that levels up to 10mg/L appear clear in normal tap water.

19. Evaluation of Optimum Design

To establish if the process was optimized from a reactant concentration point of view, as opposed to the product gas concentration, the HHV was investigated in Figure 39. The higher heating values for samples B-6-2013, B-33-2013 and B-85-2013 represent the HHV of untreated sludge for sample batch B. The experiment that was expected to result in the largest change in reactant concentration was established to be the longest kinetic run at the optimum conditions as determined by the central composite design. This experiment was then used to compare the change in the HHV of the untreated and the treated sludge. A larger change in the HHV of the reactant would mean that more of the biomass component of the reactant has been utilized in the experiment.

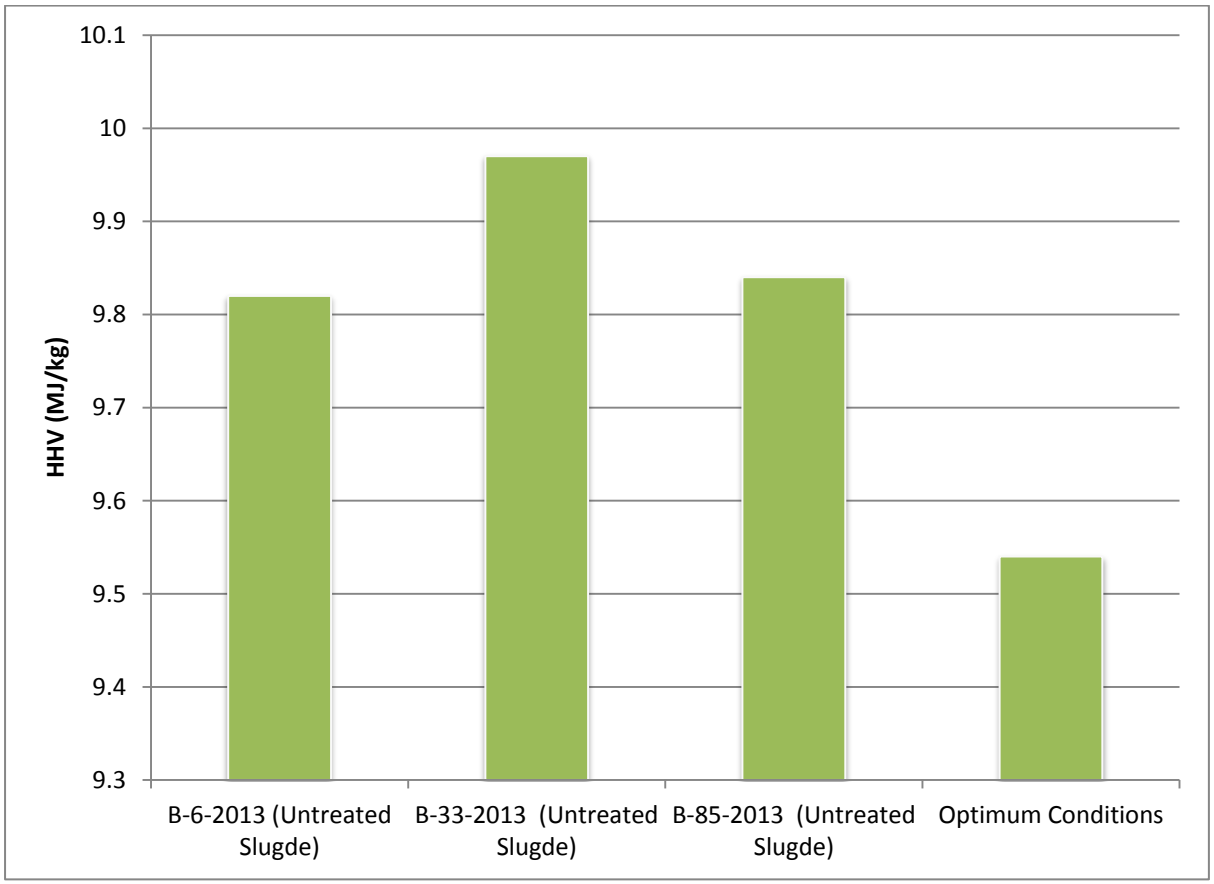

Figure 39: Higher Heating Value of untreated sludge and treated sludge at optimum conditions

In Figure 39 it can be seen that the average higher heating value for the untreated sludge was 9.81 mJ/kg with a standard deviation of 0.16 mJ/kg. The sludge treated at optimum conditions had a HHV of 9.54 mJ/kg, representing a change of 0.27 mJ/kg at the optimum conditions for the current experimental setup. Based on the unutilized energy of 9.54 mJ/kg still available in the treated sludge, the partial oxidation reaction did occur, but to a very limited extent. The biomass present in the sludge was not the limiting reactant due to its presence in the product. Oxygen was also not deemed the limiting reactant due to the formation of carbon dioxide. The extent of the reaction is, therefore, limited based on the design of the sonochemical reactor.

When considering the design of the sonochemical reactor as the extent limiting factor, several factors could have been involved. According to Santos et al. (2009), the parameters that affect ultrasonic cavitation include frequency, intensity, solvent, temperature, external pressure and direct or indirect ultrasonic application. These items were specifically discussed in chapter 2.6 under Reactor Design considerations. When studying the actual applied intensity based on the current reactor design, as seen in Figure 29 and Figure 30, it can be seen that the applied intensity was on average of 0.52 W/m^2 with a standard deviation of 0.14 W/m^2. The average applied intensity is 0.92 W/m^2 below the design intensity of 1.44 W/m^2 – operating at an efficiency of only 36%. The design intensity was not achieved due to energy being transferred to the reactor flange fitting rather than into the liquid in the reactor. This transfer of energy was due to the moving ultrasonic probe that shifted the o-ring and caused a direct contact point between the probe and the reactor flange. The result of the energy transfer was observed as a noticeable increase in the temperature of the reactor flange. With an operating efficiency at only 36%, the intensity of the ultrasound delivered to the reactant could potentially be the limiting factor for the extent to which the reaction can take place. The limited intensity can directly be seen as the cause of the small change in the reactant HHV. At a higher intensity it is expected that a larger change in the HHV of the sludge would have occurred – resulting in an increased amount of hydrogen and carbon monoxide production by the partial oxidation of biomass in the sludge.

Due to the fact that the intensity of sonication is said to be proportional to the amplitude of vibration of the converter, an increase in the amplitude would lead to increased sonochemical affects (Santos, Lodeiro, & Capelo-Martinez, 2009). According to Mason et al. (1988) a cavitation threshold exists that needs to be overcome by the intensity of the emitted ultrasound. Due to the lower than expected ultrasound intensity in the system, it could be that the minimum intensity

threshold was not achieved and as a result, the reaction was limited to only degradation of the sludge, not partial oxidation.

The external pressure exerted on the system also influenced the cavitational effects. For high pressure in the system, the energy required to achieve cavitation would also be higher (Santos, Lodeiro, & Capelo-Martinez, 2009). At a specified frequency, a pressure exists that would result in an optimum sonochemical reaction (Mason & Lorimer, 1988). Considering that the system as operated at its maximum amplitude under the experimental design, the intensity delivered to the reactor could have been reduced due to the fact that more energy would be required to achieve cavitation. It is possible that cavitation was not achieved due to the high pressure application of this study. Alternatively, the exertion of external pressure lead to the reduction of bubble size and this phenomenon significantly improved the efficiency of the sonochemical process (Entezari et al., 1994). An optimum pressure therefore exists where both the power input and the bubble size are optimized to enhance sonochemical activity. When comparing the molar percentages of hydrogen in the product gas in Table 12, it can be seen that at 12.03 minutes and 90 % amplitude, the hydrogen molar percentage in the product gas is 0.07mole % hydrogen at a pressure of 1.41 barg. At the same time and amplitude conditions, it can be seen that at a pressure of 2.59 barg, the hydrogen production was 0.12 mole % in the product gas. It was found that the reduced bubble size, due to an increase in static pressure, resulted in an increase in the sonochemical activity and favoured the production of hydrogen.

20. CCD Results and Optimization

20.1 Basic Statistical Analysis and Model determination

The objective of this study included formulating a statistical model to adequately predict the yields of hydrogen and carbon monoxide and to simultaneously optimize these models. The data from the central composite experiments were used and the model was formulated utilizing a process of backwards elimination by adjusting the model to exclude all insignificant terms based on the P-statistic value.

The H_2 model can be described as:

$$y_{H_2} = 0.44063 - 0.14673x_1 + 0.017031x_2 + 0.00588x_3 + 0.032627{x_1}^2 + 0.00076{x_2}^2 + 0.000051002{x_3}^2 \qquad eq\ (37)$$

where x_1= Pressure (barg), x_2= Time(minutes), x_3= Amplitude (%) and $y =$ fraction hydrogen present in product gas.

The CO model can be described as:

$$y_{CO} = 0.10911 - 0.22625x_1 + 0.045904x_2 + 0.000448x_3 \qquad eq\ (38)$$

where x_1= Pressure (barg), x_2= Time(minutes), x_3= Amplitude (%) and $y =$ fraction carbon monoxide present in product gas. The exact output from the original ANOVA analysis, without removing the insignificant terms, can be seen in Appendix D.

20.2 ANOVA Assumptions for the hydrogen model

Response surface methodology is a group of statistical processes that is used to develop and optimize the variables that influence the response (Montgomery, 1997). For this study, response surface methodology was used to investigate the functional relationship between the responses and the variables. A quadratic regression model was used to initially develop the response surface and was then related to the predicted response. The statistical significance of the factors was judged based on the regression coefficients. For a relatively small p-value and a large coefficient, the term is deemed to have a significant effect on the response variables (Montgomery, 1997). The analysis of variance is based on three assumptions. It is assumed that constant variance is appropriate for the model, it is assumed that the responses are independent and that the system presents normal distribution.

In Figure 40, it can be seen that all the residuals for the hydrogen production model falls within the desired horizontal band depicted by lines from the y-axis at the values of 3 and -3. These residuals are scattered around zero and only two residuals are seen between 2 and 3 on the y-axis – the rest falling in the desired -2 to 2 band. Due to this finding that all the residual fall within the allowable horizontal band, the constant variance assumption was not violated.

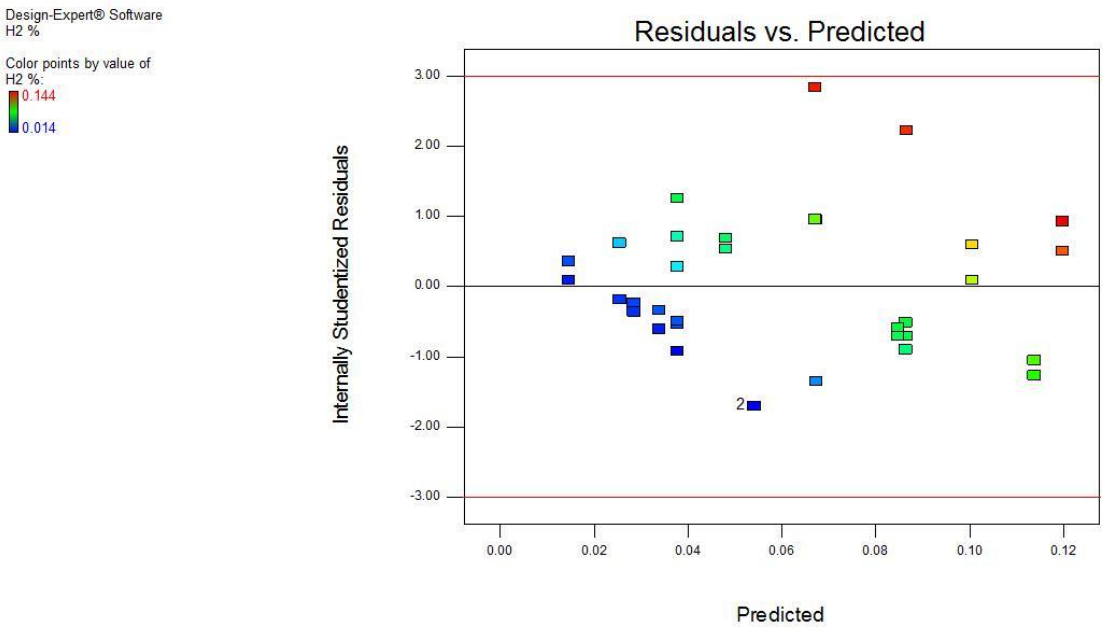

Figure 40: Constant Variance H_2 Model using data points obtained during Ultrasonic Experiments

When looking at the residuals for every run, it can be seen in Figure 41 that all the residuals are scattered around zero without a clearly visible trend.

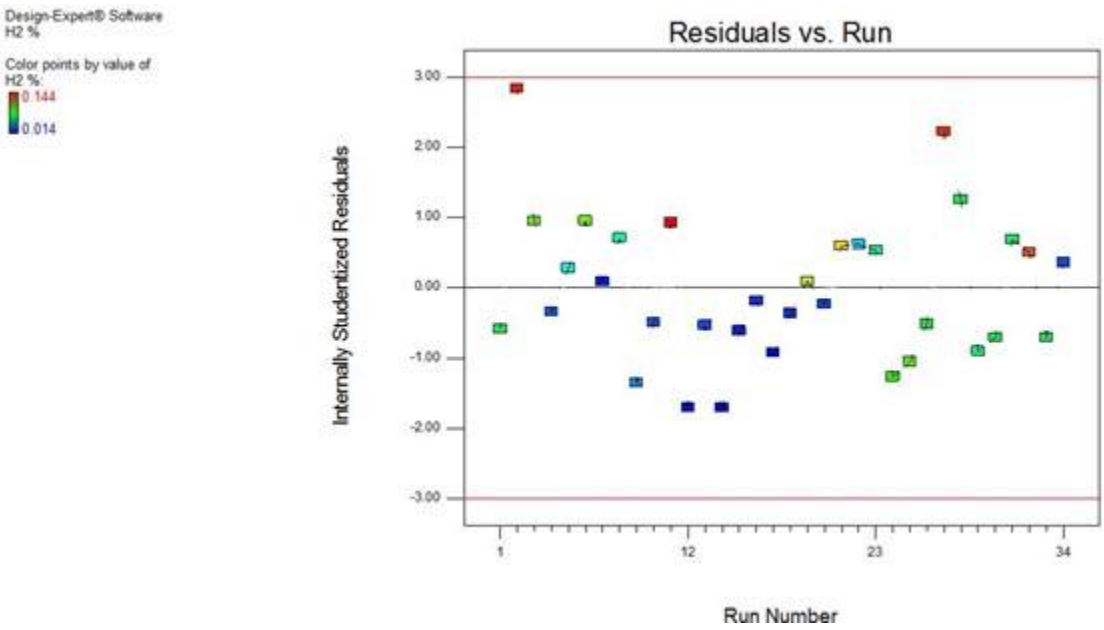

Figure 41: Independent Errors for H_2 Model using data points obtained during Ultrasonic Experiments

These residuals fall within the allowable horizontal band as well and, therefore, the error terms are considered as independent.

The normal probability plot can be seen in Figure 42. From the normal probability plot was found that the data is nearly linear, apart from outliers on the right-hand side of the plot. Due to these outliers only accounting for 2 experiments (run 2 and run 27), which are also visible as the red markers in Figure 41, the data was seen as nearly linear and that the normality assumption was not violated. None of the ANOVA assumptions are therefore violated.

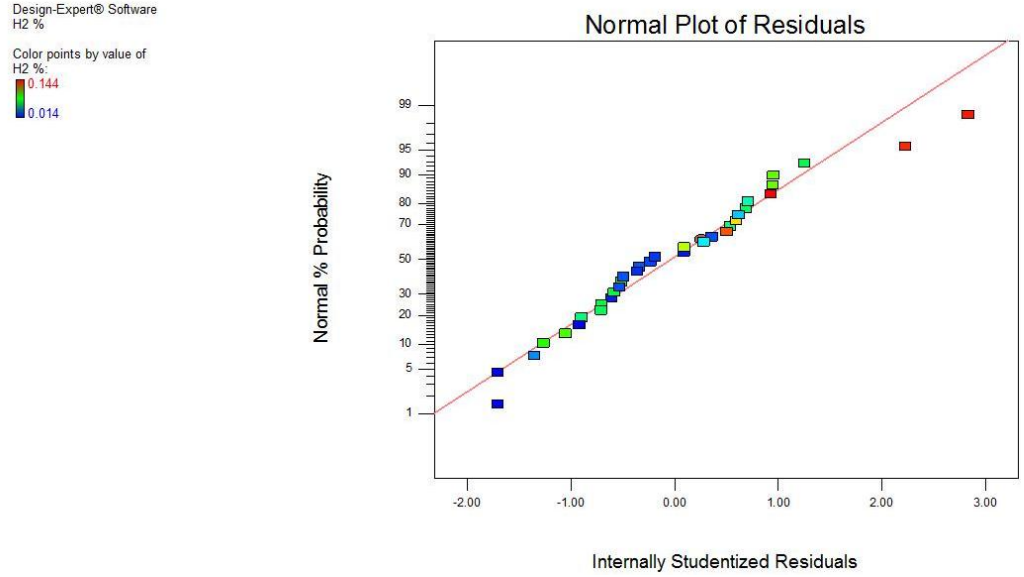

Figure 42: Normal Probability Plot for H_2 Model obtained during Ultrasonic Experiments

20.3 Adequacy of the hydrogen model

When considering the adequacy of a model, several tests can be taken into account. The most common is that of the R-Squared value. The R-Squared value is a summation of the physical distances from the measured points to the predicted line. With a rotatable central composite design with two replicas of the factorial and axial points as well as 6 replicas of the centre point, a very large data set was acquired. As discussed in section 3.1 of this study, with more data points in the experimental design, it is expected that a smaller R-Squared value would be obtained. For the given size of the data set, an R-Squared value of 0.61 in Table 16 is considered acceptable and adequately described the process. With a p-value of 0.01, the model is significant in describing the production of hydrogen by the sonochemical treatment of biomass.

Table 16: Adequacy of H_2 Model

Std. Dev	0.03	R-Squared	0.61
Mean	0.06	Adj R-Squared	0.52
p-value	0.01	Pred R-Squared	0.36

20.4 ANOVA Assumptions for the carbon monoxide model

The same procedure as discussed in chapter 21.2 was now applied to the carbon monoxide model. In Figure 43, it can be seen that all the residuals for the carbon monoxide production model falls within the desired horizontal band – apart from the residual for run 27. This point appeared as one red marker in Figure 43. This was an outlier that does not fall within the allowable limits. Due to this finding that not all the residuals fall within the allowable horizontal band, the constant variance assumption was violated.

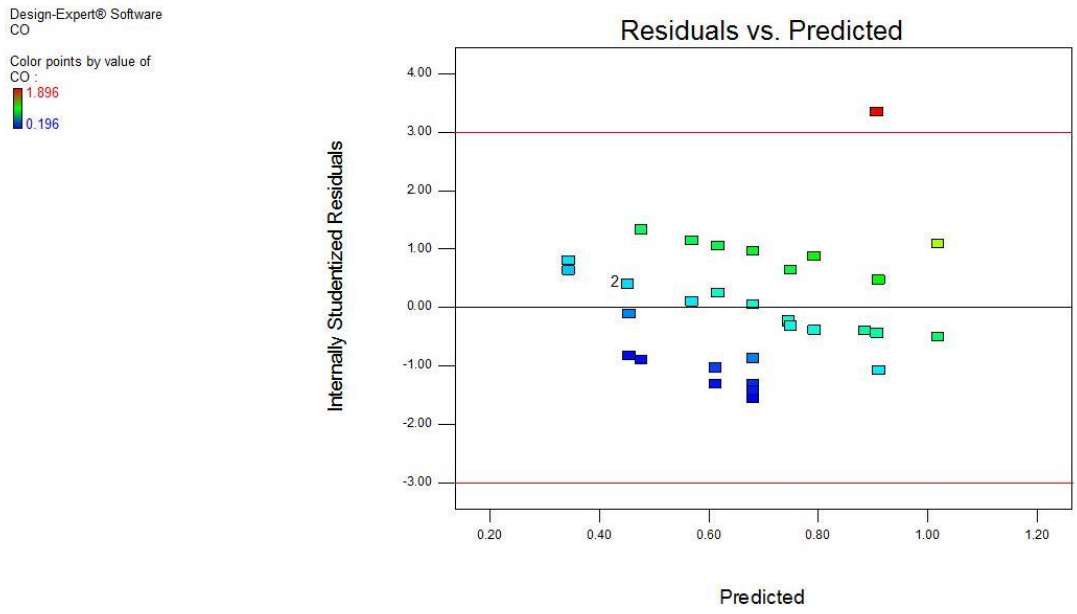

Figure 43: Constant Variance CO Model using data points obtained during Ultrasonic Experiments

The residuals for run 27 also fall outside the allowable range in Figure 44. All other residuals are randomly scattered around zero and no clearly visible trend was observed. The residuals were independent, but with an outlier outside the allowable range. The ANOVA assumption of independence is therefore violated.

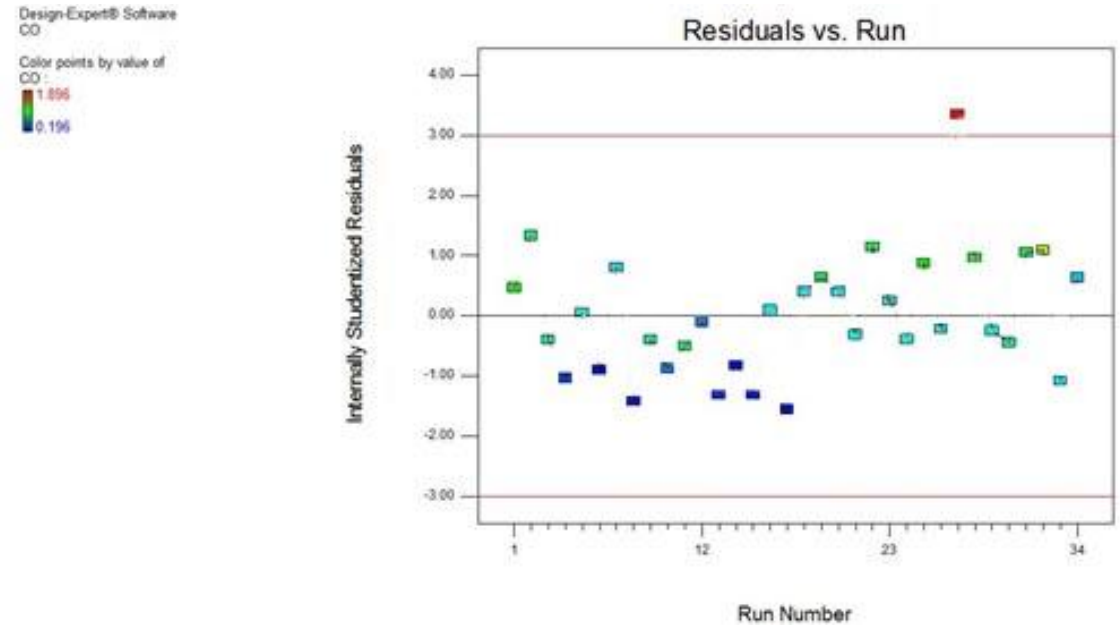

Figure 44: Independent Errors for CO Model using data obtained during Ultrasonic Experiments

The normal probability plot can be seen in Figure 45. From the normal probability plot is can be seen that the data was nearly linear, apart from outlier on the right-hand side of the plot for run 27. Due to this outlier's presence, which violates all ANOVA assumptions, the model was found to be inadequate.

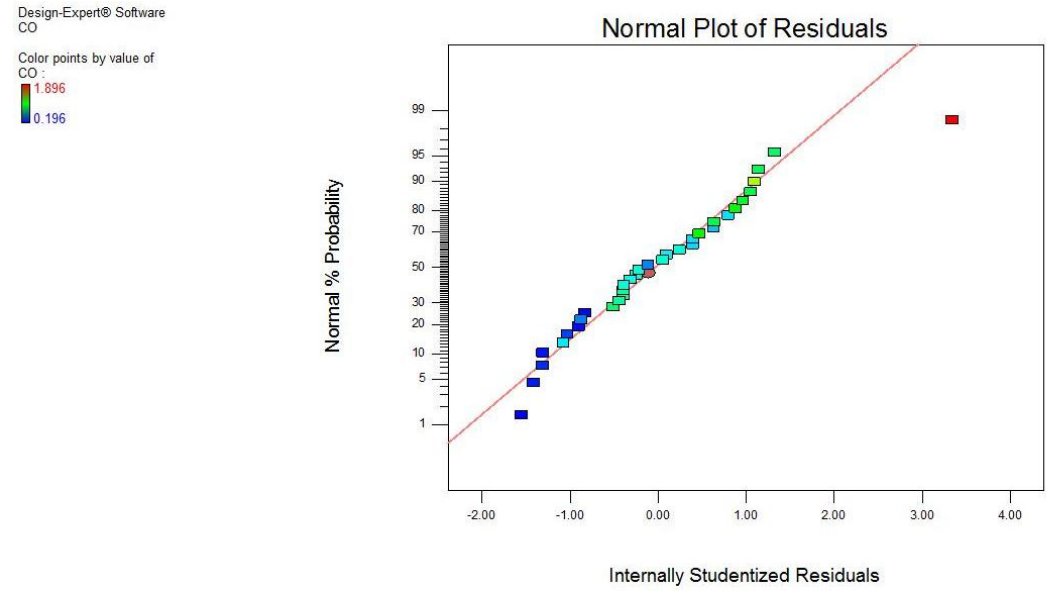

Figure 45: Normal Probability Plot for CO Model using data points obtained during Ultrasonic Experiments

20.5 Adequacy of the carbon monoxide model

Based on the violation of the ANOVA assumptions, the model for carbon monoxide was found to be inadequate to describe the production of carbon monoxide during the sonochemical treatment of biomass. This finding is confirmed by the results of the model in Table 17, where a p-value of 0.32 clearly indicates an insignificant model.

Table 17: Adequacy of CO Model

Std. Dev	0.32	R-Squared	0.27
Mean	0.68	Adj R-Squared	0.2
PRESS	3.84	Pred R-Squared	0.08
p-value	0.32		

20.6 Regression Model Description

The predicted hydrogen model can be seen in Figure 46. When investigating the distances from between the data points and the predicted line (R-squared value of 0.61) below, it was seen that outliers marked in red could potentially play a significant role in the calculated R-squared value. If these points were at a similar distance from the predicted line as the green and blue points, a larger R-squared value would be obtained.

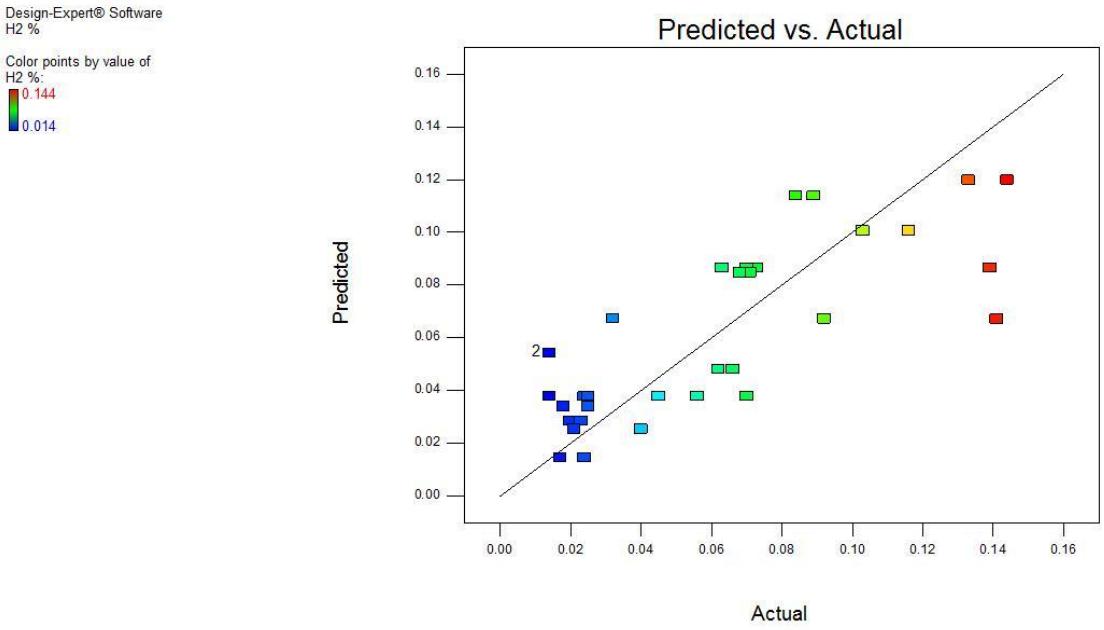

Figure 46: Comparison of predicted and actual values for H_2 Model

Due to an insignificant carbon monoxide model, it was not possible to apply the desirability approach to simultaneously optimize the hydrogen production as well as the carbon monoxide production. It was, therefore, decided to only investigate the optimization of hydrogen production.

To start the optimization process, a stationary point was calculated by partially differentiating each variable and setting it equal to zero. In this manner, the values for $x_1, x_2\ and\ x_3$ at the stationary point were obtained. By replacing these values into the hydrogen production model, a local minimum response was obtained.

By partially differentiating the equation below

$$y_{H_2} = 0.44063 - 0.14673x_1 + 0.017031x_2 + 0.00588x_3 + 0.032627{x_1}^2 + 0.00076{x_2}^2 + 0.000051002{x_3}^2 \qquad eq\ (37)$$

where x_1= Pressure (barg), x_2= Time(minutes), x_3= Amplitude (%) and $y =$ fraction hydrogen present in product gas, and setting the function equal to zero, it was found that the stationary point is at $(x_1.x_2.x_3) = (0.42.-1.25.-1.17)$ in terms of coded variables. This yielded a local minimum at y =0.01 when investigating the dataset. This value for the response was the same when using the coded or actual variables

Knowing that the stationary point was a minimum by investigating the data range, the generalized reduced gradient method was used to determine the optimum point for$x_1, x_2\ and\ x_3$. This was calculated in Excel using the Solver function and defining the constraints within the experimental design.

In terms of coded variables, the Solver function was set up to maximize the value of the response, y, by changing the values of$x_1, x_2\ and\ x_3$. The following constraints were applied:

$$-1 \le x_1 \le 1 \qquad eq\ (40)$$

$$-1 \le x_2 \le 1 \qquad eq\ (41)$$

$$-1 \le x_3 \le 1 \qquad eq\ (42)$$

$$\sum({x_1}^2, {x_2}^2, {x_2}^2) \le \propto^2 \qquad eq\ (43)$$

This resulted in a maximum response in terms of coded variables at $y = 0.12$ and in terms of actual variables, $y = 0.14$ mole % hydrogen in the product gas. This value corresponded well with the actual measured maximum of $y = 0.14$ mole % hydrogen.

This maximum point was then compared to that found in the graphic representation of the model using Design Expert Software. It can be seen in Figure 48 that the maximum predicted response for hydrogen production was at a time setting of 17.97 minutes, 1.41 barg and 100 % Amplitude, according to the contour lines. Based on the maximum calculated using Solver, the maximum settings of time=16.35 min, P=1.41 and amplitude = 100%, the predicted response from the contour plot yielded 0.14 mole % hydrogen. This value corresponds to the value obtained using Solver (y=0.14) and the actual measured maximum (y=0.14). These results are summarized in Table 18.

Table 18: Comparison of actual data with RSM and Solver results

	Excel-Solver	RSM - Contour Plot	Actual Experimental Results
Hydrogen Mole %	0.14	0.14	0.14
time (min)	16.35	17.97	17.89
Pressure (barg)	1.41	1.41	2.59
Amplitude (%)	100	100	89.97

A graphical representation of the maximum values for the response surface methodology can be seen below.

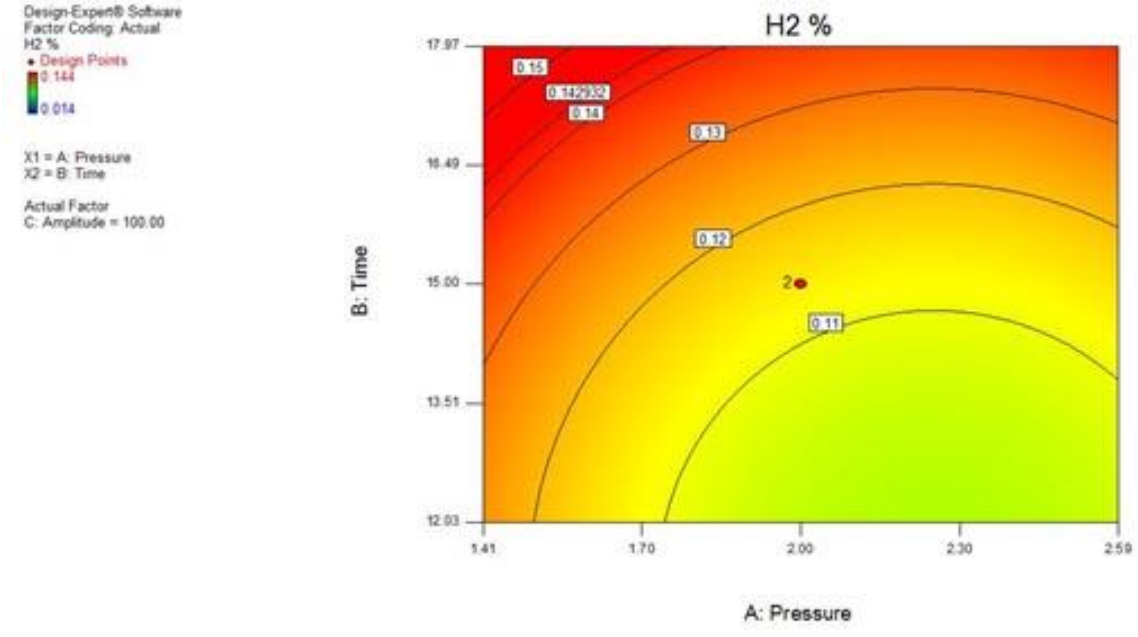

Figure 47: Contour plot of maximum values for H_2 production obtained by response surface methodology

Based on Figure 49, the local maximum point was located at pressure = 1.41 barg, time=17.97 min and an amplitude of 100%. This would yield a value of 0.16 mole % hydrogen. This corresponds to the contour plot seen in Figure 47.

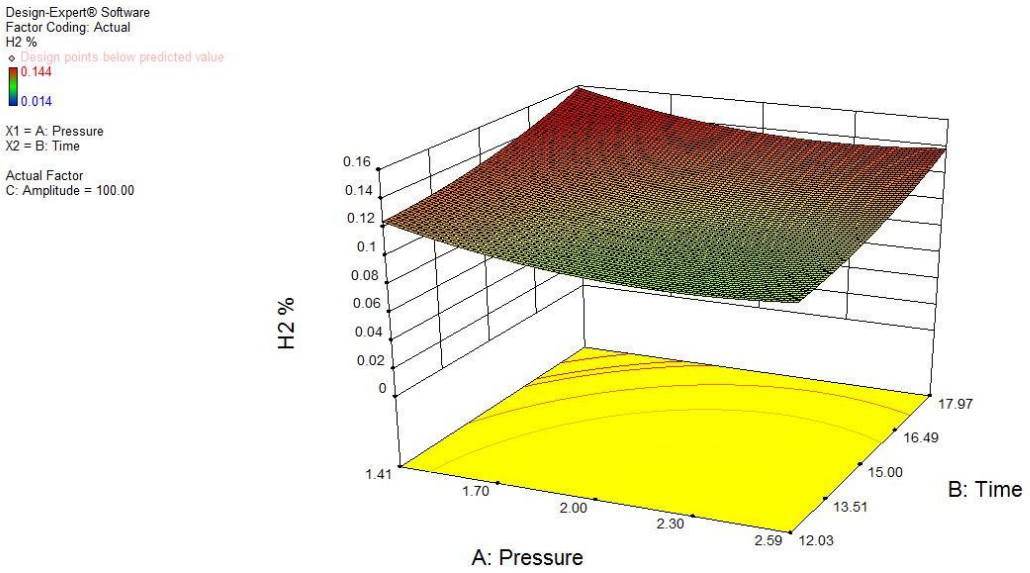

Figure 48: 3D Plots of maximum values for H_2 production obtained by response surface methodology

It can be seen that the model was successfully optimized as both the Excel Solver algorithm and the graphical representation yielded the similar results:

Table 19: Comparison of optimum responses

	H_2 %
Actual Measured Maximum	0.14
Maximum by Solver	0.14
Maximum by Contour plot	0.15
Average	0.15
Standard Deviation	0.01

The optimum expected hydrogen production is as $x_1 = 1.41\ barg$, $x_2 = 17.97\ minutes$ $and\ x_3 = 100\%$. The maximum expected hydrogen production given the process limitations was therefore 0.16 mole % hydrogen in the product gas.

21. Cavitation effect on equipment

After the experiments were conducted, the probe was removed to compare the damage with an unused titanium probe. It can be seen in Figure 49 that the probe experienced extensive damage during the experiments that were conducted.

Figure 49: Ultrasonic Probe tip damage after experiments were conducted

The probe on the left has not been used and as it can be seen on the surface of the probe on the right, extensive damage was experienced.

22. Commercial Plant input

As mentioned in the literature review of this study, Li et al. (2010) found that syngas production using steam gasification would cost of R 1.48/Nm^3 with the syngas yield at 0.67 m^3/kg. It was calculated that at the optimum conditions, using the maximum time kinetic run, the volume produced would be 0.002 m^3/kg for sludge in the energy balance section of this report. This value is significantly less than the current commercial yield using steam gasification.

A commercial GTL plant would require a syngas with a H_2/CO ratio of 1 to 2, depending on the required GTL products. The highest H_2/CO ratio found in this study was 0.43 and a commercial application would require at least double the amount of hydrogen. During conventional steam reforming, more than the required amount of hydrogen is produced and the process conditions are normally limited intentionally to reduce the amount of hydrogen formed. If economically feasible

amounts of gas were produced for the ultrasonic unit at the current H_2/CO ratio, the product gas from the ultrasonic unit could potentially be mixed with the product stream from steam reforming to obtain the required ratio. The amount of hydrogen produced by steam reforming can be adjusted by changing the process conditions of the reforming unit. Alternatively, the concentration of the carbon monoxide can be reduced by removing some of the carbon monoxide from the feed stream into the GTL process. The latter option would require a unit that utilizes a ceramic membrane to selectively remove a portion of the carbon monoxide which is illustrated in Figure 50. This would require an additional energy input into the system that was not considered in the energy balance.

The GTL process requires a feed composition of 70 mole % H_2, 24 mole % CO and 6 mole % CO_2. The required temperature and pressure are 250 °C and 22 bar, respectively. A further energy requirement would be to pressurize the gas from the operating pressure in the ultrasonic unit to that of the GTL unit.

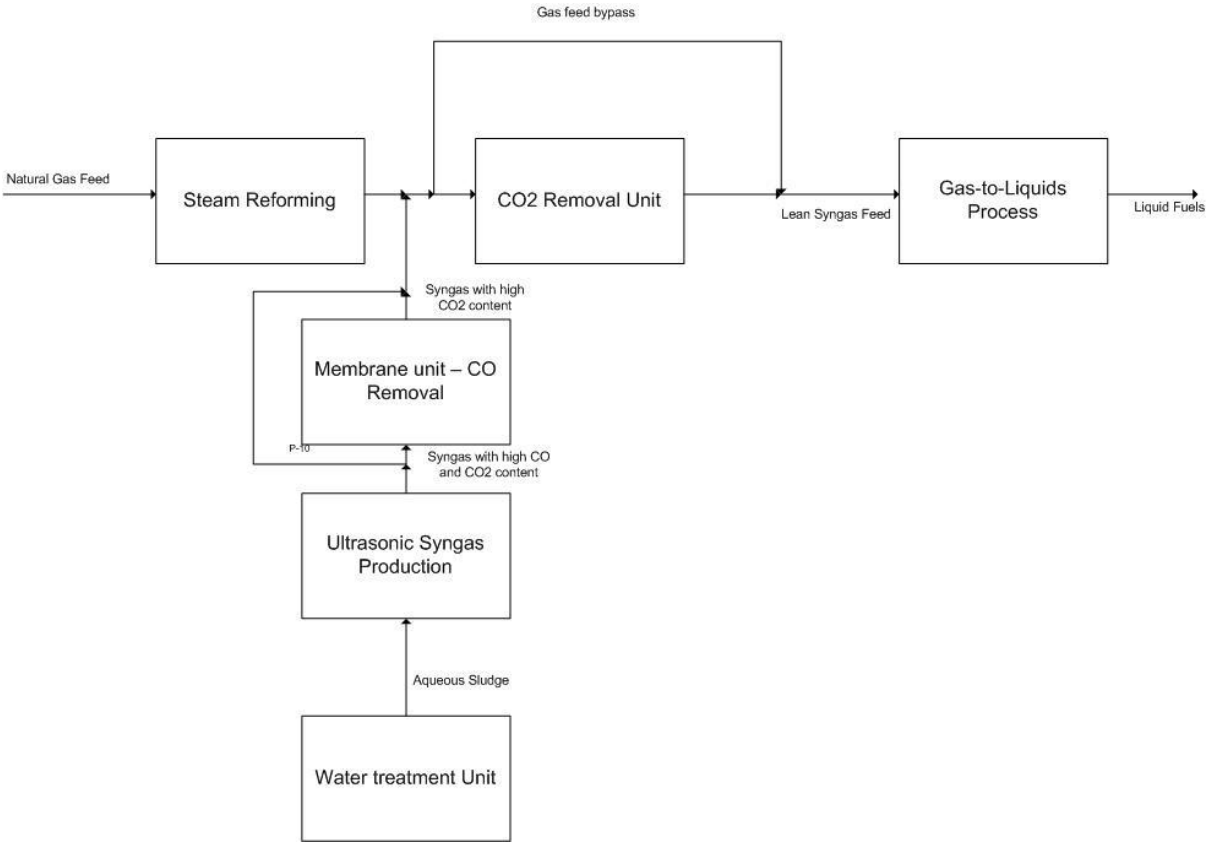

Figure 50: Ultrasonic Syngas Production Process Integration into GTL stream

A possible approach to integrating the ultrasonic syngas production unit in a GTL plant is illustrated in Figure 50. This is based on the results from this study where no methane was produced. If any methane was present during the study, the syngas from the ultrasonic unit would have entered the

main process stream before the steam reforming unit. The sludge would be fed from the water treatment unit, where it was generated, to the ultrasonic syngas production unit. The product from this unit would be sent through a membrane unit to remove CO from the gas stream to achieve the required concentration. The CO concentration is regulated by the use of a bypass stream. The flow to the bypass stream would be controlled based on the gas stream composition at the outlet of the membrane unit. The gas stream would now still contain excess amounts of carbon dioxide and this stream is mixed with the product stream from the steam reforming process. The bulk of this gas stream bypasses the carbon dioxide removal unit and the remainder of the stream is passed through the carbon dioxide removal unit to achieve the desired concentrations before the syngas can enter the GTL process.

23. Improvement on previous work

Studies conducted by Beyers (2011) yielded a maximum hydrogen production of 0.058 mole % and a maximum carbon monoxide production of 0.16 mole %. A summary can be seen in Table 20. The objective of this study was to optimize the reactor system and to improve the production of hydrogen and carbon monoxide whilst reducing the amount of carbon dioxide produced. It was found in Table 20 that the maximum amount of hydrogen produced was increased by 59% and that of carbon monoxide was increased by 92%. It was also found that a 49% reduction in the production of carbon dioxide was also achieved by the design changes conducted in this study.

Table 20: Effect of Design Changes to Equipment

Effect of Design changes			
	2011	2013	Difference
Maximum H_2 mole %	0.06	0.14	59%
Maximum CO mole %	0.16	1.9	92%
Maximum CO_2 mole %	11.8	6.01	-49%

The improvements that are listed in Table 20 can be seen as significant improvement to the process. This serves as an indication that the addition of a cooling water system and an increased static pressure is a step in a positive direction, but for the process to be feasible on a commercial scale, further improvements of the yields would be required.

24. Feasibility

The study was conducted to determine if partial oxidation of biomass using ultrasound is a feasible alternative to steam gasification. It was found that the process yield was 0.000169 Nm^3/kg feed and

the cost of syngas production at this yield would result to R 19.98/Nm^3. This cost only takes operational costs in the form of energy required into account and does not account for initial capital investment for the construction or the cost of any additional downstream processing into account. The downstream processing equipment could CO and CO_2 treatment as well as a compressor to attain the downstream required process pressure.

It was found by Li et al. (2012) that the cost of conventional steam gasification of biomass at a yield of 0.67 Nm^3/kg would result in a syngas price of R1.48/ Nm^3. Based on the operational energy required alone, the sonochemical process would be nearly 10 times more expensive than conventional steam gasification. This excludes all capex costs involved as well as all downstream processing. At the current yield of only 0.002 Nm^3/kg feed, the sonochemical process is not feasible as an alternative to steam gasification due to extremely low yields. A significant improvement in the yield would present a case worth investigating initial capital investment and rate of repayment, but under the current yield, no such study can be conducted. Based on the improvements in the process yields, as seen in Table 20, a significant improvement would be required to reach a yield of 0.67 Nm^3/kg. Due to the large quantities of water present in the sludge samples, the production of hydrogen from partial oxidation is already supported by the sonolysis of water. The production of carbon monoxide from partial oxidation is also supported by the thermal degradation of the lime. Possible changes to the reactor would include a design where the probe does not get in to contact with the reactor flange and the distance between the reactor wall and the probe would be minimized. The design change between the probe and the flange would result in operation at higher pressures and for longer periods as the flange would no longer heat up. Even with all these changes, an increased amount of sonochemical activity leads to an increased amount of cavitation around the probe tip. With an increased amount of cavitational events, the titanium probe would be severely damaged in a short period of time. The yield of the process is ultimately limited by the damage of the titanium probe tip at increased sonochemical activity.

SECTION IV – CONCLUSIONS AND RECOMMENDATIONS

25. CONCLUSIONS

By the redesigning and reconfiguration of the sonochemical reactor to conduct the sonochemical treatment of biomass, it was concluded that the process was successfully optimized. The hypothesis that the partial oxidation, sonolysis and lime degradation process using ultrasound can be optimized was therefore confirmed. The hydrogen production shows a 58% improvement, the carbon monoxide showed a 92 % improvement and the carbon dioxide was reduced by 49% from the work conducted by Beyers (2011). As a result, it was also concluded that the addition of argon positively influenced the sonochemical reactions. It was concluded that the reduction in carbon dioxide is due to not feeding any oxygen to the system under the assumption that enough oxygen is present in the air that is initially dissolved in the liquid. This assumption was confirmed by the presence of an increased amount of nitrogen present after the reaction took place, than in the beginning – showing that dissolve air was present and degassing of the sample occurred. The ratio of carbon monoxide to hydrogen was not optimized and a maximum of only 0.438 was achieved and the hypothesis that a ratio of 2 can be achieved was, therefore, not confirmed. All the product gas analysis was conducted by means of gas chromatography and as a result, the GC was successfully commissioned and calibrated.

As it was found that more hydrogen is produced at higher pressures (whilst other parameters are kept constant), it can be concluded that the static pressure increase resulted in smaller cavitational bubble sizes which lead to an increased in the extent of the hydrogen production reaction.

Representative sludge samples were analysed to characterize the composition of the sludge prior to conducting the experiments. Due to limited time and resources, it was not possible to fully characterise the sludge after experiments were conducted and only prioritized analysis occurred in terms of HHV.

The reactor design optimization was also concluded as successful due to the significant improvement in the product yields as well as repeatability of the experiments. It was found that the application of cooling to the reactor ensured that no water vapour formed during the experiments and the experiments could be conducted for a longer period of time as boiling of the contents was

successfully avoided. All experiments were conducted at least twice and based on the adequate model fit for hydrogen production; it was found that the process conveyed good reproducibility.
A central composite design was conducted and from the results, it was concluded that both hydrogen and carbon monoxide yields increased with an increase in time and amplitude. The hydrogen to carbon monoxide ratio varied considerably and did not reach the desired ratio of 2. The energy potential (HHV) in the feed changed with only 3% at the optimum reactions conditions and it was concluded that the presence of reactive carbon in the feed is not the limiting factor for the partial oxidation of biomass using ultrasound. From the central composite design, the hydrogen production model adequately described the system and identified that time, amplitude and pressure influences the hydrogen yield. The rate equation for hydrogen and carbon monoxide production was found to be zero order and therefore, independent of feed concentration. This supports the small change in the HHV of the feed for the experiment that should have induced the most significant effect on the feed. The hydrogen production model, a manual statistical solution as well as physical testing yielded that the maximum possible hydrogen production under the current conditions, was a value of 0.16 mole % hydrogen at a pressure of 1.42 barg, 17.97 minutes and 100 % amplitude.

It was also concluded that the reactor only operated at a 36% efficiency due to the actual energy intensity reaching an average value of 0.52 W/m^2 and the actual design intensity was 1.44 W/m^2. The energy intensity was also found to be directly proportional to the amplitude of operation.

From the control experiments, it was concluded that hydrogen in produced during the sonolysis of distilled water as a result, this should also occur during the partial oxidation of the biomass sludge as the sludge consists mostly of water. This was found to be the largest contributor to hydrogen production during this study. It was also concluded from the control experiments that carbon monoxide was formed by the thermal degradation of lime into calcium oxide and carbon dioxide, followed by the Boudouard reaction to produce carbon monoxide.

Based on the production of no methane during the course of this study, the sonochemical process can be tied into the GTL process after the steam reforming unit. Due to the relatively high carbon dioxide content, the process will need to join the main feed gas stream that is past into the carbon dioxide removal unit before it enters the GTL process to correct the desired feed gas ratio.

Based on the very low syngas yields, the low hydrogen to carbon monoxide ratio in comparison to the required ratio of 2 as well as the high energy intensity required for this process, it was concluded

that the partial oxidation of biomass sludge in a sonochemical reactor is not feasible as an alternative technology to conventional steam gasification. The process yield of 0.002 Nm^3/kg feed resulted in the cost of syngas production at this yield to reach R 19.98/Nm^3. As a result, this production process was not comparable to conventional steam gasification that delivered a yield of 0.67 Nm^3/kg which resulted in a syngas price of R1.48/ Nm^3. This process was therefore not economically feasible as an alternative to steam gasification. The operating costs of the sonochemical unit would be nearly ten times that of steam gasification and is therefore concluded to not be a competitive technology to conventional steam gasification.

26. RECOMMENDATIONS

It is recommended that the reactor is redesigned to improve the energy intensity delivered to the feed material. By reducing the reactor volume and increasing the contact area between the probe and the feed sample, the intensity should improve. The contact area between the liquid and the probe can be improved by the utilization of a spiral probe that does not have a tip where the ultrasonic effects are intensified – it is dispersed evenly along the length. The contact between the vibration probe and the reactor flange should also be investigated and a more suitable material selected to produce the seal between the flange and the probe.

It is recommended that the argon gas is continuously bubbled to avoid the degassing effect experienced during operation where the batch system is pressurized and sealed before emitting the ultrasound. With continuous bubbling, it is recommended that the product gas is fed continuously through an online GC that has been fitted with column that leads to a TCD that then proceeds into a column that is connected to a FID with a methanizer. This would eliminate analytical errors and the analysis is conducted on the TCD and FID with the same gas sample as the TCD does not destroy the sample. It is also recommended that a gas standard is used with low concentrations to calibrate the FID methanizer and TCD.

The use of a radical scavenger during the sonolysis of water can be investigated to establish the radical behaviour. This process can then be repeated without the scavenger to establish the radical behaviour during the ultrasonic treatment of biomass sludge.

The sludge that contained a significant amount of lime produced favourable results with regards to carbon monoxide production. It is recommended that pure calcium carbonate mixed with water be tested under the same conditions to determine the degree to which partial oxidation occurred and to what degree thermal decomposition of the calcium carbonate occurred. If more carbon dioxide is formed during this test, then the Boudouard reaction is not supported under these conditions and carbon monoxide was formed due to the partial oxidation of biomass that was present in the sample.

It is also recommended that the sludge characterization experiments are conducted after every experiment to measure the extent to which the elemental composition was changed during this experiment.

Due to the large number of data points, unnecessary errors were encountered. It is therefore recommended to reinvestigate the experimental design and choose a design that will deliver the same information utilizing fewer data points. Based on this model as well as further kinetic testing, it is recommended that a complete ASPEN model is developed to simulate the energy requirements to tie the ultrasonic process into the commercial plant. The possibility of mixing the product gas from the improved sonochemical unit with that of the steam reforming unit, can be investigated as higher than the required amount of hydrogen is produced in steam reforming and higher than the required amount of carbon monoxide is produced during the sonochemical process. Based on this model, a complete feasibility study can then be conducted to determine the capital costs involved, the operating costs, the repayment period as well as taking the current costs of sludge disposal into account.

REFERENCES

1. Adbel-Kreem, M., Bassyouni, M., Abdel-Hamid, S., & Abdel-Aal, H. (2009). The Role of GTL Technology as an Option to Exploit Natural Gas Resources. *The Open Fuels Cells Journal (2)*, 5-10.
2. Adewuyi, Y. (2001). Sonochemistry: Environmental Science and Engineering Applications. *Ind. Eng Chem, 40*, 4681.
3. Administration, U. S. (2010). *Index Mundi*. Retrieved March 13, 2013, from World Oil Consumption oer Year: http://www.indexmundi.com/energy.aspx
4. Asakura, Y., Maebayashi, M., & Koda, S. (2005). Study on Efficiency and Characterization in a cylindrical Sonochemical Reactor. *Journal of Chemical Engineering of Japan (38)*, 1008-1014.
5. Bas, D., & Boyaci, I. (2009). Modeling and optimization I: Usability of response surface methodology. *Journal of Food Engineering*, 836-845.
6. Beer, D., & McMurrey, D. (2009). *A guide to Writing as an Engineer - 3rd Edition.* Don Fowley.
7. Beyers, A. (2011). *Partial Oxidation of Bacterial Sludge in a Sonochemical Reactor.* Stellenbosch: Stellenbosch Unviversity.
8. Boyd, J., Deacon, S., & van Niekerk, A. (2009). *Solar drying and compostign of sewage sludge without a bulking agent.* Johannesburg: Johannesburg Water.
9. *Carbon Monoxide Survivior*. (2012). Retrieved November 2013, 9, from http://www.carbon-monoxide-survivor.com/carbon-monoxide-levels-in-the-air.html
10. Chaing, K., Chou, C., & Liu, N. (2009). Application of response surface methodology in describing the thermal performaces of a pin-fin heat sink. *International Journal of Thermal Sciences*, 1196-1205.
11. Chendke, P., & Fogler, H. (1974). Second-Order Sonochemical Phenomena-Extensions of Previous Work. *The Chemical Engineering Journal (8)*, 165-178.
12. Cho, I., & Zoh, K. (2007). Photocatalytic degradation of azo dye in TiO2/UV system: Optimization and modeling using a response surface methodology based on central composite design. *Dyes and Pigments*, 533-543.
13. Ciferno, J. P., & Marano, J. (2002). *Hydrogen Production*. Retrieved March 15, 2011, from http://www.netl.gov/technologies/coalpower/gasification/pubs/market.html
14. Colussi, A., Weavers, L., & Hoffmann, M. (1998). Chemical Bubble Dynamics and Quantitatice Sonochemistry. *Jouranl of Physics and Chemistry*, 6927-6934.

15. Couppiss, E., & Klinzing, G. (1974). Effect of cavitation on reacting systems. *AIChE*, 485 (20).
16. Cravotto, G., Omicciolo, G., & Stevanato, L. (2005). An Improved Sonochemical Reactor. *Ultrasonics Chemistry (12)*, 213-217.
17. Dehghani, K., Nekahi, A., & Mirzaie, M. (2010). Optimizing the bake hardening behaviour of Al7075 using response surface methodology. *Materials and Design*, 1768-1775.
18. Edgar, T., & Himmelblau, D. (2001). *Optimization of Chemical Processes.* Singapore: McGraw-Hille Higher Education.
19. Entezari, M. K. (1997). The effect of Frequency on sonochemical reactions 111: dissociation of carbon disulfide. *Ultrasound Sonochemicstry, 4*, 49.
20. Felder, R., & Rousseau, R. (2005). *Elementary Principles of Chemical Processes.* Hoboken: John Wiley & Sons.
21. Fuel.com, N. E. (2008). *New Energy and Fuel.com*. Retrieved November 04, 2013, from http://newenergyandfuel.com/http:/newenergyandfuel/com/2008/04/18/a-biomass-to-biofuel-watershed-event/
22. *Gas Chromatography*. (2009). Retrieved November 8, 2013, from Chem Pages - Laboratory Resources: http://chem.wisc.edu/deptfiles/genchem/lab/labdocs/modules/gaschrom/gaschromdesc.htm
23. Gautam, G., Adhikari, S., & Bhavnani, S. (2012). Estimation of Biomass Synthesis Gas Composition using Equilibrium Modeling. *Energy Fuels , 24*, 2693-2698.
24. Gogate, P. R., & Pandit, A. B. (2003). A review of imperative technologeis for the watstewater treatment 1: oxidation technologies at ambient conditions. *Advances in Envionmental Research, 8*, 501-551.
25. H., S.-R. (2000). *Writing for Science and Engineering.* Burlington: Butterworth-Heinemann.
26. Hatambeygri, N., Abedi, G., & Talebi, M. (2011). Method development and validation for optimised separation of salicylic, acetyl salicylic and ascorbid acid in pharmaceutical formulations by hydrophillic interaction chromatography and response surface methodology. *Journal of Chromatograpy*, 5995-6003.
27. Horst, C., Chen, Y., Kunz, U., & Hoffman, U. (1996). Design, Modelling and Performance of a novel Sonochemical Reactor for Heterogeneous Reactions. *Chemical Engineering Science (51)*, 1837-1846.
28. Kupiec, T. (2004). Quality-Control Analytical Methods: Gas Chromatogaphy. *International Journal of Pharmaceutical Compounding (vol. 8) 4*, 305-309.

29. Li, L., Song, Z., Ma, C., & Zhao, X. (2012). *Technical and Economic Analysis on Syngas Produciton from Biomass Gasification.* Jinan, China: National Engineering Laboratory for Coal Combustion Pollutants Reduciton.
30. Lorimer, J. M. (1987). Sonochemistry part 1 – the physical aspects. . *Chem.Soc.*
31. Lucchesi, A., & Stoppato, G. (1994). Production of Syngas from Biomass. *Bioresource Technology (48)*, 119-126.
32. Lux Research Inc. (2009). *Technologies tutn waste to proft.*
33. Mabizela, P. M. (n.d.). Thermal characterization of various biomass materials for co-gasification with coal.
34. Mabizela, P., Meyer, E., & Mamphweli, N. (2006). Thermal characterization of various biomass materials for co-gasification with coal.
35. Mann, M. (1995). Technical and Economic Assesment of Producing Hydrogen by Reforming Syngas from the Batelle Indirectly heated biomass gasifier. In *National Renewable Energy Laboratory.* Tsk No. TP-431-8143.
36. Marda, J. D. (2009). Non-catalytic partial oxidation of bio-oil to synthesis gas for distributed hydrogen production. *International Journal of Hydrogen Energy, 34*, 8519-8534.
37. Mason, T. J. (2009). *Sonochemistry beyond synthesis*. Retrieved November 26, 2013, from RSC Advanced Chemical Sciences: http://www.rsc.org/education/eic/issues/2009Sept/SonochemistryBeyondSynthesis.asp
38. Mason, T., & Lorimer, J. (1988). *Sonochemistry - theory, applications and uses of ultrasound in chemistry.* Chichester, West Sussex: Ellis Horwood Ltd.
39. *Mid Year Pricing Determination*. (2013, July). Retrieved November 12, 2013, from ESKOM: http://www.eskom.co.za/CustomerCare/MYPD3/Pages/MYPD3_Toolkit.aspx
40. Miller, N. (1950). The Reaction Sites in a Field of Stationary Ultrasonic Waves. *Trans. Faraday Soc.(46)*, 546.
41. Montgomery, D. C. (1997). *Design and Analysis of Experiments.* Westford: John Wiley & Sons.
42. *Multiple responses: The desirability approach*. (n.d.). Retrieved November 11, 2013, from Nist - Engineering Statistics Handbook: http://www.itl.nist.gov/div898/handbook/pri/section5/pri5322.htm
43. Naidu, D. R. (1994). Modeling of a batch sonochemical reactor. *Chem. Eng. Sci. , 49*(6), 377.
44. Peters, T. J. (2003). *Organic Chemistry Portal*. Retrieved November 4, 2013, from http://www.organic-chemistry.org/topics/sonochemistry.shtm

45. Piga, A., & Verykios, X. (2000). An advanced reactor configuration for the partial oxidation of methane to synthesis gas. *Catalysis Today*, 63-71.
46. Probstein, R., & Hicks, R. (1982). *Synthetic Fuels.* McGraw-Hill Inc.
47. Reed, T., & Siddhartha, G. (2001). *A Survey of Biomass Gasification.* 2nd Edition.
48. Rekab, K., & Shaikh, M. (2005). *Statistical Design of Experiments with Engineering Applications.* Boca Raton, Florida: Chapman & Hall/CRC.
49. Rennard, D. F. (2010). Production of synthesis gas by partial oxidation and steam reforming of biomass pyrolysis oils. *Internaitonal Journal of Hydrogen Energy, 35*, 4048-4059.
50. Riesz, P., Makino, K., & Mossoba, M. (1983). Chemical effects of ultrasound on aqueous solutions. Formation of hydroxyl radicals and hydrogen atoms. *Journal of Physical Chemistry 87 (8)*, 1369-1377.
51. Roberts, G. (2009). *Chemcial Reactions and Chemical Reactors.* Hoboken: John Wiley & Sons.
52. RSCI. (2008). *Thermal Decomposition of Calcium Carbonate.* 2008: Royal Society of Chemistry.
53. Santos, H., Lodeiro, C., & Capelo-Martinez, J. (2009). *The Power of Ultrasound.* Weinheim: Wiley-VCH.
54. Seymour, J., Wallace, H., & Gupta, R. (1997). Sonochemical reactions at 640kHz using an efficient reactor. Oxidation of potassium iodide. *Ultrasonics Sonochemistry*, 289-293.
55. Shah, Y. P. (1999). *Cavitation Reaction Engineering.* USA: Plenum Publishers.
56. Shell. (2011, June 13). *Pearl GTL - An overview*. Retrieved December 1, 2013, from Shell: http://www.shell.com/global/aboutshell/major-projects-2/pearl/overview.html
57. *Simplifying a Multiple Regression Equation*. (n.d.). Retrieved September 30 , 2011, from Jerry Dallal: http://www.jerrydallal.com/LHSP/simplify.htm
58. Sokhansanj, S. (2011). *Biomass Energy Data Book.* September: Oak Ridge National Laboratory.
59. Song, M., Branford-White, C., Nie, H., & Zhu, L. (2011). Optimization of adsorption conditions of BSA on thermosensitive magnetic composite particles using response surface methodology. *Colloids and Surfaces B: Biointerfaces*, 477-483.
60. Suslick, K. S., Mdleleni, K. M., & Reis, J. T. (1997). Chemistry induced by hydrodynamic cavitation. *American Chemical Society, 119*, 9303.
61. Suslick, K., Schubert, P., & Goodale, J. (1981). *Ultrasonics Symposium*, (p. 612).
62. Trabelsi, F. A.-L., Ratsimba, B., Wilheml, A., Delmas, H., Fabre, P., & Berlan, J. (1996). Oxidation of Phenol in wastewater by sonoelectrochemistry. *Chemical Engineering Science*, 1857-1865.

63. *Thermal Decomposition of Calcium Carbonate*. (2013, July 31). Retrieved November 10, 2013, from Nuffield Foundation: http://www.nuffieldfoundation.org/practical-chemistry/thermal-decomposition-calcium-carbonate

64. Van Aken, D., & Hosford, W. (2008). *Reporting Results: A practical guide for Engineers and Scientists.* New York: Cambrigde University Press.

65. Xu, X., Goa, Y., Liu, G., Wang, Q., & Zhao, J. (2008). Optimization of superscitical carbon dioxide extraction of sea buckthorn oil using response surface methodology. *Food Science and Technology*, 1223-1231.

66. Zhong, K., & Wang, Q. (2010). Optimization of ultrasonic extraction of Flammulina Velutipes polysaccharides and evaluation of its acetylcholinesterase inhibitory activity. *Carbohydrate Polymers*, 19-25.

67. Zhu, L. W. (2010). Synthetic Fuels and Chemicals from biomass synthesis gas. *Journal Number 978-4244-7739-5/10*.

Appendix

A. Personal Protective Equipment and Safety Considerations

The aqueous sludge mixture contains bacterial matter that could potentially cause an adverse reaction when coming into contact with skin, eyes and respiratory system. As the exact bacterial content of the sludge varies, it is recommended that precaution be taken by using a mask, safety glasses, a lab coat, closed shoes and gloves at all times when handling the bacterial sludge.

As the gases produced consisted of hydrogen, methane and unreacted oxygen, a potentially explosive mixture was present at all times in the reactor setup. The system was therefore not exposed to any source of ignition, friction or sudden pressure changes. The flammability limit of hydrogen in oxygen is 4 % to 74 % and as a special precaution, the system was diluted with inert argon to ensure that the process was controlled outside the flammability range.

The presence of carbon monoxide posed a threat and as a precaution, a carbon monoxide detector, Draeger X-am 500 Multigas Monitor was present in the laboratory in close proximity to the reactor set up at all times. The Draeger gas monitor was calibrated with a High Alarm at 30 ppm and a High High Alarm at 60 ppm. As a sample loop was used in the GC setup, the GL loop needed to be purged of all air prior to running the analysis. As a result, carbon monoxide could be present at the outlet of the GC sample loop. The carbon monoxide detector was therefore also present during all sample gas analysis.

After gas samples were analysed, the Tedlar gas sample bag's outlet valve was connected to a vacuum system. The remaining gas was then removed from the bags. The gas bags were then purged with compressed air and evacuated using the vacuum connection again. This also served as a check to see if the bag is air tight, as a small air leak would result in a loss of vacuum in the bag.

A build-up of pressure was expected as gasification of a solid was expected to occur. As a result, the pressure gauge on the reactor was monitored carefully. In the event of a pressure build up, the seal between the o-ring and the ultrasonic probe would be released by the upwards motion of the ultrasonic equipment by the pressure inside the reactor. The ultrasonic processor was fitted to an adjustable rod that facilitates this upward movement. The pressure would then escape the system via this route and no damage would occur to the equipment.

B. GC Method Used

Manuals: Varian 3300

Typical Instrument Parameters:

TCD:

Columns: 15’ x 1/8” SS 60/80 Carboxen-1000

Injector: not installed – gas sampling valve fitted to oven

Oven Temperature Program: Method 1

120 ◦C for 10 minutes

Detector: Detector Block - 160 ◦C

TCD Filament - 170 ◦C

TCD Polarity - negative

TCD Initial attenuation - 4

Initial Range - 0.5

Sensitivity: $8 \times 10^{-0.50}$

Gas Flow Rate: Carrier gas is ARGON

Front column pressure = 9.5 psi

Rear column Pressure = 9.9 psi

Relays: Relay 1 corresponds to the column switching valve

Time = 0.00 min -1

Time = 5.00 min +1

FID Methanizer:

Column: as installed

Injector: syringe injection into heated port

Oven Temperature Program: Method 1

120 ◦C for 10 minutes

Detector: FID Oven - 280 ◦C

Methanizer - 380 ◦C

Sensitivity: $8 \times 10^{-0.50}$

Gas Flow Rate: Carrier gas is helium

Front column pressure = 9.5 psi

Rear column Pressure = 9.9 psi

Relays: Relay 1 corresponds to the column switching valve

Time = 0.00 min -1

Time = 5.00 min +1

C. GC Calibration Curves

For the Thermal Conductivity Detector:

Clarity - Chromatography SW
DataApex 2006
www.dataapex.com

C:\Documents and Settings\hp\Desktop\Analene & Max\Max\Max

Calibration	: final calibr	By	: Administrator
Description	:		
Created	: 2013/10/21 16:15:27	Modified	: 2013/11/03 09:03:51

Calculation	: ESTD	Mode	: Calibrate
Calibrate	: Automatic	Recalibration Type	: Average
Change Response	: Enable	Weight	: 0.25
Update Reten. Time	: Enable	Search Criteria	: 0.00%
Default Injected Volume	: Not Used		

Calibration Summary Table (ESTD - C:\Documents and Settings\hp\Desktop\Analene & Max\Max\Max final calibr - Signal 1)

Used	Compound Name	Reten.Time	Left Window	Right Window	Peak Type	Peak Color	LOD	LOQ	R B	Resp. Factor
☒	Hydrogen	1.367	0.200	0.200	Ordnr		0.000	0.000	A	0.0000
☒	Nitrogen	2.390	0.200	0.200	Ordnr		0.000	0.000	A	0.0000
☒	Carbon Monoxide	2.843	0.200	0.200	Ordnr		0.000	0.000	A	0.0000
☒	Methane	5.293	0.200	0.200	Ordnr		0.000	0.000	A	0.0000

Hydrogen - Signal 1 - 1.367 min.

Peak Type	: Ordnr
Left Window	: 0.2 min
Right Window	: 0.2 min
Response Base	: Area
Curve Fit Type	: Quadratic
Zero Type	: Curve from Zero
Weighting Method	: None
Subst. Equation	: Y = 1047.47557*X^2 + 1622.6298*X
Correlation Coef.	: 0.9998613
Residuum	: 5.83697 [mV.s]

	Response	Amount	Resp. Factor	Rec No.	Used
1	1006.5421	0.4782	0.0005	1	☒
2	1024.4045	0.4782	0.0005	1	☒
3	1601.3556	0.6837	0.0004	1	☒
4	1596.7043	0.6837	0.0004	1	☒
5	0.0000	0.0000	0.0000	0	☒
6	0.0000	0.0000	0.0000	0	☒
7	0.0000	0.0000	0.0000	0	☒
8	0.0000	0.0000	0.0000	0	☒
9	0.0000	0.0000	0.0000	0	☒
10	0.0000	0.0000	0.0000	0	☒
11	0.0000	0.0000	0.0000	0	☒
12	0.0000	0.0000	0.0000	0	☒
13	0.0000	0.0000	0.0000	0	☒
14	0.0000	0.0000	0.0000	0	☒
15	0.0000	0.0000	0.0000	0	☒
16	0.0000	0.0000	0.0000	0	☒
17	0.0000	0.0000	0.0000	0	☒
18	0.0000	0.0000	0.0000	0	☒
19	0.0000	0.0000	0.0000	0	☒
20	0.0000	0.0000	0.0000	0	☒
BL	0.0000	Blank	0.0000	0	☒

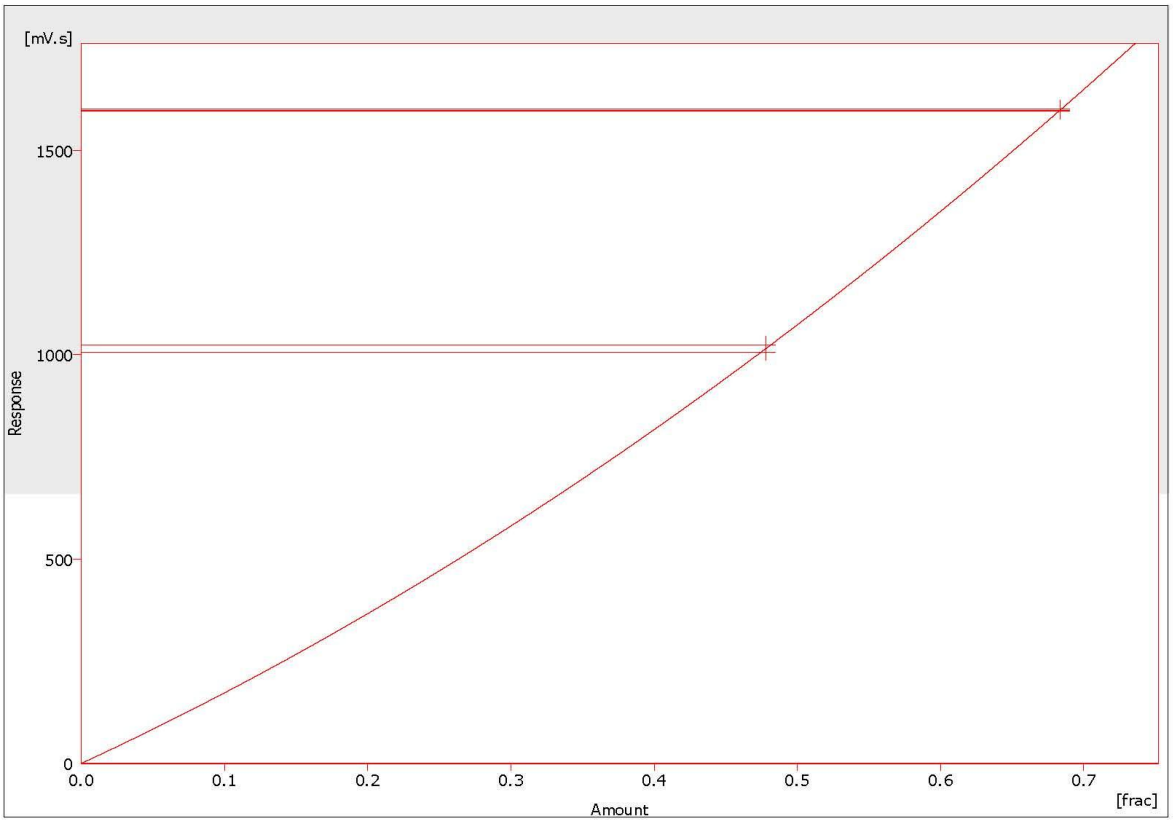

Nitrogen - Signal 1 - 2.39 min.

Peak Type	: Ordnr
Left Window	: 0.2 min
Right Window	: 0.2 min
Response Base	: Area
Curve Fit Type	: Linear
Zero Type	: Curve from Zero
Weighting Method	: None
Subst. Equation	: Y = 202.51135*X
Correlation Coef.	: 0.9999242
Residuum	: 1.42198 [mV.s]

	Response	Amount	Resp. Factor	Rec No.	Used
1	0.0000	0.0000	0.0000	1	☐
2	203.4312	1.0000	0.0049	1	☒
3	201.0732	1.0000	0.0050	1	☒
4	203.4312	1.0000	0.0049	1	☒
5	0.0000	0.0000	0.0000	1	☒
6	20.1883	0.1135	0.0056	1	☒
7	22.2434	0.1135	0.0051	1	☒
8	0.0000	0.0000	0.0000	0	☒
9	0.0000	0.0000	0.0000	0	☐
10	0.0000	0.0000	0.0000	0	☒
11	0.0000	0.0000	0.0000	0	☒
12	0.0000	0.0000	0.0000	0	☒
13	0.0000	0.0000	0.0000	0	☒
14	0.0000	0.0000	0.0000	0	☒
15	0.0000	0.0000	0.0000	0	☒
16	0.0000	0.0000	0.0000	0	☒
17	0.0000	0.0000	0.0000	0	☒
18	0.0000	0.0000	0.0000	0	☒
19	0.0000	0.0000	0.0000	0	☒
20	0.0000	0.0000	0.0000	0	☒
BL	0.0000	Blank	0.0000	0	☒

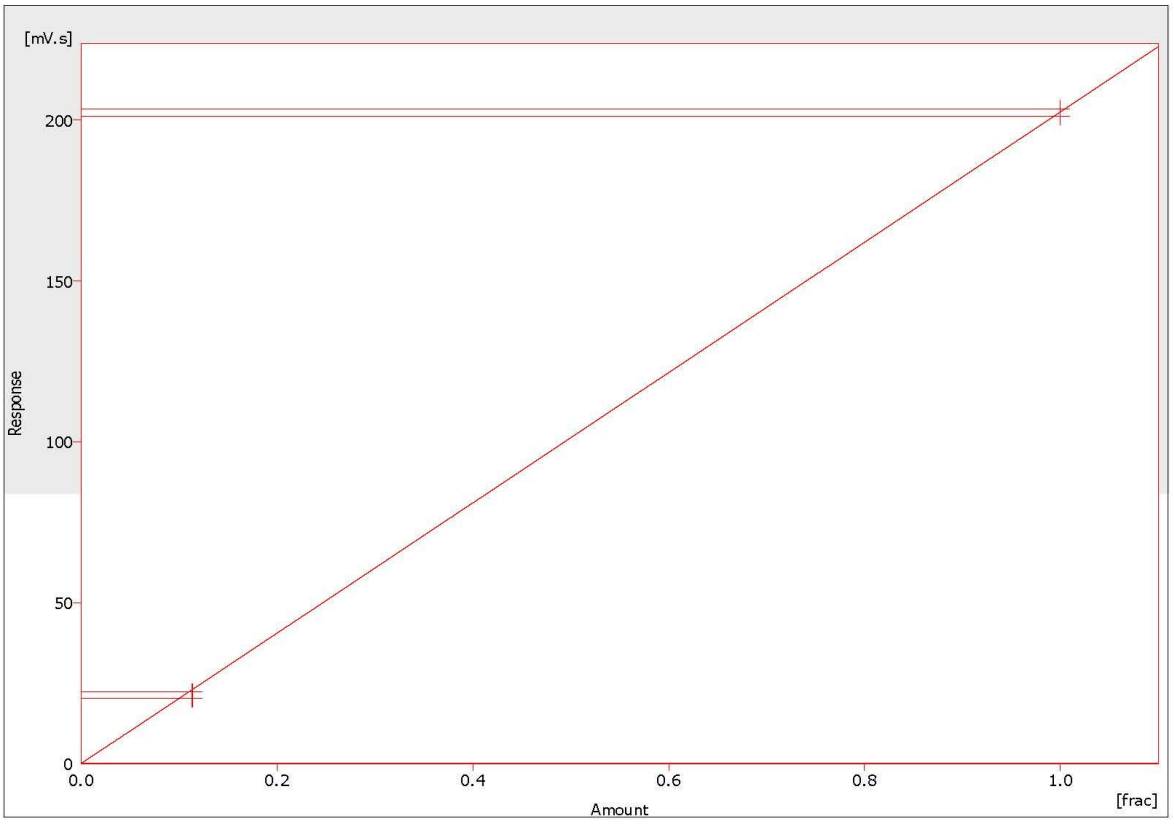

Carbon Monoxide - Signal 1 - 2.843 min.

Peak Type	: Ordnr
Left Window	: 0.2 min
Right Window	: 0.2 min
Response Base	: Area
Curve Fit Type	: Linear
Zero Type	: Curve from Zero
Weighting Method	: None
Subst. Equation	: Y = 200.16469*X
Correlation Coef.	: 0.9999912
Residuum	: 0.48742 [mV.s]

	Response	Amount	Resp. Factor	Rec No.	Used
1	4.5658	0.0243	0.0053	1	☒
2	4.0338	0.0243	0.0060	1	☒
3	185.2902	0.9279	0.0050	1	☒
4	186.1257	0.9275	0.0050	1	☒
5	0.0000	0.0000	0.0000	0	☒
6	0.0000	0.0000	0.0000	0	☒
7	0.0000	0.0000	0.0000	0	☒
8	0.0000	0.0000	0.0000	0	☒
9	0.0000	0.0000	0.0000	0	☒
10	0.0000	0.0000	0.0000	0	☒
11	0.0000	0.0000	0.0000	0	☒
12	0.0000	0.0000	0.0000	0	☒
13	0.0000	0.0000	0.0000	0	☒
14	0.0000	0.0000	0.0000	0	☒
15	0.0000	0.0000	0.0000	0	☒
16	0.0000	0.0000	0.0000	0	☒
17	0.0000	0.0000	0.0000	0	☒
18	0.0000	0.0000	0.0000	0	☒
19	0.0000	0.0000	0.0000	0	☒
20	0.0000	0.0000	0.0000	0	☒
BL	0.0000	Blank	0.0000	0	☒

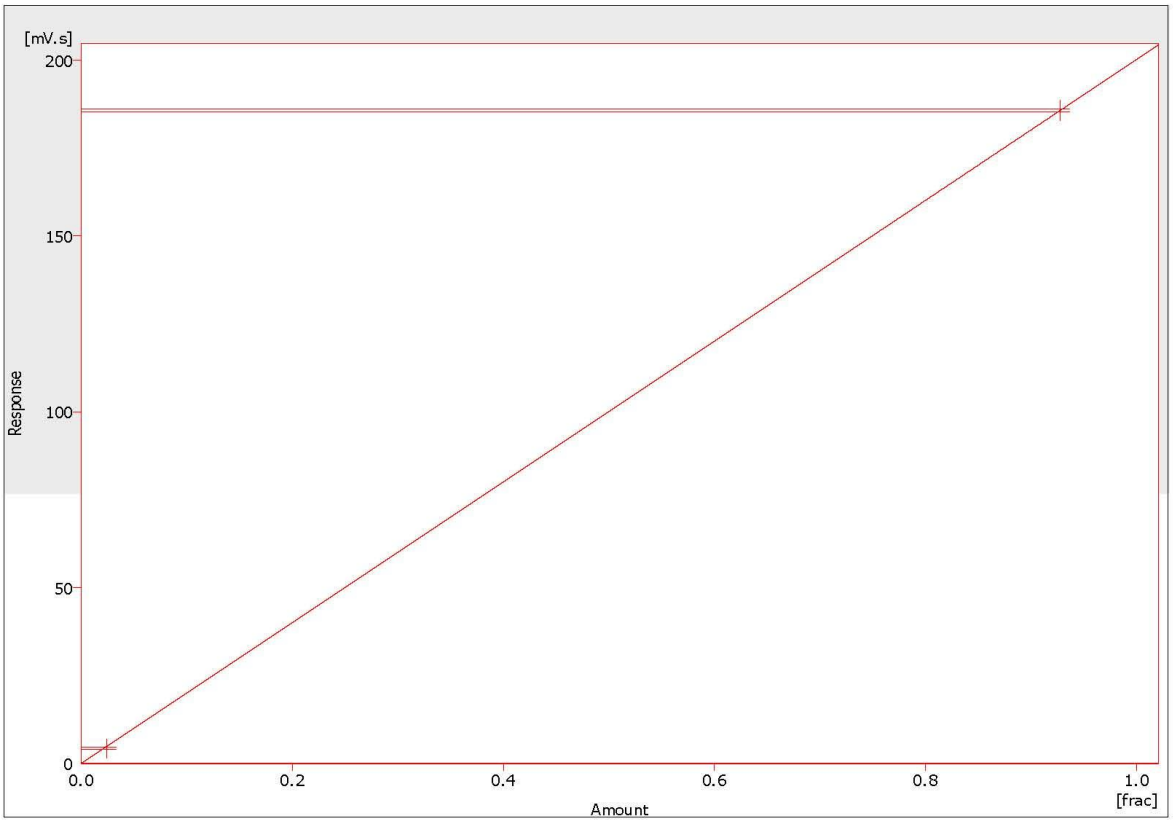

Methane - Signal 1 - 5.293 min.

Peak Type : Ordnr

Left Window : 0.2 min

Right Window : 0.2 min

Response Base : Area

Curve Fit Type : Quadratic

Zero Type : Curve from Zero

Weighting Method : None

Subst. Equation : Y = -245.18039*X^2 + 735.61039*X

Correlation Coef. : 0.9988831

Residuum : 8.08479 [mV.s]

	Response	Amount	Resp. Factor	Rec No.	Used
1	92.6060	0.1307	0.0014	1	☒
2	91.2571	0.1307	0.0014	1	☒
3	474.8625	0.8849	0.0019	1	☒
4	453.7936	0.8861	0.0020	1	☒
5	448.5419	0.8848	0.0020	1	☒
6	0.0000	0.0000	0.0000	0	☒
7	0.0000	0.0000	0.0000	0	☒
8	0.0000	0.0000	0.0000	0	☒
9	0.0000	0.0000	0.0000	0	☒
10	0.0000	0.0000	0.0000	0	☒
11	0.0000	0.0000	0.0000	0	☒
12	0.0000	0.0000	0.0000	0	☒
13	0.0000	0.0000	0.0000	0	☒
14	0.0000	0.0000	0.0000	0	☒
15	0.0000	0.0000	0.0000	0	☒
16	0.0000	0.0000	0.0000	0	☒
17	0.0000	0.0000	0.0000	0	☒
18	0.0000	0.0000	0.0000	0	☒
19	0.0000	0.0000	0.0000	0	☒
20	0.0000	0.0000	0.0000	0	☒
BL	0.0000	Blank	0.0000	0	☒

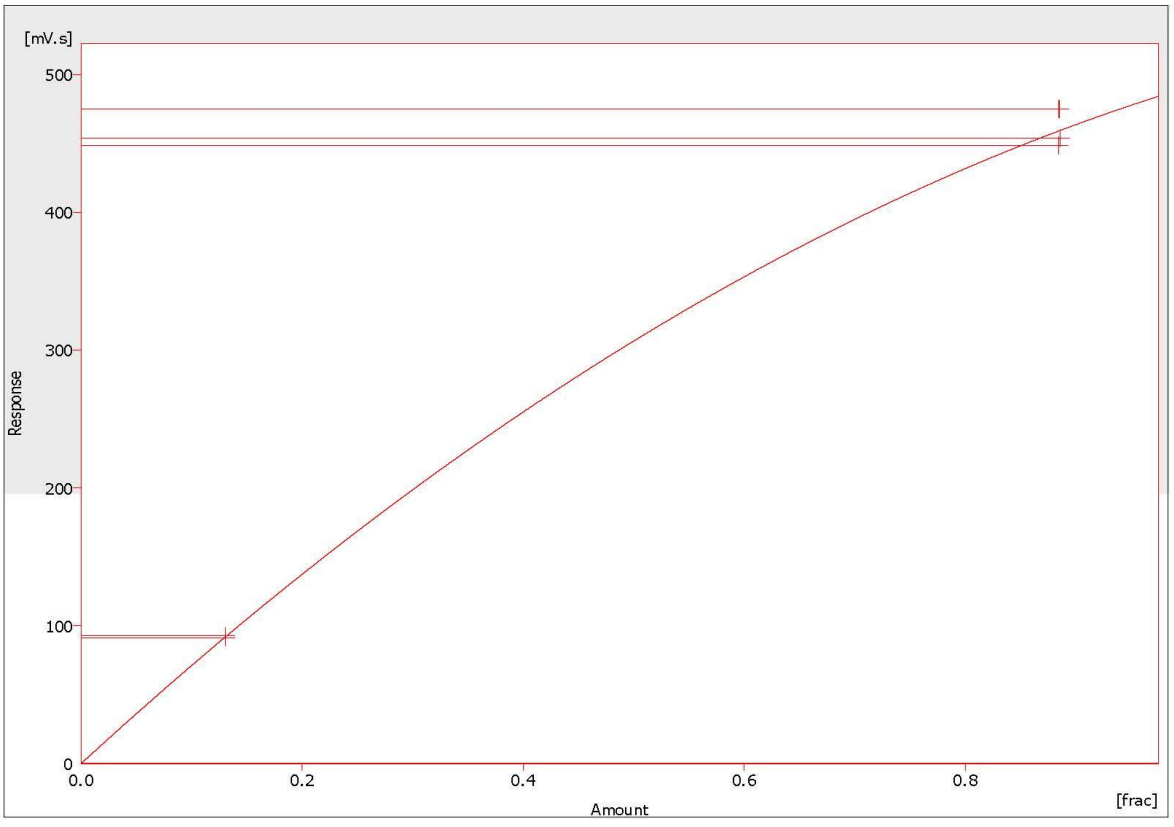

For the FID with a Methanizer:

Clarity - Chromatography SW
DataApex 2006
www.dataapex.com

C:\Documents and Settings\hp\Desktop\Analene & Max\Max\Max
Calibration : final Calib FID
Description :
Created : 2013/10/22 15:15:00
By : Administrator
Modified : 2013/11/03 09:06:16

Calculation	: ESTD	Mode	: Calibrate
Calibrate	: Automatic	Recalibration Type	: Replace
Change Response	: Enable	Weight	: 0.25
Update Reten. Time	: Enable	Search Criteria	: 0.00%
Default Injected Volume	: Not Used		

Calibration Summary Table (ESTD - C:\Documents and Settings\hp\Desktop\Analene & Max\Max\Max final Calib FID - Signal 1)

Used	Compound Name	Reten.Time	Left Window	Right Window	Peak Type	Peak Color	LOD	LOQ	R B	Resp. Factor
☒	Carbon Monoxide	0.973	0.200	0.200	Ordnr		0.000	0.000	A	0.0000
☒	Carbon Dioxide	1.173	0.200	0.200	Ordnr		0.000	0.000	A	0.0000

Carbon Monoxide - Signal 1 - 0.973 min.

Peak Type : Ordnr

Left Window : 0.2 min

Right Window : 0.2 min

Response Base : Area

Curve Fit Type : Linear

Zero Type : Curve from Zero

Weighting Method : None

Subst. Equation : Y = 847.24561*X

Correlation Coef. : 0.9970329

Residuum : 14.16207 [mV.s]

	Response	Amount	Resp. Factor	Rec No.	Used
1	839.0377	1.0000	0.0012	1	☒
2	832.6252	1.0000	0.0012	1	☒
3	870.0739	1.0000	0.0011	1	☒
4	0.0000	0.0000	0.0000	0	☒
5	0.0000	0.0000	0.0000	0	☒
6	0.0000	0.0000	0.0000	0	☒
7	0.0000	0.0000	0.0000	0	☒
8	0.0000	0.0000	0.0000	0	☒
9	0.0000	0.0000	0.0000	0	☒
10	0.0000	0.0000	0.0000	0	☒
11	0.0000	0.0000	0.0000	0	☒
12	0.0000	0.0000	0.0000	0	☒
13	0.0000	0.0000	0.0000	0	☒
14	0.0000	0.0000	0.0000	0	☒
15	0.0000	0.0000	0.0000	0	☒
16	0.0000	0.0000	0.0000	0	☒
17	0.0000	0.0000	0.0000	0	☒
18	0.0000	0.0000	0.0000	0	☒
19	0.0000	0.0000	0.0000	0	☒
20	0.0000	0.0000	0.0000	0	☒
BL	0.0000	Blank	0.0000	0	☒

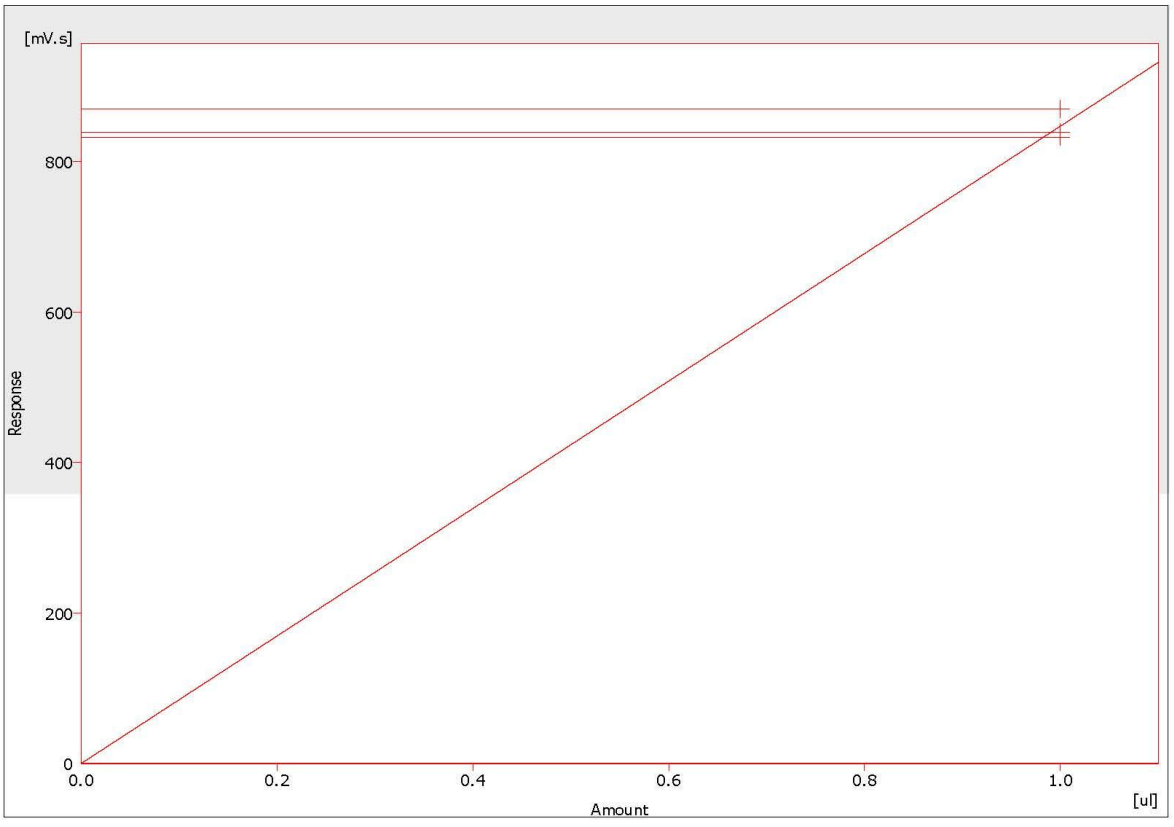

Carbon Dioxide - Signal 1 - 1.173 min.

Peak Type : Ordnr

Left Window : 0.2 min

Right Window : 0.2 min

Response Base : Area

Curve Fit Type : Linear

Zero Type : Curve from Zero

Weighting Method : None

Subst. Equation : Y = 228.96743*X

Correlation Coef. : 0.9910359

Residuum : 8.4006 [mV.s]

	Response	Amount	Resp. Factor	Rec No.	Used
1	239.2560	1.0000	0.0042	1	☒
2	218.6788	1.0000	0.0046	1	☒
3	3224.9637	0.0000	0.0000	1	☒
4	0.0000	0.0000	0.0000	0	☒
5	0.0000	0.0000	0.0000	0	☒
6	0.0000	0.0000	0.0000	0	☒
7	0.0000	0.0000	0.0000	0	☒
8	0.0000	0.0000	0.0000	0	☒
9	0.0000	0.0000	0.0000	0	☒
10	0.0000	0.0000	0.0000	0	☒
11	0.0000	0.0000	0.0000	0	☒
12	0.0000	0.0000	0.0000	0	☒
13	0.0000	0.0000	0.0000	0	☒
14	0.0000	0.0000	0.0000	0	☒
15	0.0000	0.0000	0.0000	0	☒
16	0.0000	0.0000	0.0000	0	☒
17	0.0000	0.0000	0.0000	0	☒
18	0.0000	0.0000	0.0000	0	☒
19	0.0000	0.0000	0.0000	0	☒
20	0.0000	0.0000	0.0000	0	☒
BL	0.0000	Blank	0.0000	0	☒

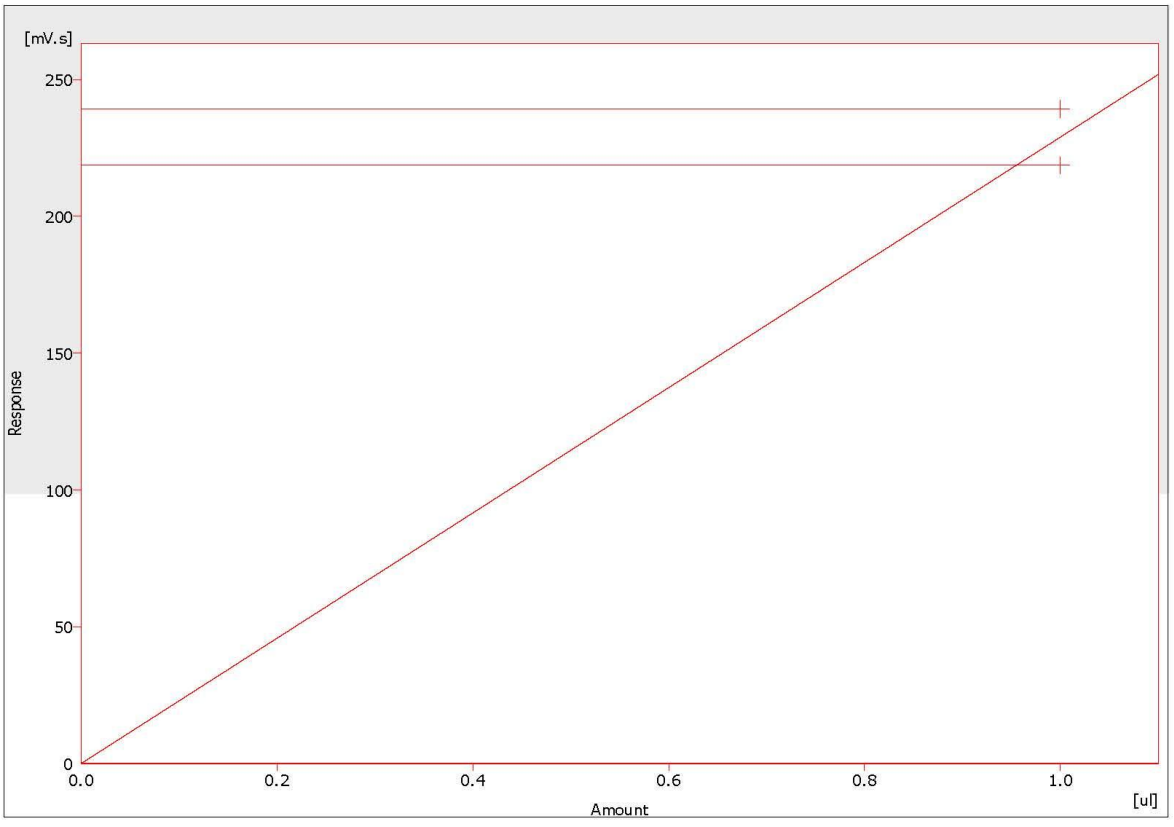

D. RAW Data Tables

DE Order	Experiment Number	Date	Pressure	Time (min)	Amplitude	Concentration	Samples	Mass Sample	Water	Exp Start Time	Hydrogen Area 1	Hydrogen Area 2	Hydogen 3	Nitrogen Area 1	Nitrogen Area 2	Nitrogen Area 3	CO ppm	CO area 1	CO area 2	CO area 3	CO2 Area 1	CO2 Area 2	CO2 Area 3
23	1.2	23/10/2013	2	20.00	75	2/3	B-255, B-2	133.94	70	10:57	0.78	0.85	0.91	2.72	2.73	2.79	216.00	5.85	7.33	6.28	0.98	1.40	1.45
12	2	2/10/2013	2.59	12.03	89.87	2/3	B-81, B-36	141.58	70	15:40	2.021	2.084		1.412	1.424		248	5.669	7.344	6.828	1.669	17.344	16.828
6	3	2/10/2013	1.41	17.97	60.13	2/3	B-46, B-66	143.79	70	13:34	0.84	0.98	0.89	7.34	7.47	7.66	262.00	3.78	4.05	3.93	2.78	4.05	3.932
1	4	3/10/2013	1.41	12.03	60.13	2/3	B-95, B-45	159.69	70	15:40	0.233	0.242	0.216	1.518	1.542	1.64	158	1.888	1.439	1.046	1.88	1.439	1.046
30	5.1	23/10/2013	2	15.00	75	2/3	B-249, B-229	130.07	70	11:59	0.484	0.584	0.534	1.707	1.713	1.771	126	4.26	4.316		0.446	0.712	
11	6	3/10/2013	2.59	12.03	89.87	2/3	B-44. B-88	139.15	70	17:33	1.4	1.337	1.351	5.346	5.539	5.726	260	1.668	1.373	1.814	1.668	1.313	1.814
4	7.1	23/10/2013	2.59	12.03	60.13	2/3	B-232, B-234	130.15	70	14:25	0.246	0.23	0.238	1.63	1.641	1.766	54	3.875	4.498		0.329	0.593	
34	8	4/10/2013	2	15.00	75	2/3	B-76, B-26	138.82	70	14:25	0.731	0.577	0.686	1.368	1.335	1.356	128	1.724	1.236		1.724	1.236	
5	9.1	23/10/2013	1.41	17.97	60.13	2/3	B-240, B-252	130.2	70	14:45	0.346	0.353	0.231	1.746	1.769	1.707	58	3.919	3.882		0.313	0.289	
33	10	7/10/2013	2	15.00	75	2/3	B-18, B-77	164.49	70	14:50	0.308	0.292	0.282	1.585	2	1.746	54	2.845	1.936	2.802	2.845	1.936	2.802
14	11.1	23/10/2013	1.41	17.97	89.97	2/3	B-238, B-235	130.11	70	16:02	1.124	1.149	1.123	1.23	1.347	1.321	246	4.904	4.075		0.335	0.101	
20	12	9/10/2013	3	15.00	75	2/3	B-68, B-249	143.21	70	13:36	0.223	0.225		21.671	22.008		42	3.626	3.358		3.868	4.229	
32	13	9/10/2013	2	15.00	75	2/3	B-99, B-30	131.9	70	15:12	0.213	0.377	0.29	5.535	5.725	5.829	62	2.264	1.55	1.366	2.259	1.204	1.139
19	14	9/10/2013	3	15.00	75	2/3	B-58, B-28	147.05	70	17:57	0.261	0.192	0.222	4.217	4.469	4.621	46	1.946	1.533		2.791	1.956	
2	15	10/10/2013	1.41	12.03	60.13	2/3	B-47, B-208	126.06	70	13:56	0.174			5.011	5.189			0.735	1.512		0.412	0.529	
25	16.1	23/10/2013	2	15.00	50	2/3	B-246, B-226	131.8	70	7:26	0.219	0.305	0.189	1.506	1.571	1.672	28	3.457	3.552		0	0	
31	17	10/10/2013	2	15.00	75	2/3	B-257, B-14	128.62	70	16:50	0.217	0.156	0.142	4.452	4.649	4.76		1.461	0.987	1.173	0.187	0.05	0.23
21	18.1	10/10/2013	2	10.00	75	2/3	B-263, B-245	130.8	70	11:43	0.279	0.231	0.212	1.389	1.585	1.501	60	3.587	3.471		0.138	0.079	
15	19.1	11/10/2013	2.59	17.97	89.97	2/3	B-262, B-246	130.2	70	13:05	1.465	1.471	1.41	2.301	2.39	2.383	362	7.272	6.53		0.582	0.179	
22	20	11/10/2013	2	10.00	75	2/3	B-220, B-245	130.17	70	14:45	0.264	0.193	0.303	1.363	1.383	1.411		3.22	2.915	3.654	0	0	0
16	21	19/10/2013	2.59	17.97	89.97	2/3	B-8, B-261	134.75	70	10:47	1.669	1.725	1.682	3.412	3.547	3.492	404	5.583	4.416		12.121	9.43	

26	22	19/10/2013	2	15.00	50	2/3	B-236, B-227	130.17	70	11:58	0.451	0.537	0.383	1.536	1.497	1.528	102	4.711	6.207		4.678	7.529	
7	23	19/10/2013	2.59	17.98	60.12	2/3	B-258, B-224	130.07	70	14:16	0.865	0.878	0.845	1.665	2	1.691	188	5.16	4.788		8.628	8.065	
27	24	19/10/2013	2	15.00	100	2/3	B-218, B-1	136.47	70	16:00	1.04	0.996	0.998	1.183	1.116	1.136	232	3.876	4.62		9.369	10.953	
27	25	24/10/2013	2	15.00	100	2/3	B-205, B-224	130.13	70	15:34	1.069	1.076	1.06	3.665	3.743	3.763	316	6.598	6.54		0.339	0.31	
10	26	20/10/2013	1.41	12.03	89.97	2/3	B-221, B-217	130.17	70	11:23	0.712	0.712	0.747	2.16	2.081	2.326	164	3.574	3.473		3.362	3.48	
18	27	20/10/2013	1	15.00	75	2/3	B-15, B-281	133.15	70	12:38	1.112	1.115	1.094	2.199	2.059	2.333	310	7.955	7.787		2.264	2.249	
29	28	20/10/2013	2	15.00	75	2/3	B-19, B-223	134.88	70	13:48	0.908	0.809	0.744	1.781	1.929	1.88	202	5.623	6.309		2.463	2.995	
9	29	20/10/2013	1.41	12.03	89.97	2/3	B-214, B-27	135.03	70	15:20	0.794	0.492	0.593	1.538	1.494	1.554	120	3.979	3.001		1.934	2.434	
17	30	20/10/2013	1	15.00	75	2/3	B-252, B-253	130.07	70	16:37	0.558	0.538	0.653	4.266	4.258	5.022	126	3.295	3.422		1.946	1.23	
8	31	20/10/2013	2.59	17.97	60.13	2/3	B-248, B-220	130.28	70	17:44	0.971	0.879	0.906	1.612	1.608	1.611	242	5.833	7.577		1.725	2.154	
13	32	21/10/2013	1.41	17.97	89.97	2/3	B-250, B-212	130.23	70	10:48	1.319	1.318	1.33	2.688	2.681	2.735	316	6.398	7.512		1.236	1.319	
24	33	21/10/2013	2	20.00	75	2/3	B-215, B-209	130.17	70	12:03	0.8	0.803	0.824	2.007	2.135	2.116	170	3.718	4		0.76	0.708	
3	34	21/10/2013	2.59	12.03	60.13	2/3	B-203, B-247	130.16	70	13:15	0.344	0.292	0.377	1.391	1.398	1.401	68	3.216	4.386		0.514	0.739	

E. ANOVA Outputs

Hydrogen

Use your mouse to right click on individual cells for definitions.

Response 2 H2 %

ANOVA for Response Surface Quadratic Model

Analysis of variance table [Partial sum of squares - Type III]

Source	Sum of Squares	df	Mean Square	F Value	p-value Prob > F	
Model	0.035	9	3.908E-003	4.71	0.0011	significant
A-Pressure	2.540E-003	1	2.540E-003	3.06	0.0930	
B-Time	7.628E-003	1	7.628E-003	9.19	0.0058	
C-Amplitude	0.019	1	0.019	22.70	< 0.0001	
AB	1.388E-003	1	1.388E-003	1.67	0.2083	
AC	8.556E-005	1	8.556E-005	0.10	0.7509	
BC	1.051E-004	1	1.051E-004	0.13	0.7251	
A^2	3.000E-003	1	3.000E-003	3.61	0.0693	
B^2	1.004E-003	1	1.004E-003	1.21	0.2822	
C^2	2.864E-003	1	2.864E-003	3.45	0.0755	
Residual	0.020	24	8.300E-004			
Lack of Fit	0.012	5	2.350E-003	5.47	0.0028	significant
Pure Error	8.167E-003	19	4.298E-004			
Cor Total	0.055	33				

The Model F-value of 4.71 implies the model is significant. There is only a 0.11% chance that a "Model F-Value" this large could occur due to noise.

Values of "Prob > F" less than 0.0500 indicate model terms are significant.
In this case B, C are significant model terms.
Values greater than 0.1000 indicate the model terms are not significant.
If there are many insignificant model terms (not counting those required to support hierarchy), model reduction may improve your model.

The "Lack of Fit F-value" of 5.47 implies the Lack of Fit is significant. There is only a 0.28% chance that a "Lack of Fit F-value" this large could occur due to noise. Significant lack of fit is bad -- we want the model to fit.

Std. Dev.	0.029	R-Squared	0.6384
Mean	0.061	Adj R-Squared	0.5028
C.V. %	46.91	Pred R-Squared	0.2482
PRESS	0.041	Adeq Precision	6.736

The "Pred R-Squared" of 0.2482 is not as close to the "Adj R-Squared" of 0.5028 as one might normally expect. This may indicate a large block effect or a possible problem with your model and/or data. Things to consider are model reduction, response transformation, outliers, etc.

"Adeq Precision" measures the signal to noise ratio. A ratio greater than 4 is desirable. Your ratio of 6.736 indicates an adequate signal. This model can be used to navigate the design space.

Coefficient Factor	Estimate	df	Standard Error	95% CI Low	95% CI High	VIF
Intercept	0.038	1	0.012	0.014	0.062	
A-Pressure	-9.644E-003	1	5.512E-003	-0.021	1.733E-003	1.00
B-Time	0.017	1	5.512E-003	5.334E-003	0.028	1.00
C-Amplitude	0.026	1	5.512E-003	0.015	0.038	1.00
AB	-9.313E-003	1	7.202E-003	-0.024	5.552E-003	1.00
AC	2.312E-003	1	7.202E-003	-0.013	0.017	1.00
BC	-2.563E-003	1	7.202E-003	-0.017	0.012	1.00
A^2	0.012	1	6.067E-003	-9.868E-004	0.024	1.16
B^2	6.674E-003	1	6.067E-003	-5.848E-003	0.019	1.16
C^2	0.011	1	6.067E-003	-1.252E-003	0.024	1.16

Final Equation in Terms of Coded Factors:

H2 % =

+0.038
-9.644E-003 * A
+0.017 * B
+0.026 * C
-9.313E-003 * A * B
+2.312E-003 * A * C
-2.563E-003 * B * C
+0.012 * A^2
+6.674E-003 * B^2
+0.011 * C^2

Final Equation in Terms of Actual Factors:

H2 % =
+0.25661
-0.087329 * Pressure
-2.14653E-003 * Time
-5.53714E-003 * Amplitude
-5.26795E-003 * Pressure * Time
+2.61630E-004 * Pressure * Amplitude
-5.79828E-005 * Time * Amplitude
+0.032627 * Pressure^2
+7.55073E-004 * Time^2
+5.10029E-005 * Amplitude^2

The Diagnostics Case Statistics Report has been moved to the Diagnostics Node.
In the Diagnostics Node, Select Case Statistics from the View Menu.
Proceed to Diagnostic Plots (the next icon in progression). Be sure to look at the:

1) Normal probability plot of the studentized residuals to check for normality of residuals.
2) Studentized residuals versus predicted values to check for constant error.
3) Externally Studentized Residuals to look for outliers, i.e., influential values.
4) Box-Cox plot for power transformations.

If all the model statistics and diagnostic plots are OK, finish up with the Model Graphs icon.

Carbon Monoxide:

Use your mouse to right click on individual cells for definitions.

Response 1 CO

ANOVA for Response Surface Quadratic Model

Analysis of variance table [Partial sum of squares - Type III]

Source	Sum of Squares	df	Mean Square	F Value	p-value Prob > F	
Model	1.68	9	0.19	1.81	0.1193	not significant
A-Pressure	0.49	1	0.49	4.79	0.0385	
B-Time	0.51	1	0.51	4.93	0.0361	
C-Amplitude	0.12	1	0.12	1.17	0.2895	
AB	0.044	1	0.044	0.42	0.5214	
AC	0.15	1	0.15	1.44	0.2417	
BC	1.225E-003	1	1.225E-003	0.012	0.9141	
A^2	0.24	1	0.24	2.37	0.1371	
B^2	0.075	1	0.075	0.73	0.4027	
C^2	0.22	1	0.22	2.10	0.1599	
Residual		2.48	24	0.10		
Lack of Fit		0.72	5	0.14	1.55	0.2212 not significant
Pure Error		1.76	19	0.093		
Cor Total		4.15	33			

The "Model F-value" of 1.81 implies the model is not significant relative to the noise. There is a 11.93 % chance that a "Model F-value" this large could occur due to noise.

Values of "Prob > F" less than 0.0500 indicate model terms are significant.
In this case A, B are significant model terms.
Values greater than 0.1000 indicate the model terms are not significant.
If there are many insignificant model terms (not counting those required to support hierarchy), model reduction may improve your model.

The "Lack of Fit F-value" of 1.55 implies the Lack of Fit is not significant relative to the pure error. There is a 22.12% chance that a "Lack of Fit F-value" this large could occur due to noise. Non-significant lack of fit is good -- we want the model to fit.

Std. Dev.	0.32	R-Squared	0.4039
Mean	0.68	Adj R-Squared	0.1803
C.V. %	47.16	Pred R-Squared	-0.1895
PRESS	4.94	Adeq Precision	4.614

A negative "Pred R-Squared" implies that the overall mean is a better predictor of your response than the current model.

"Adeq Precision" measures the signal to noise ratio. A ratio greater than 4 is desirable. Your ratio of 4.614 indicates an adequate signal. This model can be used to navigate the design space.

Coefficient Factor	Estimate	df	Standard Error	95% CI Low	95% CI High	VIF
Intercept	0.47	1	0.13	0.20	0.74	
A-Pressure	-0.13	1	0.061	-0.26	-7.698E-003	1.00
B-Time	0.14	1	0.061	9.641E-003	0.26	1.00
C-Amplitude	0.067	1	0.061	-0.060	0.19	1.00
AB	-0.052	1	0.080	-0.22	0.11	1.00
AC	-0.096	1	0.080	-0.26	0.069	1.00
BC	-8.750E-003	1	0.080	-0.17	0.16	1.00
A^2	0.10	1	0.068	-0.036	0.24	1.16
B^2	0.058	1	0.068	-0.082	0.20	1.16
C^2	0.098	1	0.068	-0.041	0.24	1.16

Final Equation in Terms of Coded Factors:

CO =
+0.47
-0.13 * A
+0.14 * B
+0.067 * C

-0.052 * A * B

-0.096 * A * C

-8.750E-003 * B * C

+0.10 * A^2

+0.058 * B^2

+0.098 * C^2

Final Equation in Terms of Actual Factors:

CO =

+2.29656

-0.14206 * Pressure

-0.075711 * Time

-0.037341 * Amplitude

-0.029557 * Pressure * Time

-0.010904 * Pressure * Amplitude

-1.97990E-004 * Time * Amplitude

+0.29423 * Pressure^2

+6.51930E-003 * Time^2

+4.43972E-004 * Amplitude^2

The Diagnostics Case Statistics Report has been moved to the Diagnostics Node.

In the Diagnostics Node, Select Case Statistics from the View Menu.

Proceed to Diagnostic Plots (the next icon in progression). Be sure to look at the:

1) Normal probability plot of the studentized residuals to check for normality of residuals.

2) Studentized residuals versus predicted values to check for constant error.

3) Externally Studentized Residuals to look for outliers, i.e., influential values.

4) Box-Cox plot for power transformations.

If all the model statistics and diagnostic plots are OK, finish up with the Model Graphs icon.

F. Particle Size Analysis

micromeritics®

Micromeritics Instrument Corporation

Saturn DigiSizer 5200 V1.10 Saturn DigiSizer 5200 V1.10 5200 LSHU V2.01 S/N 216 Page 1

Sample: A-80 (A Beyers/M van Baarsel)
Operator: H Botha
Submitter:
File: C:\5200\DATA\STD\002-264.SMP

Test Number: 3
Analyzed: 2013/10/18 10:42:43PM
Reported: 2013/10/24 9:45:31PM
Background: 2013/10/18 10:07:28PM

Model: (1.550, 0.1000000), 1.331
Material: Calcium Carbonate / Water
Background: Water RI 1.331
Smoothing: Medium

Comments: 0.0005% TSPP

Combined Report

Volume Frequency vs. Diameter

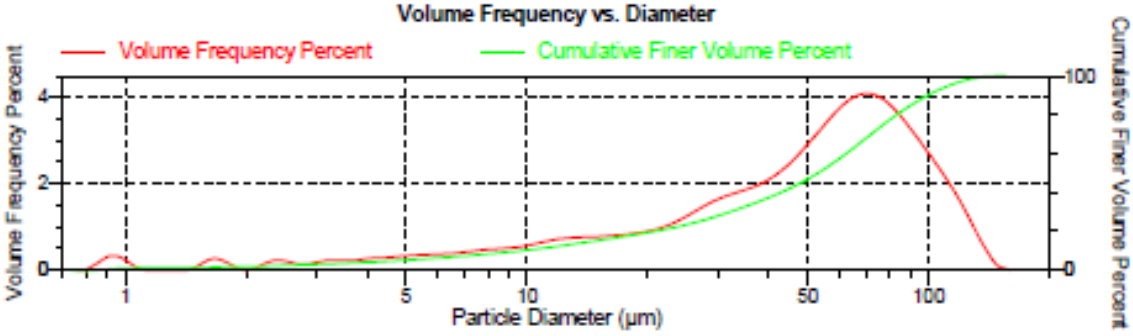

Summary Report

Analysis Conditions

FlowRate: 12.0 l/m
Circulation time: 60 sec
Ultrasonic intensity: 60 %
Ultrasonic time: 60 sec

Sample

Sample Concentration: 0.02572 %
Obscuration: 20.0 %

Volume Distribution Arithmetic Statistics

		Std Dev of 3			Std Dev of 3
Mean	53.98	2.803	Mode	71.22	2.437
Median	53.05	1.227			

Selected Sizes

Diameter (µm)	Percent Finer
100.0	90.2
50.00	46.9
20.00	19.4
10.00	10.3
1.000	0.9

Peaks

Peak Number	% of Dist.*	% of Dist. Std Dev of 3	Mean	Mean Std Dev of 3	Median	Median Std Dev of 3	Mode
1	96.4	0.2	55.93	2.960	54.77	1.330	71.22

* Peaks must comprise at least 5.00 % of the distribution.

micromeritics®

Micromeritics Instrument Corporation

Sample: A-80 (A Beyers/M van Baarsel)
Operator: H Botha
Submitter:
File: C:\5200\DATA\STD\002-264.SMP

Test Number: 3
Analyzed: 2013/10/18 10:42:43PM
Reported: 2013/10/24 9:45:31PM
Background: 2013/10/18 10:07:28PM

Model: (1.550, 0.1000000), 1.331
Material: Calcium Carbonate / Water
Background: Water RI 1.331
Smoothing: Medium

Comments: 0.0005% TSPP

Report by Size Table

Low Diameter (µm)	Cumulative Volume Finer (Percent)	Low Diameter (µm)	Cumulative Volume Finer (Percent)	Low Diameter (µm)	Cumulative Volume Finer (Percent)	Low Diameter (µm)	Cumulative Volume Finer (Percent)
150.000	100.0	50.000	46.9	9.000	9.3	3.000	2.9
100.000	90.2	40.000	37.3	8.000	8.3	2.000	1.8
90.000	84.7	30.000	28.0	7.000	7.3	1.000	0.9
80.000	77.4	25.000	23.4	6.000	6.2	0.900	0.3
70.000	68.1	20.000	19.4	5.000	5.1	0.800	0.0
60.000	57.4	10.000	10.3	4.000	4.0		

micromeritics®

Micromeritics Instrument Corporation

Sample: A-80 (A Beyers/M van Baarsel)
Operator: H Botha
Submitter:
File: C:\5200\DATA\STD\002-264.SMP

Test Number: 3
Analyzed: 2013/10/18 10:42:43PM
Reported: 2013/10/24 9:45:31PM
Background: 2013/10/18 10:07:28PM

Model: (1.550, 0.1000000), 1.331
Material: Calcium Carbonate / Water
Background: Water RI 1.331
Smoothing: Medium

Comments: 0.0005% TSPP

Report by Volume Percent

Low Diameter (µm)	Cumulative Volume Finer (Percent)	Low Diameter (µm)	Cumulative Volume Finer (Percent)	Low Diameter (µm)	Cumulative Volume Finer (Percent)
99.589	90.0	53.048	50.0	9.712	10.0

micromeritics®

Micromeritics Instrument Corporation

Sample: A-80 (A Beyers/M van Baarsel)
Operator: H Botha
Submitter:
File: C:\5200\DATA\STD\002-264.SMP

Test Number: 3
Analyzed: 2013/10/18 10:42:43PM
Reported: 2013/10/24 9:45:31PM
Background: 2013/10/18 10:07:28PM

Model: (1.550, 0.1000000), 1.331
Material: Calcium Carbonate / Water
Background: Water RI 1.331
Smoothing: Medium

Comments: 0.0005% TSPP

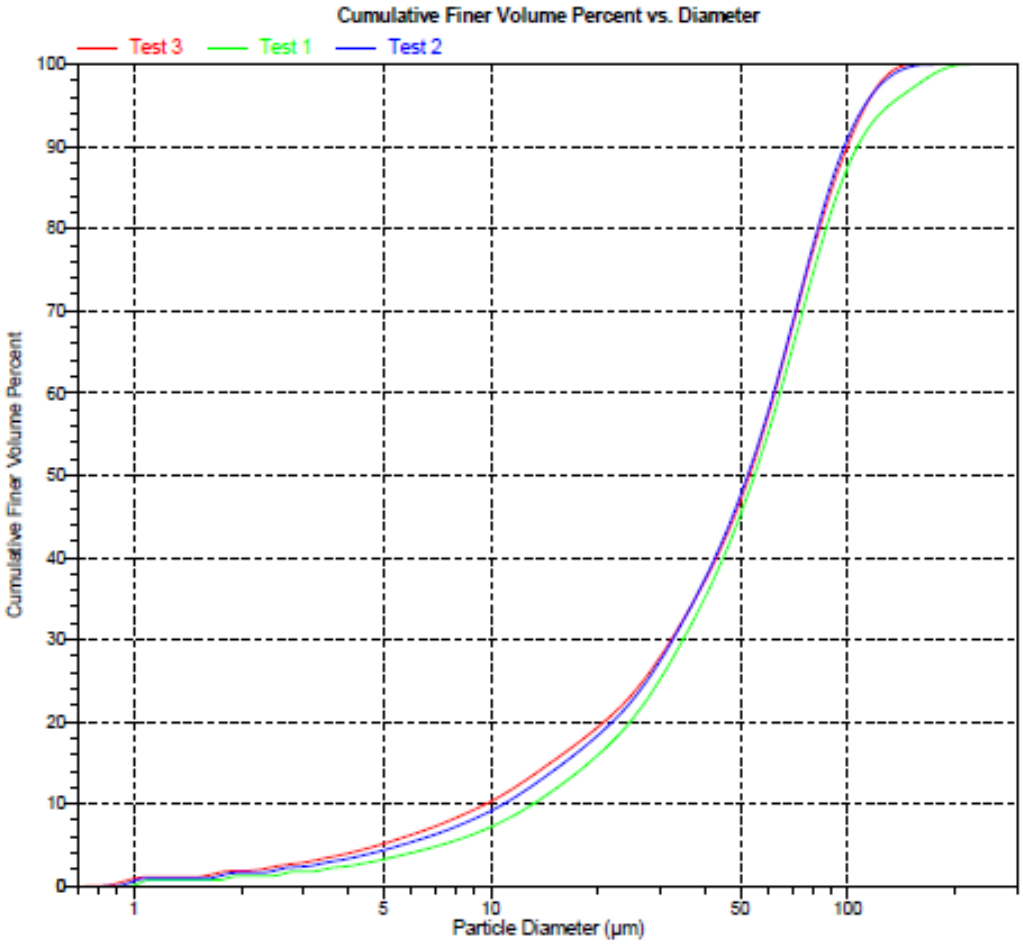

Sample: A-80 (A Beyers/M van Baarsel)
Operator: H Botha
Submitter:
File: C:\5200\DATA\STD\002-264.SMP

Test Number: 3
Analyzed: 2013/10/18 10:42:43PM
Reported: 2013/10/24 9:45:31PM
Background: 2013/10/18 10:07:28PM

Model: (1.550, 0.1000000), 1.331
Material: Calcium Carbonate / Water
Background: Water RI 1.331
Smoothing: Medium

Comments: 0.0005% TSPP

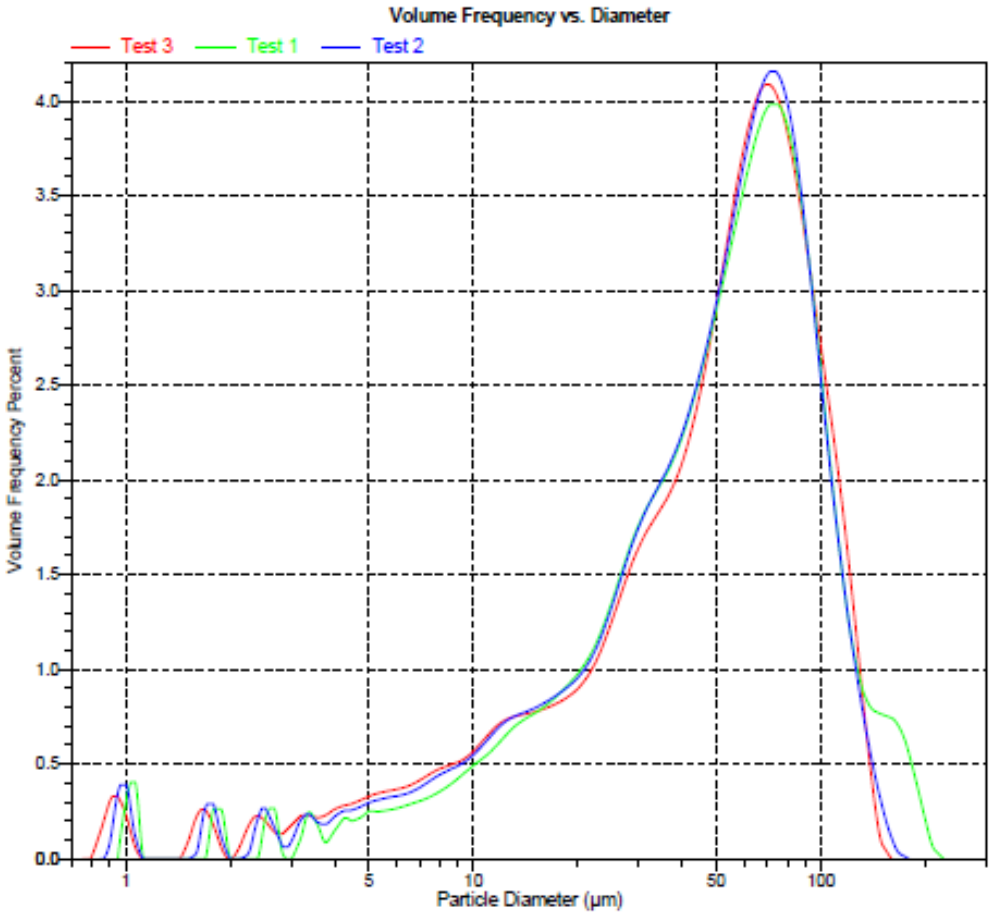

micromeritics®

Micromeritics Instrument Corporation

Sample: B-242 (A Beyers/M van Baarsel)
Operator: H Botha
Submitter:
File: C:\5200\DATA\STD\002-265.SMP

Test Number: 3
Analyzed: 2013/10/18 11:18:52PM
Reported: 2013/10/24 9:48:33PM
Background: 2013/10/18 10:07:28PM

Model: (1.550, 0.1000000), 1.331
Material: Calcium Carbonate / Water
Background: Water RI 1.331
Smoothing: Medium

Comments: 0.0005% TSPP

Combined Report

Volume Frequency vs. Diameter

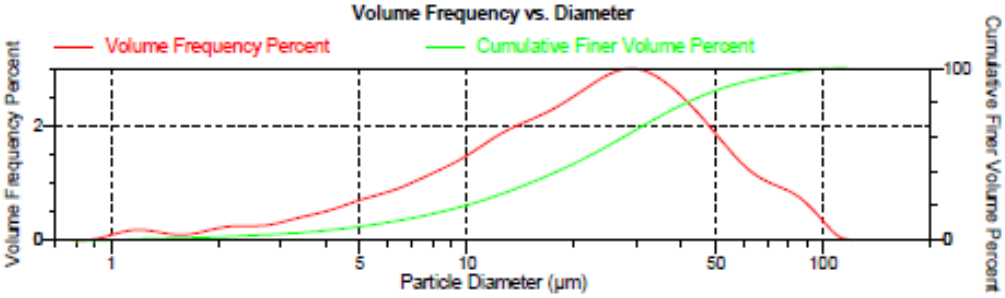

Summary Report

Analysis Conditions

FlowRate: 12.0 l/m
Circulation time: 60 sec
Ultrasonic intensity: 60 %
Ultrasonic time: 60 sec

Sample

Sample Concentration: 0.01317 %
Obscuration: 16.0 %

Volume Distribution Arithmetic Statistics

		Std Dev of 3			Std Dev of 3
Mean	27.21	3.704	Mode	28.36	1.730
Median	22.53	3.059			

Selected Sizes

Diameter (µm)	Percent Finer
100.0	99.6
50.00	87.0
20.00	44.6
10.00	20.4
1.000	0.1

Peaks

Peak Number	% of Dist.*	% of Dist. Std Dev of 3	Mean	Mean Std Dev of 3	Median	Median Std Dev of 3	Mode
1	97.1	0.5	27.96	3.649	23.22	2.976	28.36

* Peaks must comprise at least 5.00 % of the distribution.

micromeritics®

Micromeritics Instrument Corporation

Sample: B-242 (A Beyers/M van Baarsel)
Operator: H Botha
Submitter:
File: C:\5200\DATA\STD\002-265.SMP

Test Number: 3
Analyzed: 2013/10/18 11:18:52PM
Reported: 2013/10/24 9:48:33PM
Background: 2013/10/18 10:07:28PM

Model: (1.550, 0.1000000), 1.331
Material: Calcium Carbonate / Water
Background: Water RI 1.331
Smoothing: Medium

Comments: 0.0005% TSPP

Report by Size Table

Low Diameter (µm)	Cumulative Volume Finer (Percent)	Low Diameter (µm)	Cumulative Volume Finer (Percent)	Low Diameter (µm)	Cumulative Volume Finer (Percent)	Low Diameter (µm)	Cumulative Volume Finer (Percent)
100.000	99.6	40.000	78.5	8.000	15.3	2.000	1.8
90.000	98.7	30.000	64.5	7.000	12.8	1.000	0.1
80.000	97.2	25.000	55.1	6.000	10.3	0.900	0.0
70.000	95.0	20.000	44.6	5.000	7.9		
60.000	92.0	10.000	20.4	4.000	5.6		
50.000	87.0	9.000	17.8	3.000	3.5		

micromeritics®

Micromeritics Instrument Corporation

Sample: B-242 (A Beyers/M van Baarsel)
Operator: H Botha
Submitter:
File: C:\5200\DATA\STD\002-265.SMP

Test Number: 3
Analyzed: 2013/10/18 11:18:52PM
Reported: 2013/10/24 9:48:33PM
Background: 2013/10/18 10:07:28PM

Model: (1.550, 0.1000000), 1.331
Material: Calcium Carbonate / Water
Background: Water RI 1.331
Smoothing: Medium

Comments: 0.0005% TSPP

Report by Volume Percent

Low Diameter (µm)	Cumulative Volume Finer (Percent)	Low Diameter (µm)	Cumulative Volume Finer (Percent)	Low Diameter (µm)	Cumulative Volume Finer (Percent)
55.406	90.0	22.528	50.0	5.866	10.0

micromeritics®

Micromeritics Instrument Corporation

Sample: B-242 (A Beyers/M van Baarsel)
Operator: H Botha
Submitter:
File: C:\5200\DATA\STD\002-265.SMP

Test Number: 3
Analyzed: 2013/10/18 11:18:52PM
Reported: 2013/10/24 9:48:33PM
Background: 2013/10/18 10:07:28PM

Model: (1.550, 0.1000000), 1.331
Material: Calcium Carbonate / Water
Background: Water RI 1.331
Smoothing: Medium

Comments: 0.0005% TSPP

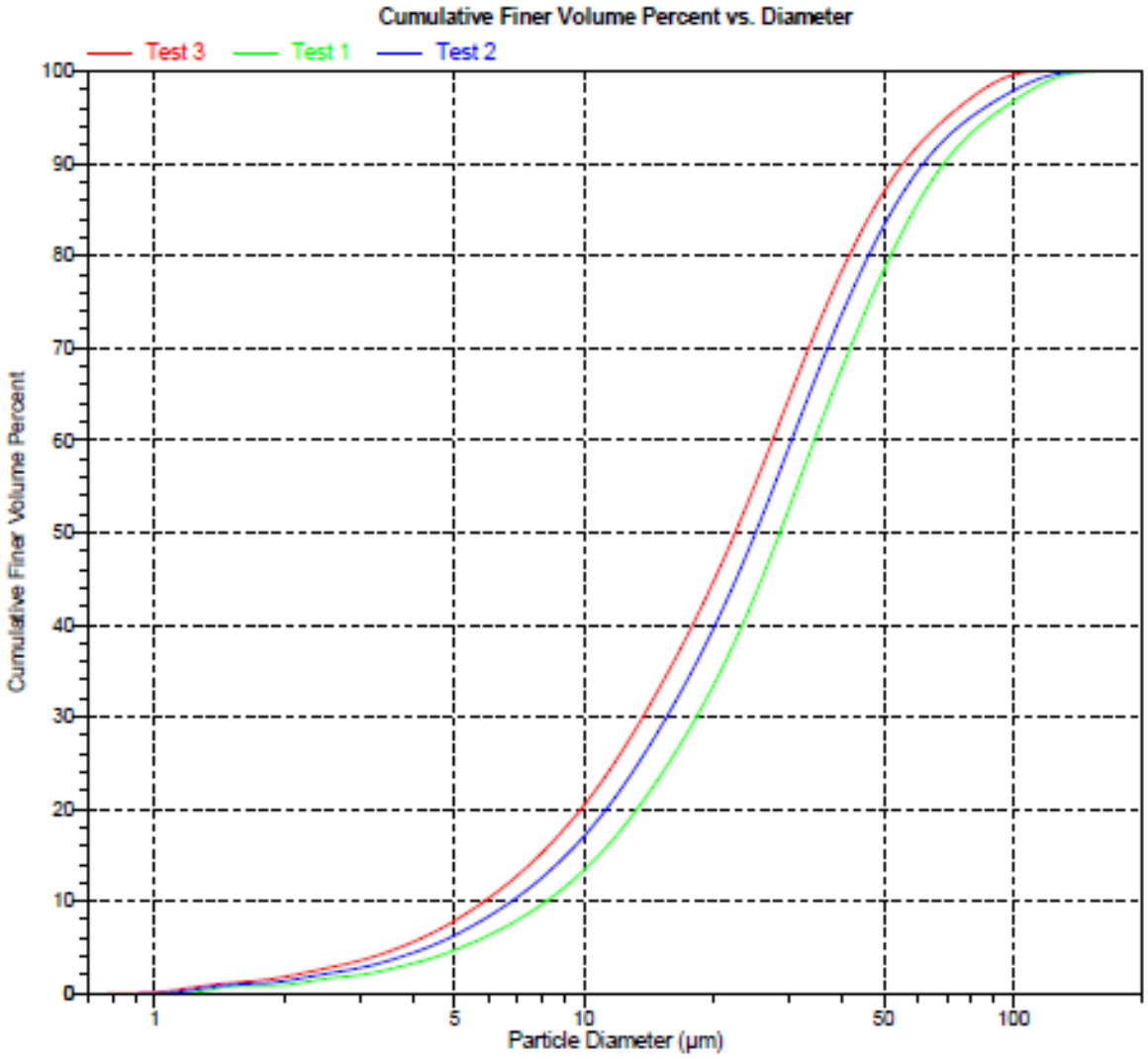

micromeritics®

Micromeritics Instrument Corporation

Sample: B-242 (A Beyers/M van Baarsel)
Operator: H Botha
Submitter:
File: C:\5200\DATA\STD\002-265.SMP

Test Number: 3
Analyzed: 2013/10/18 11:18:52PM
Reported: 2013/10/24 9:48:33PM
Background: 2013/10/18 10:07:28PM

Model: (1.550, 0.1000000), 1.331
Material: Calcium Carbonate / Water
Background: Water RI 1.331
Smoothing: Medium

Comments: 0.0005% TSPP

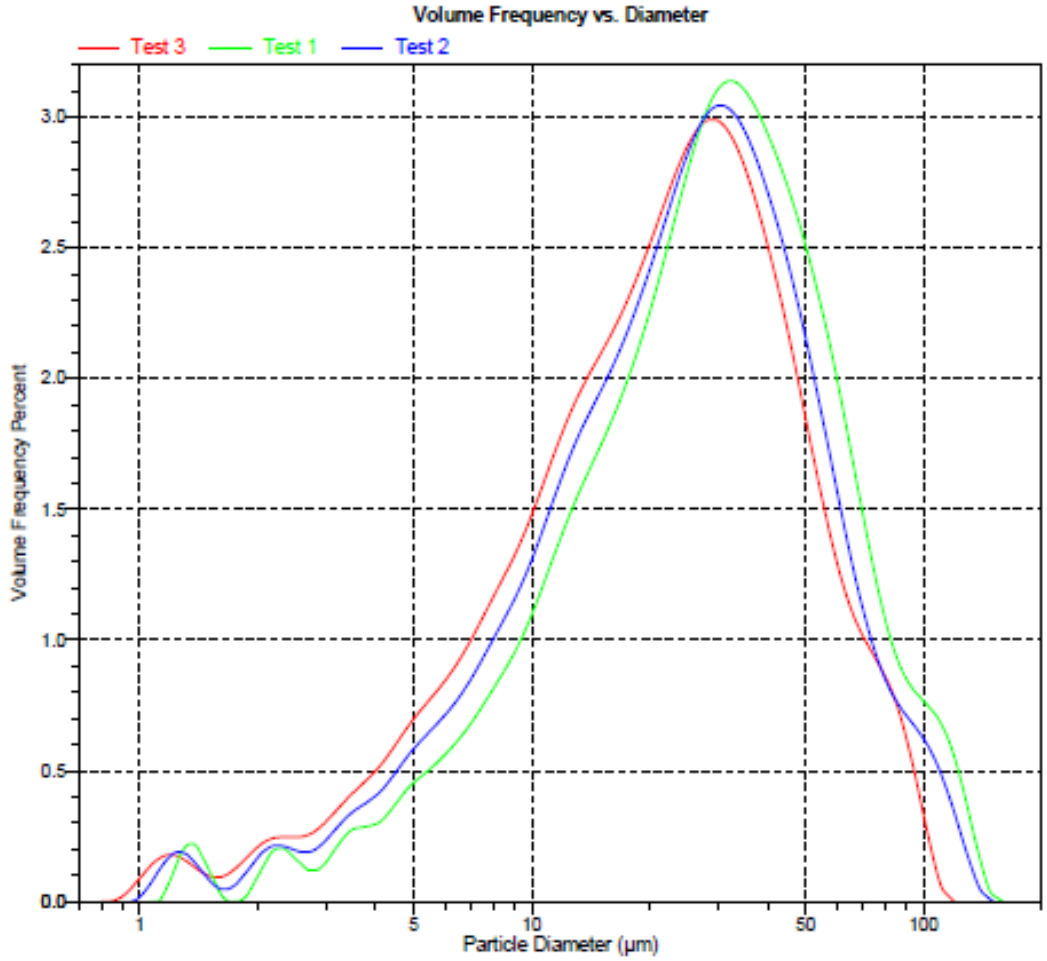

Micromeritics Instrument Corporation

Sample: B-242 (A Beyers/M van Baarsel)
Operator: H Botha
Submitter:
File: C:\5200\DATA\STD\002-265.SMP

Test Number: 3
Analyzed: 2013/10/18 11:18:52PM
Reported: 2013/10/24 9:48:33PM
Background: 2013/10/18 10:07:28PM

Model: (1.550, 0.1000000), 1.331
Material: Calcium Carbonate / Water
Background: Water RI 1.331
Smoothing: Medium

Comments: 0.0005% TSPP

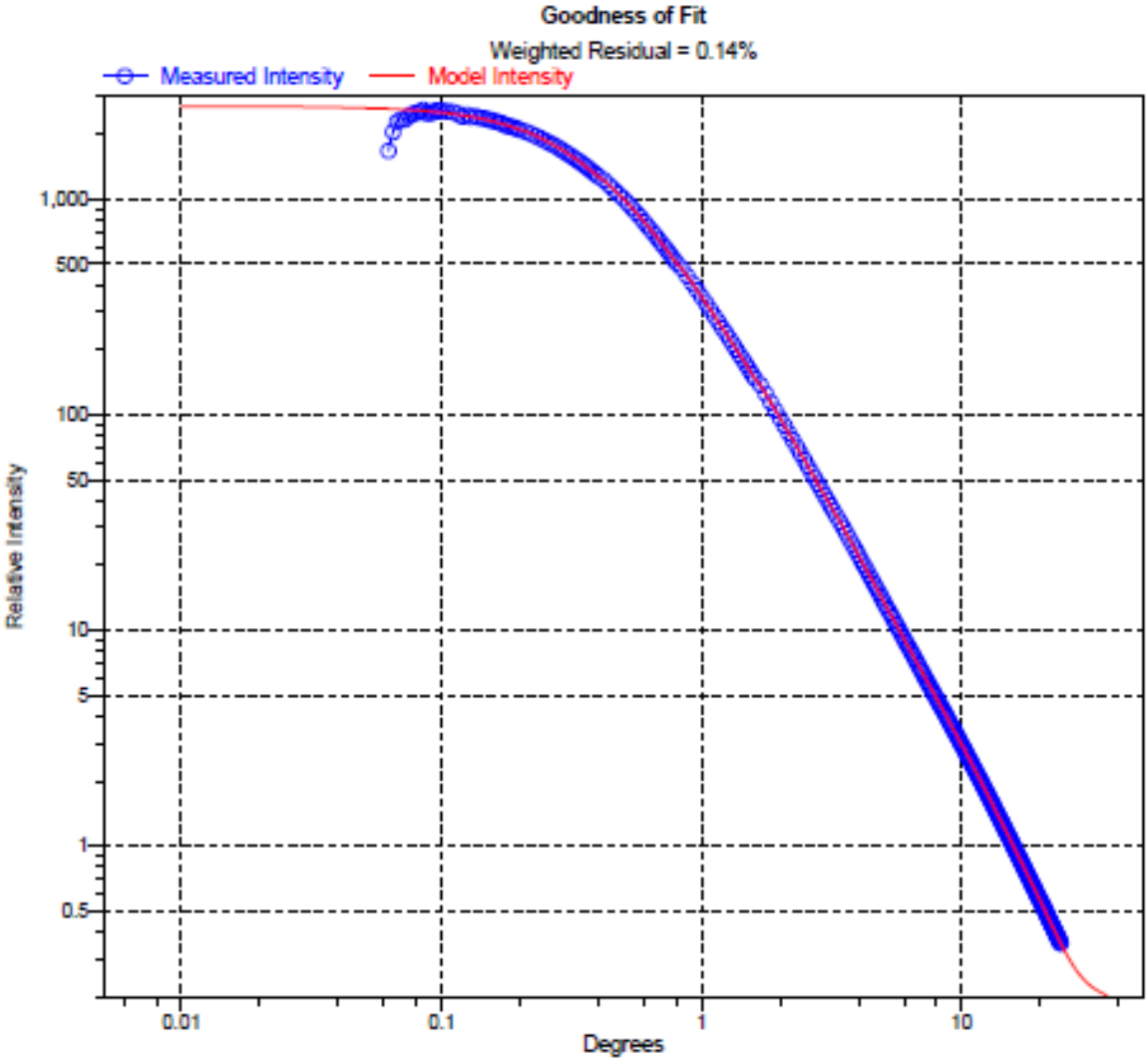

G. Materials used

Apart from the reactor setup described in the previous section, the following items were also used:

Tedlar gas sample bags – To contain hydrogen and all other gasses for up to 3 days

Teflon tubing – To connect the gas sampling lines

Teflon tape – To seal all tubing connections

Digital Scale – To measure sludge mass before and after experiments

Temperature controlled oven – To dry all samples to determine the water content

Muffle oven – To determine the ash content of the biomass samples

Porcelain oven-save Bowl – Used to dry the samples in the oven

Acetone – For cleaning of the equipment

Distilled water – Used to dilute the original sludge sample

Gas Chromatograph with TCD - for gas analysis

Gas Chromatograph with and FID and Methanizer- for gas analysis

Design Expert Statistical software by Statease ® - To evaluate statistical model

Draeger X-am 500 Multigas Monitor - CO Personal Protection

Sludge Sampling vessel – to split sludge into representative samples

EnvironServe Waste container – waste management

Snoop Liquid detection – gas leak detection on fittings

Personal Protective Equipment: lab coat, hearing protection, safety glasses, latex gloves

Gases used for calibration: argon, hydrogen, carbon monoxide, carbon dioxide, methane, instrument grade air, helium

100 µl Gas tight syringe – to inject into FID injection port

Inlet Liners: Replacement liners for GC injection ports

Replacement septa – to replace septa on Tedlar bags once worn from needle insertion

Excel-XLSTAT Software – for simple regression analysis

Glass Thermometer – to measure the temperature in cooling bath